UNIVERSITY OF NAPLES FEDERICO II

DEPARTMENT OF PHARMACY

PhD programme in Pharmaceutical Sciences

Targeting enzymes with marine-derived small molecules in search of new multitarget inhibitors to develop new treatments for type 2 diabetes mellitus and inflammatory diseases

PhD student

ALESSIO VITO

Coordinator

Prof.

ROSARIA MELI

Tutor

Prof. MARIALUISA MENNA

Cotutor

Prof. ANNA AIELLO

XXXVI CYCLE (2021-2023)

INDEX

ABSTRACT 1

LIST OF ABBREVIATIONS 3

INTRODUCTION 4

CHAPTER 1. A spotlight on bioactive marine natural products and their potential in drug discovery 11

1.1 Marine natural products in drug discovery 11

1.2 The role of marine natural products in the drug discovery for Type 2 Diabetes Mellitus 16

1.3 Identifying new designed multiple ligands in marine resources for the treatment of multifactorial diseases 26

CHAPTER 2. Current methodologies for unlocking the potential of marine natural products 31

2.1 Target-oriented (semi)synthesis (TOS) 31

2.2 From the TOS to the Diversity Oriented Synthesis (DOS) 36

2.3 Fragment-based drug discovery approach 38

2.4 Methods for assigning absolute configuration in natural and synthetic small molecules 40

CHAPTER 3. The phosphoeleganin, a promising antidiabetic and anti-inflammatory lead of marine origin 45

3.1 An overview on the antidiabetic properties of a phosphorylated metabolite isolated from *Sidnyum elegans* 45

3.2 Fighting hepatic insulin resistance for the treatment of NAFLD/MAFLD 50

3.3 Isolation of phosphoeleganin (44) and oxidative cleavage for the synthesis of 45 and 46 52

3.4 Pharmacological studies on 44-46 54

3.5 Materials and method 58

3.5.1 Isolation of phosphoeleganin (44) 58

3.5.2 Semisynthesis of compounds 45 and 46 58

3.5.3 Pharmacological assays on 44-46 59

CHAPTER 4. Merging FBDD and DOS to explore the antidiabetic chemical space of phosphoeleganin 62

4.1 Design of a NP-fragments library 62

4.2 Synthesis of compound 47a-50b 64

4.3 Pharmacological screening of compounds 45-46 and 47a-50b 67

4.3.1 Pharmacological characterization of compound 46 and 49a 70

4.3.2 Docking of compound 46 and 49a 76

4.4 Conclusions 79

4.5 Material and methods 80

4.5.1 Synthesis of compounds 47a-50b 80

4.5.2 Pharmacological assays on 47a-50b 87

CHAPTER 5. Targeting human 15-lipoxygenase-1 with phosphoeleganin and its analogues 92

5.1 Human 15-lipoxygenase-1 (15-LOX-1): an emerging target for drug discovery 92

5.2 Targeting 15-LOX-1 with marine natural products 94

5.3 Pharmacological evaluation of phosphoeleganin (44) and its derivatives on 15-LOX-1 97

5.4 Generating regiochemical and stereochemical diversity within a phosphorylated fragments library: synthesis of compounds 71-72 98

5.5 Materials and methods 101

CHAPTER 6. Synthesis of a second-generation library inspired to phosphoeleganin 103

6.1 Design and synthesis of compounds 73a-75b 103

6.2 Determination of the absolute configurations of diols 73a-75b 108

6.2.1 Structural characterization of diols 73a-73b 110

6.2.2 Structural characterization of diols 74a-74b 113

6.2.3 Structural characterization of diols 75a-75b 117

6.3 Materials and methods 117

CONCLUDING REMARKS 125

CHAPTER 7. Spectroscopic data 128

REFERENCES 167

ABSTRACT

Even more than their terrestrial counterpart, marine natural products are considered privileged structures capable to bind and modulate a plethora of protein targets, positioning them as pre-validated starting points for the design of compounds libraries for new pharmaceutical leads discovery. The wide chemical space covered by the unique and often complex scaffolds of marine metabolites can be indeed explored and exploited for drug discovery through the design and production of libraries of diverse natural product-inspired compound. These tasks can take full advantage of current medicinal chemistry strategies and methodologies. In this context, the research work reported below focused on the pharmacological characterization of phospoeleganin, a phosphorylated polyketide of marine origin endowed with antidiabetic properties, performed also by using several fragments libraries inspired to the natural product and generated by organic synthesis. These focused chemical libraries have been developed combining the principles of fragment-based drug discovery and diversity-oriented synthesis. They were composed of both semi-synthetic fragments of the polyketide and small molecules representative of its most functionalized portion, aiming both at investigating the essential requirements necessary to ensure pharmacological activities and at identifying new small molecules with multitarget activity to be further optimized in search of new therapeutics for multifactorial diseases. The study confirmed the insulin-sensitizing behavior of the polyketide, clarified its effects on insulin resistance and glucose homeostasis in liver cells, as well as demonstrated it as a promising multitarget agent capable of interacting with as many as three

targets involved in metabolic diseases. Moreover, it pointed out to some new candidates as antidiabetic leads with more synthetic tractability with respect to the natural complex metabolite.

Part of the topic of this PhD thesis has been published in three papers:

- Casertano, M.; Genovese, M.; Piazza, L.; Balestri, F.; Del Corso, A.; Vito, A.; Paoli, P.; Santi, A.; Imperatore, C.; Menna, M. Identifying Human PTP1B Enzyme Inhibitors from Marine Natural Products: Perspectives for Developing of Novel Insulin-Mimetic Drugs. *Pharmaceuticals* **2022**, *15*, 325, doi: 10.3390/ph15030325.
- Casertano, M.; Vito, A.; Aiello, A.; Imperatore, C.; Menna, M. Natural Bioactive Compounds from Marine Invertebrates That Modulate Key Targets Implicated in the Onset of Type 2 Diabetes Mellitus (T2DM) and Its Complications. *Pharmaceutics* **2023**, *15*, 2321, doi: 10.3390/pharmaceutics15092321.
- Agognon A.L.; Casertano, M.; Vito, A.; Orso, S.; Cabaro, S.; Mormone, F.; Morelli, C.; Perruolo, G.; Formisano, P.; Menna, M.; Imperatore, C.; Oriente, F.; Exploring the hepatic insulin sensitivity and inflammatory response via natural products: a spotlight on the marine-derived molecule phosphoeleganin and its semisynthetic derivatives. *International Journal of Molecular Sciences* **2024**, accepted.

LIST OF ABBREVIATIONS

SMs, small molecules; HTS, high throughput screening; NPs, natural products; SARs, structure-activity relationships; FBDD, fragment-based drug discovery; DOS, diversity-oriented synthesis; FDA, Food and Drug Administration; EMA, European Medicines Agency; T2DM, type 2 diabetes mellitus; T1DM, type 1 diabetes mellitus; MS, metabolic syndrome; PPAR, proliferator activated receptor; GLP-1, Glucagone-like peptide 1; DPP-IV, dipeptidyl peptidase IV; SGLT2, sodium–glucose cotransporter type 2; FBPase, fructose-1,6-bisphosphatase; GSK-3, glycogen synthase kinase 3; PTP1B, protein tyrosine phosphatase 1B; AR, aldose reductase; NAFLD, non-alcoholic fatty liver disease; NASH, non-alcoholic steatohepatitis; MAFLD, metabolic dysfunction–associated fatty liver disease; IRS, insulin receptor substrate; PI3K, phosphatidylinositol 3-kinase; SOCS, suppressors of cytokine signaling; ERK, extracellular signal-regulated kinases; pINSR, insulin receptor tyrosine phosphorylation; LOXs, lipoxygenases; PUFAs, polyunsaturated fatty acids; HPETEs, hydroperoxyeicosatetraenoic acids; 15-LOX-1, 15-lipoxygenase-1; phGPx, phospholipid hydroperoxide glutathione peroxidase; COPD, chronic obstructive pulmonary disease; HETE, hydroxyeicosatetraenoic acid; CNS, central nervous system; NMR, nuclear magnetic resonance; CDA, chiral derivatizing agent; CSA, chiral solvating agent; MPA, methoxyphenylacetic acid; 9-AMA, 9-anthrylmethoxyacetic acid; MTPA, methoxytrifluorphenylacetic acid; 4-DMAP, 4-dimethylaminopyridine; EDC, 3-(3-dimethylaminopropyl) carbodiimide;

INTRODUCTION

Drug discovery is a multidisciplinary process which lead to the identification of therapeutic agents useful in treating or managing a pathological condition. Aided by progresses and discoveries in different scientific fields, drug discovery requires a connection between biologists, chemists, clinicians, computational experts, and other specialists which synergistically cooperate to address the continuous demand of new medicines [1,2].

The drug target

The first step in drug discovery is to understand as completely as possible the biological and molecular mechanisms that underlie the onset of a given disease; this allows us to identify and validate appropriate pharmacological targets that can be modulated to restore health conditions. Pharmacological targets include receptors, enzymes, ion channels, transporters, nucleic acids, structural proteins, and second messengers whose activities influence various physiological processes and pathways. An ideal target, in addition to being safe and endowed with a therapeutic efficacy due to avoid failure in clinical trials, should be mostly "druggable", where this term refers to the possibility of being regulate by small molecules (SMs). This last requisite is mostly possessed by protein targets such as ion channel, G-coupled protein and enzymes. Enzymes stand out as highly effective drug targets because of the central role in disease onsets and the specificity of enzyme-inhibitor interactions. Compared with the other types of targets, enzymes offer advantages such as the possibility to have different mechanisms of action depending on the

site of interaction and the nature of interaction. The success of enzyme-targeted drugs, as demonstrated by statins, protease inhibitors, and tyrosine kinase inhibitors, underscores the efficacy and versatility of enzymes as valuable targets in pharmacotherapy. Nowadays, advances in the field of genomics have made it possible to identify tens of thousands of potential drug targets [2–5].

The biologically relevant small molecules chemical space

However, when many pharmacological targets have been discovered and vallidate, the source of molecules remains the main concern in drug discovery. The lead identification, which follows the previously discussed stage in drug discovery, requires libraries of SMs to be screened in search of bioactive ones. SMs dominate our ability to treat disease, indeed many drugs are small carbon-based chemical compounds. On the other hand, SMs advance our knowledge of biological processes: they are such chemical probes, compounds that can be used both for studying disease and as starting points for making drugs. These molecules can fill the gap between understanding and treating disease, namely between chemistry and biology. Discovery of useful SMs in this sense requires the ability to navigate efficiently the chemical space of biological interest efficiently, considering previously unexplored regions. SMs can modulate the selected targets acting as agonists or antagonists, activators or inhibitor and openers or blockers in case of G-coupled receptors, enzymes or ion channel, respectively [2,6]. The ability to assay large libraries of SMs is related to the development of modern screening techniques such as high throughput screening (HTS), which involve automated equipment to quickly test thousands of molecules for identifying the most promising chemical entities based on their biological activity [7]. Generally, HTS has been

coupled with combinatorial chemistry that consists in the generation of large libraries of structurally diverse compounds through systematic, repetitive, and covalent linkage of several selected building blocks. However, even if this approach has brought a great innovation in drug discovery in late 1990, the probability of success in lead identification does not depend only on the number of available molecules. The resulting combinatorial libraries usually lack structural variation and favorable pharmacokinetic and pharmacodynamic properties [8].

The natural products

The vastness of the bioactive SMs chemical space prevents exploration by synthesis alone; in addition, it should be considered that bioactivity is actually concentrated in a few small regions in the SMs chemical space. One strategy could be to start the exploration with molecules that already show a certain bioactivity and look for ones that are structurally related. Much of the chemical space with pharmacological value is occupied by natural products (NPs). They are of intrinsic chemical and biological importance due to their high chemical diversity improved through evolutionary selection to interact with biological macromolecules-binding sites. Historically, small organic NPs have played a pivotal role in health promotion and diseases treatment. In ancient times, drugs were entirely of natural origin and composed of plants, animal byproducts and inorganic materials. Many natural matrices, especially derived from plants, have been showed to be effective healthy treatments and, therefore, they have been subsequently recorded and documented in herbals [9,10]. Over the years with the rise of new scientific technologies, however, interest in the natural world has shifted to the identification of the molecules responsible for the therapeutic activity of that matrix. This goal was then pursued

through the systematic study of natural metabolites, a field of organic chemistry focused on the isolation of such molecules from the natural source by chromatographic techniques and subsequent structural characterization by spectroscopic and spectrometric techniques. All organisms share about the same crucial biochemical pathways necessary for life processes but, in addition to these, they also possess secondary biosynthetic pathways that produce unique and often complex metabolites. These "secondary metabolites" are low molecular weight molecules with different chemical structures and biological activities. The term "secondary" refers to the initial observation that their production is not necessary for the growth and reproduction of organisms; however, it is now accepted that secondary metabolites play key roles in the survival of the organisms that produce them because they determine interactions with their environment. Today, the chemical investigation of the secondary metabolites produced by different living organisms is an important field of research for organic chemists, molecular biologists, and bioinformaticians [11,12]. Even after the advent of combinatorial chemistry and HTS, nature is still considered the most valuable and prolific source of chemical entities. Unsurprisingly, it has been estimated that more than 65% of clinical drugs marketed from 1981 to 2019 are derived from natural matrices or have been designed employing NPs scaffolds as inspiring tools [9,13,14]. NPs, both of terrestrial and marine origin, are characterized by enormous chemical diversity and complexity, unmatched by synthetic chemical libraries, and occupy a wide unexplored chemical space which provides a rich arsenal of promising bioactive compounds more attractive as leads and more drug-like than the compounds obtained by combinatorial chemistry processes [15–18]. Moreover, NPs offer unique features compared with synthetic molecules,

which confer both benefits and challenges for lead discovery stage. They are often characterized by high content of sp^3-hybridized carbon atoms, relevant molecular rigidity, and several chiral center. These features increase the value of these metabolites in lead discovery processes since an excess of flat moieties has been identified as a source of undesirable properties while the higher rigidity and the fixed stereochemistry can be valuable in drug discovery for tackling protein–protein interactions, improving pharmacodynamics properties [15,19,20].

Synthesis and medicinal chemistry of NPs

It should be considered that unaltered NPs generally possess suboptimal pharmacological properties and, therefore, strategies to obtain more active, better absorbed, and less toxic analogues are almost always required to design valuable new drugs [15]. In this scenario, organic synthesis proves to be a consolidated tool to enhance the potential of NPs; their total chemical synthesis, production of semi-synthetic derivatives using NPs as a starting point, and synthesis of analogs are some of the feasible strategies to enrich screening libraries with an adequate number of NPs and NP-inspired molecules [16,21]. The advent of NPs chemistry was immediately followed by the challenging procedures of total synthesis of bioactive molecules. In fact, in some cases, one of the limiting factors for the use of nature in drug discovery is the low amount of compound that can be obtained from the isolation processes and that often does not allow the complete pharmacological characterization. However, total synthesis is a complicated and laborious process, characterized by numerous synthetic steps that are necessary to obtain the complex structures provided by nature [22,23]. Sometimes it has been possible to facilitate total synthesis by starting from natural intermediates that can be isolated in large

quantities or the production of which can be carried out through biotechnological techniques. In this context, modifying a natural product to synthesize another or performing chemical manipulations of a bioactive metabolite to evaluate and study structure-activity relationships (SARs) [24,25]. To date, total synthesis is gradually declining. In fact, from the perspective of versatile, efficient and green processes, total synthesis should be avoided in favor of other methods that yield optimized NP-derived SMs with a less complex structure. The role of bioactive NPs, therefore, remains crucial as inspiring factor for the synthesis of SMs due to their intrinsic pharmacological activity and unique scaffolds which provide chemical diversity. In recent decades, the structural models provided by nature have inspired drug discovery campaigns through two different approaches, fragment-based drug discovery (FBDD) and diversity-oriented synthesis (DOS), both of which can include a bioactive natural metabolite as the cornerstone of the search for new active SMs. While DOS involves the synthesis of chemical libraries in which chemical diversity is enhanced both from a structural and stereochemical point of view, FBDD consists in the design and synthesis of low molecular weight fragments to be functionalized further in the optimization processes [26–29]. NPs match perfectly with these two methods; in fact, the great structural diversity provided by nature is incomparable with combinatorial chemistry and can inspire the design of focused liberations through DOS, while through FBDD approach consists in the design of fragments representative of some portions of the entire natural model structure in order to study its pharmacological properties and identify the pharmacophore of the natural bioactive molecule, avoiding the total synthesis process. These are just two of the possible ways to unlock the great potential of natural metabolites, whose role in the drug discovery

seems everlasting as long as it is possible to merge them with the most modern approaches for the identification of new therapeutics[30,31].

The aim of The PhD

In this context, the aim of my PhD project was to exploit the potential of a secondary marine metabolite endowed with antidiabetic and anti-inflammatory properties by merging the FBDD and DOS approaches. Furthermore, by framing diabetes as a multifactorial disease, our aim was also to be able to identify novel multitarget ligands inspired by the natural metabolite. In fact, the innovative therapeutic approach for the treatment of diseases in which several molecular systems are impaired is to simultaneously modulate multiple targets to have a favorable synergistic effect. This purpose can be achieved by using molecules which are endowed with such structural promiscuity that allow interactions with multiple biological macromolecules. The potential of this marine NPs has been widely explored during my PhD activity under the supervision of Proff. Marialuisa Menna and Anna Aiello at the Department of Pharmacy of University of Naples "Federico II". Specifically, I dealt with the ex-novo isolation of the bioactive marine metabolite for its in-depth pharmacological investigation and then, with the synthesis of its derivatives in search of new multitarget leads. The performed studies join a multidisciplinary work in which further national and foreign research groups have been involved, too.

CHAPTER 1. A spotlight on bioactive marine natural products and their potential in drug discovery

1.1 Marine natural products in drug discovery

Although the systematic study of terrestrial organisms has driven drug discovery in the past and is widely validated in the identification of new bioactive compounds, natural resources are far of being completely explored. In this view, oceans, which occupy more than 70% of the Earth's surface and represent one of the richest components of the Earth's biosphere, have become attractive because of the wide variety of animal, plant and microorganism interacting species. Therefore, marine environment has been as a rich source of secondary metabolites to fully explore in drug discovery [32,33]. In recent years, the interest in marine environment grown up due to the enormous chemodiversity provided by marine NPs which are structurally distinct from terrestrial ones by unusual scaffolds and functional groups because of the different and extreme life conditions. Marine NPs, thus, represent a rich arsenal of bioactive molecules to which a high potential for discovering new lead compounds with peculiar mechanisms of action is associated [14,15,34]. Despite their applicability in drug discovery, marine NPs are usually isolated in low amounts which is enough for the determination of planar structures but not adequate for the assignment of absolute stereochemistry and complete pharmacological characterization. Therefore, it is often necessary turn to the re-isolation of marine NPs or to the total synthesis of the natural model, generally a laborious and expensive procedure characterized by several steps according to its structure complexity. Moreover, this low synthetic accessibility of marine NPs, which also reduce the possibility of scale up,

together with poor pharmacokinetics properties, represent the main drawbacks which hinder the marketing of unaltered marine NPs as drugs [25,35,36].

Systematic investigation of the metabolic content of marine organisms has long been limited because of the few methods of collecting living material, which were limited to skin diving. Most of the bioactive NPs from sea have been isolated from marine invertebrates: sponges are the most prolific source of new compounds (almost 47%), followed by corals (34%) and then echinoderms and tunicates (about 18%) [33]. Since the 1970s, with the development of modern diving techniques that allowed exploration of the deep-sea environment, bioprospecting of marine organisms rise the interest of chemists and biologists. In fact, most of the approved drugs occurred in the 21st century while other interesting bioactive marine NPs and derivatives are in clinical trials, mostly as anticancer drugs [37,38]

Historically, the first marine derived approved drug from Food and Drug Administration (FDA) was cytarabine, a cytosine arabinoside isolated from Caribbean sponge *Cryptothethya crypta*, marketed as Cytosar-U® for the treatment of different types of leukemia [39,40]. Cytarabine belongs to the antimetabolites family which are produced by organisms and microorganisms to block the growth of competitors or predators. The antimetabolites are chemically similar to natural produced metabolites, but they hamper with some biological activities, in particular interfering with cellular proliferation. The discovery of cytarabine from *Cryptotethya crypta* paved the way for the introduction of marine NPs in drug discovery, laying foundations for anticancer and antiviral therapy by nucleoside antimetabolite drug identification. Mainly used in association with other anticancer drugs, cytarabine formed the principal chemotherapeutic of the most frequently adopted regimens such as MEC (mitoxantrone, etoposide

and cytarabine), DHAP (dexamethasone, cytarabine and cisplatin), and the ESHAP (etoposide, methylprednisolone, high dose cytarabine and cisplatin). Few years later, vidarabine, an adenine arabinoside was isolated from the same sponge and marketed as antiviral drug against herpes simplex 1, even if it was later removed from trade since it was identified as less efficient and more toxic than the drug acyclovir. Therefore, these two nucleosides played a precious implementation of cancer and viral therapy as well as a pivotal role in the use of marine NPs in drug discovery [40,41]. All the marine NPs marketed as drugs are reported in Table 1.

Another example of anticancer marine metabolite is ecteinascidin (Yondelis), an alkaloid extracted from the colonial tunicate *Ecteinascidia turbinate* which received the orphan drug status in 2007. This alkaloid is an FDA approved compound for treatment of soft tissue sarcomas and in 2009 gained the approval by European Medicines Agency (EMA) for ovarian cancer along with doxorubicin, too. Currently, this compound is additionally involved in several clinical trials of multiple countries for prostate, breast and paediatric sarcomas [42,43].

Although marine metabolites were funneled into the anticancer lead discovery since their cytotoxic nature, some marine compounds got approval as a drug for analgesic properties (zicotonide, marketed as Prialt) and for hypotriglyceridemic effect (ethyl esters of ω-3 polyunsaturated fatty acids, marketed in Europe as Eskim). Frequently employed as integrators, ethyl esters of ω-3 PUFAs, isolated from fish's oil, were approved ad drugs in 2004 by the FDA and in 2005 by the EMA for severe hypertriglyceridemia. Although the mechanism of action is not completely clear, their ability in reducing blood triglycerides is well confirmed. Reduction of hepatic lipogenesis, cholesterol incorporation into VLDLs,

cholesterol secretion and improved clearance of triglycerides from VLDL particles were proposed to explain the hypotriglyceridemic action [43–45]

Table 1. Marine-derived marketed drugs

Compounds	Brand Name	Natural Source	Clinical Use
Cytarabine	Cytosar-U	Sponge	Leukemia
Vidarabine	Vira-A	Sponge	Antiviral
Fludarabine	Fludara	Sponge	Leukemia
Ziconotide	Prialt	Mollusk	Chronic pain
Omega-3 acid ethyl esters	Eskim (EU)	Fish	Hypertriglyceridemia
Nelarabine	Atriance (EU)	Sponge	Leukemia
Trabectedin	Yondelis	Tunicate	Ovarian cancer, soft tissue sarcoma
Eribulin	Halaven	Sponge	Breast cancer
Brentuximab vedotin	Adcetris	Mollusk/ cyanobacterium	Lymphomas
Lurbinectedin	Zepzelca	Tunicate	Ovarian cancer

Polatuzumab vedotin	Polivy	Mollusk/ cyanobacterium	Breast cancer
Enfortumab vedotin	Padcev	Mollusk/ cyanobacterium	Urothelial cancer
Belantamab mafodotin	Blenrep	Mollusk/ cyanobacterium	Multiple myeloma

During years, marine NPs have, thus, gained an election position in the discovery of new lead candidates due to their fascinating chemical structures. Because of the different conditions of salinity, pressure and temperature that influence biosynthetic pathways, marine environment offers an enormous pool of chemical structures with uncommon and different structural motifs which are different from terrestrial ones for uncommon chemical scaffolds and functional groups [46]An additional feature of the marine environment is the symbiotic association that could exist between different microorganisms such as bacteria and fungi, and marine invertebrates. About 40% of the biomass often consists of microorganisms that are primarily responsible for the synthesis of many bioactive compounds [47]. Taken together, these corroborations highlight the marine environment as a rich and unexplored arsenal of bioactive molecules to which a high potential for discovering new lead compounds with peculiar mechanisms of action is associated.

1.2 The role of marine natural products in the drug discovery for Type 2 Diabetes Mellitus

Type 2 diabetes mellitus (T2DM) is a metabolic and multifactorial disorder where the β-cells of endocrine pancreas does not produce adequate levels of insulin or peripheric tissues do not effectively respond to the insulin. This disease is a burning and risky health problem that also impact health system expenditure which account for about 90% of all diabetes cases. In fact, diabetes is classified into type 1 diabetes mellitus (T1DM) and T2DM [48]. The incidence of diabetes has increased most rapidly in low- and middle-income countries due to globalization, but also with respect to changes in lifestyle and an ageing population. The number of people with diabetes has reached a total of 422 million cases in 2014, and that number that is predicted to rise [48,49]. Moreover, managing T2DM and its comorbidities with monotherapy is usually ineffective leading to the administration of several hypoglycaemic drugs increasing the risk of side effects. In fact, despite several drugs are available, glycaemic control is not easy to reach [50].

T2DM is mainly caused by insulin resistance, a pathological state in which muscle, adipose cells, and liver cells do not effectively respond to insulin and are not able to consume hematic glucose for metabolic reactions. Increased blood glucose leads to the condition of hyperglycemia which predispose to several long-term complications, such as nephropathy, retinopathy, neuropathy, and angiopathy [48,51]. The onset of insulin resistance is promoted by high-calorie dietary habits, ageing, and genetic predisposition. Moreover, a relationship between insulin resistance and obesity, which is connected to bad dietary routines, has been confirmed [52]. At least, insulin resistance, together with dyslipidemia, hypertension, and abdominal obesity, is part of the metabolic syndrome (MS), which

includes a cluster of predisposing factors of T2DM [53]. Certainly, healthy diet and moderate exercise are necessary to manage T2DM and reduce obesity, but lifestyle changes must be coupled, in many cases, with drug therapy. Considering that T2DM is a multifactorial disease and found on several risk factors and is associated with many complications, combination of several hypoglycemic drugs is required to control the progression of the disease [54,55]. The main classes of drugs to treat T2DM aim to counteract hyperglycemia through different mechanisms of action. Insulin secretagogues, whose main representative class are sulfonylureas, stimulate pancreatic cells to secrete more insulin[56]. Biguanides, instead, do not influence the insulin secretion directly, but improve the response to natural insulin of peripheral tissues reducing hepatic glucose production and increasing glucose uptake and utilization by muscle, adipose and hepatic cells [57]. Insulin mimetic sensitizers, whose peroxisome proliferator activated receptor (PPAR) agonists belong to, act by lowering blood glucose levels both by the activation of the glucose transporters on muscle and fat cells or by increasing insulin sensitivity. The activation of PPARα affects the glucose metabolism since it causes a decrease in hepatic gluconeogenesis and increase the utilization of peripheral glucose. Moreover, PPAR agonists increase the sensitivity of the cells to insulin, improve glucose uptake by skeletal muscles, and decrease the glucose production by retarding gluconeogenesis. Thus, dual PPARα/γ agonists have been also identified with synergistic action in maintaining insulin sensitivity and inflammation control, with reduced side effects with respect to using PPAR agonists alone [58]. However, all these classes of drugs are affected by side effects that are exacerbated when the drugs are administered concurrently. The not so thriving landscape of therapeutic options and the incidence of the disease in the

population drives scientific research to identify new targets and new drugs. Glucagone-like peptide 1 (GLP-1) receptor agonists and dipeptidyl peptidase IV (DPP-IV) inhibitors are considered part of incretin-mimetic drugs since both cases interact with incretin system. GLP-1 receptor agonists bind the receptor for the considered incretin hormone which is secreted after nutrient intake and increases insulin release leading to a decrease in blood glucose levels. DPP-is responsible for the degradation of GLP-1 and, thus, its inhibition DPP-IV increases the half-life of GLP-1 and its activity[59,60]. The inhibition of hydrolyzing enzymes α-amylase and α-glucosidase is considered an interesting prophylactic approach for T2DM and insulin resistance prevention. In fact, both enzyme inhibitors can control blood glucose homeostasis by limiting the final stages of carbohydrate digestion, and they could be used to control postprandial hyperglycemia [61]. The sodium–glucose cotransporter type 2 (SGLT2), which mediate glucose reabsorption from the glomerular filtrate, is considered a recently approved target for the treatment of T2DM. SGLT2 inhibitors act as hypohlycemic drugs by controlling the glucose elimination, reducing the reabsorption of glucose and enhancing the excretion of glucose in urine[62]. Fructose-1,6-bisphosphatase (FBPase) is an enzyme involved in gluconeogenesis and its inhibition has proved to be effective in glucose homeostasis by the reduction of the synthesis of endogenous glucose [63]. Glycogen synthase, a glycosyltransferase that catalyzes glycogen chain elongation promoting the conversion of glucose to glycogen, is negatively regulated from the glycogen synthase kinase 3 (GSK-3). GSK-3 selective inhibition in insulin-resistant skeletal muscle causes not only the increase in glycogen synthesis reducing blood glucose but also improvements in insulin-stimulated glucose transport activity [64]. Two promising and emergent targets are protein tyrosine phosphatase

1B (PTP1B) and aldose reductase (AR), which also represent the main targets investigated during my PhD work. PTP1B acts as a negative regulator of insulin action, by dephosphorylating specific residues of phosphotyrosine both of the activated insulin receptor and its substrates and, thus, interrupting the signaling pathways mediated by the hormone. PTP1B also downregulates leptin pathway, an adipocyte-derived hormone which controls food intake and increases energy expenditure. PTP1B overexpression is strictly related to insulin resistance, and it has been demonstrated that the inhibition or genetic ablation of this phosphatase can improve glucose homeostasis, cellular sensitivity to both insulin and leptin, and resistance to diet-induced obesity, without inducing hypoglycemia or toxic effects [65]. AR is a cytoplasmatic NADPH-dependent aldo-keto reductase critically involved in the onset and progression of side diseases associated with T2DM. AR catalyzes the first reaction of polyol pathway, in which glucose is converted to sorbitol, and plays a crucial role in hyperglycemia-induced oxidative stress and in cellular osmolarity. Therefore, AR inhibitors are useful to prevent or slow the progression of T2DM-associated complications [66]. The review published during my PhD from our research group, whose title is "*natural bioactive compounds from marine invertebrates that modulate key targets implicated in the onset of type 2 diabetes mellitus (T2DM) and its complications*", highlighted that more than 200 marine and marine-derived molecules resulted active against crucial targets of T2DM [67]. In this review, we analyzed the literature from the last thirty years on marine NPs that were isolated from marine invertebrates, and the collected molecules were first categorized according to their mechanism of action. The high chemical diversity associated with the reported bioactive marine NPs outlined marine resources as a key tool to advance understanding in the

field of T2DM research and antidiabetic drug discovery. In fact, targeting the already discussed targets involved in the etiopathogenesis and progression of T2DM with molecules characterized by different chemical scaffolds also allows new mechanisms of action to be discovered. We provided an overview on the great chemical diversity of natural metabolites, derived from marine invertebrates, which belong to different chemical family such as terpenes, alkaloids, halogenated compounds, polyketides, sterols and fatty acids, glycosides and peptides. The purpose of this review was to prove the potential of marine invertebrate-derived bioactive compounds in the discovery of novel lead compounds for targeting the main enzymes, receptors and, more generally, proteins involved in the onset of T2DM [67]. The current literature show that a variety of promising bioactive scaffolds associated with different and peculiar mechanism of action are available from marine invertebrates, even if unmodified marine NPs are not easily marketed as drugs due to failures in preclinical and clinical trials. At least, this review can serve as instrument for exploiting known marine NPs by synthetic approaches to generate inspired marine-derived SMs as synthetic leads as well as useful for outlining SARs of parent compounds. Despite the many reported proteins involved in T2DM, only a few of them have been targeted with marine invertebrate-derived molecules. As showed in Figure 1, most of the reported marine NPs and marine NP-derived compounds from marine invertebrates have been demonstrated to act as PTP1B inhibitors.

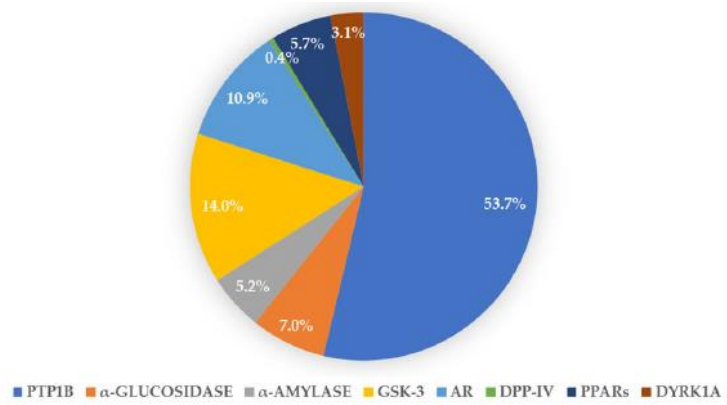

Figure 1. Relative percentage of bioactive marine NPs and marine NP-derived compounds with respect to the selected targets

Among the listed marine bioactive compounds with antidiabetic potential, dysidine (**1**, Figure 2) represent the most promising drug candidate since it is currently in preclinical trials for the treatment of T2DM and obesity [68].

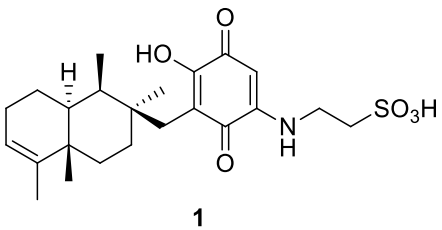

1

Figure 2. Structure of dysidine (**1**).

Dysidine is a sesquiterpene quinone isolated from Hainan sponge *Dysidea villosa* and was proved to inhibit PTP1B, with an IC_{50} of 1.5 ± 0.4 μM. Further pharmacological studies revealed that **1** behaved as a reversible and competitive inhibitor of PTP1B with a mechanism that is still not entirely clear but certainly does not involve the quinone moiety [68]. Avapyran (**2**, IC_{50} = 11.0 μM), avarol (**3**, IC_{50} = 12.0 μM), neoavarol (**4**, 35% inhibition at 44 μM), 3′-aminoavarone (**5**, IC_{50} = 18.0 μM), 17-*O*-

acetylavarol (**6**, IC_{50} = 9.5 μM), 17-*O*-acetylneoavarol (**7**, IC_{50} = 6.5 μM), 20-*O*-acetylavarol (**8**, IC_{50} = 10.0 μM), and 20-*O*-acetylneoavarol (**9**, IC_{50} = 8.6 μM) were isolated from *Dysidea* sp. collected in Okinawa (Figure 3). All these metabolites share the same scaffold with dysidine **1** and their pharmacological screening on PTP1B highlighted compound **10** as the most promising of the series [69].

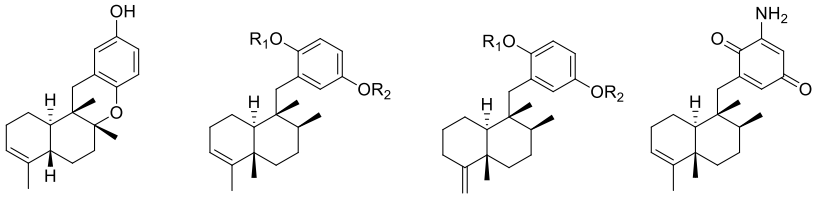

Figure 3. Structure of sesquiterpenes **2**-**9**.

The most potent terpenes certainly include frondoplysins A (**10**) and B (**11**, Figure 4), isolated from the marine sponge *Dysidea frondosa*, which are two uncommon sesquiterpenes composed of meroterpene and psammaplysin alkaloid scaffolds. Compounds **10** and **11** showed a considerable inhibitory activity with IC_{50} values of 0.39 and 0.65 μM, respectively [70].

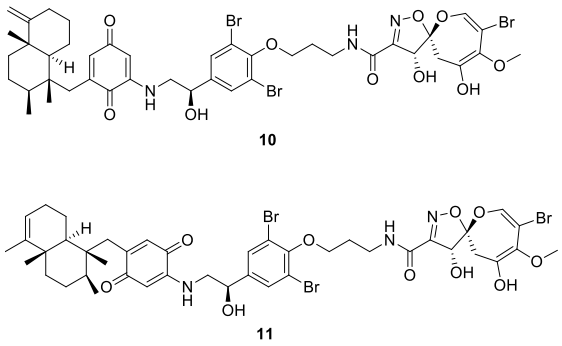

Figure 4. Structures of frondoplysins A (**10**) and B (**11**)

Not only terpenes, but also SMs belonging to other chemical families such as sterols, alkaloids, and brominated compounds have proven to be a valuable resource of PTP1B inhibitors. The marine sterol **12** isolated from the sponge *Xestospongia testudinaria* was identified as PTP1B inhibitor (Figure 5), showing an IC_{50} value of 4.27 μM while the bromodiphenyl ether **13**, isolated from Indonesian marine sponge *Lamellodysidea herbacea* inhibits the same enzyme with an IC_{50} value in the low-micromolar range (0.85 μM) [71,72].

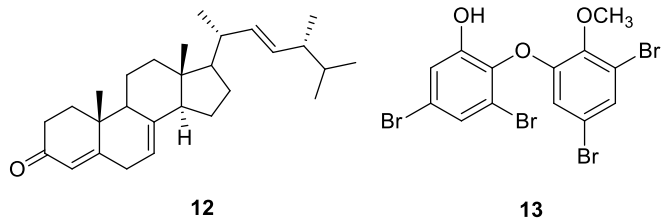

12 **13**

Figure 5. Structures of compounds **12** and **13**.

Few carbolytic enzymes inhibitors have been isolated from marine invertebrates. Examples are schulzeines A-C (**14-16**, Figure 6), isolated from the marine sponge *Penares schulzei*, are three isoquinoline-derived alkaloids characterized by a long fatty acid chain endowed with a trisulphate moiety and were found out as potent α-glucosidase inhibitors with IC_{50} values within 48-170 nM [73].

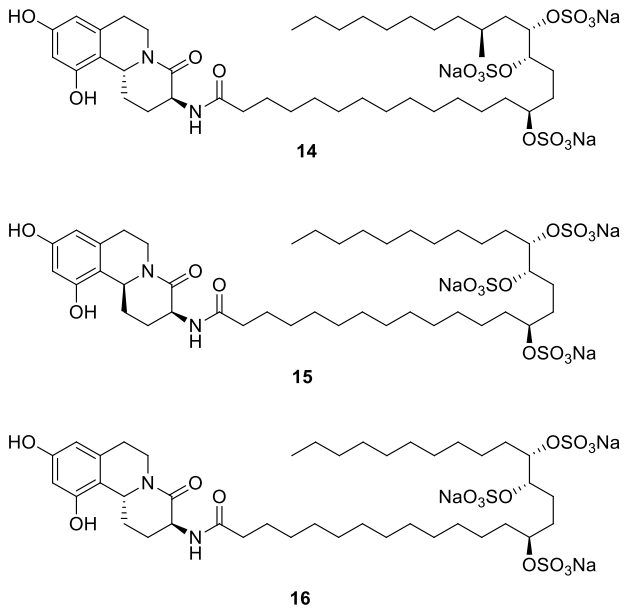

Figure 6. Structures of compounds **14-16**.

Likewise, not many inhibitors of AR were identified from marine invertebrates. The polybrominated diphenyl ether **17** (Figure 7), isolated from the marine sponge Dysidea herbacea, was proved to be an AR inhibitor with an IC_{50} value of 6.4 ± 1.1 μM [74]. Rubrolides are alkaloids characterized by two p-hydroxyphenyl rings linked to a γ-lactone ring isolated from ascidians *Ritterella rubra* and *Synoicum blochmanni*, and, among them, compound **18**, which displayed a chlorine atom in γ-lactone ring, inhibits AR with an IC_{50} of 0.8 μM [75].

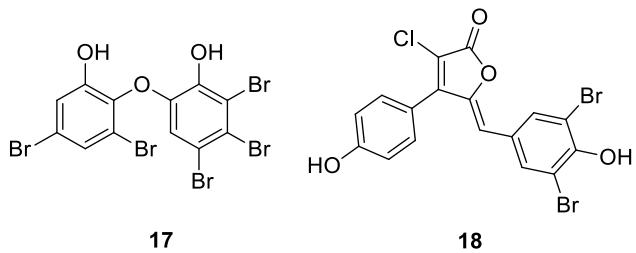

Figure 7. Structures of compounds **17-18**.

For decades, scientific research has been directed in the discovery of new molecules that could act on kinases, so natural marine molecules were initially tested on these targets. These include the aforementioned GSK-3β, which turns out to be inhibited by a class of marine molecules called manzamines. Manzamines are β-carboline alkaloids characterized by a polycyclic complex isolated from the Indonesian marine sponge Acanthostrongylophora sp. and, some of them, were identified as GSK-3β inhibitors. Manzamine A (**19**), 8-hydroxymanzamine A (**20**), 6-hydroxymanzamine A (**21**), and manzamine E (**22**, Figure 8) were found to be inhibitors of the considered enzyme, with IC_{50} values of 10.2, 4.8, 16.6, and 25.0 μM, respectively [76].

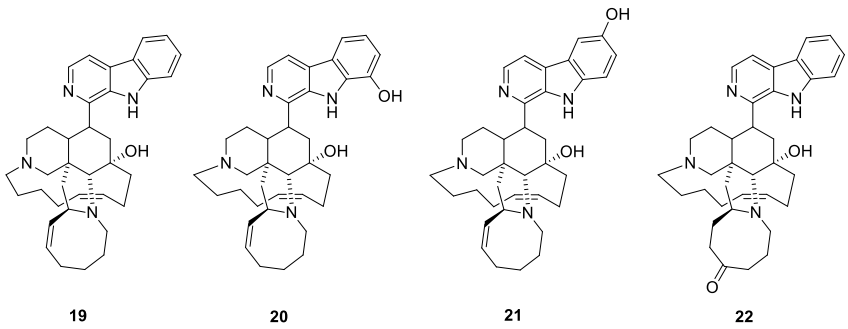

Figure 8. Structures of compounds **19**-**22**.

Among PPARγ inhibitors, some polyketides isolated from Plakortis simplex can be mentioned. Three molecules characterized by furanylidene scaffold (**23**-**26**, Figure 9) were identified as selective PPARγ agonists exerting a 2-fold induction at 50 μM [77]. Since other congeners of these marine NPs were validated as PPAR-γ agonists [78], the furanylidene acetate scaffold can be considered as a possible chemotype to be explored for the development of new potential covalent agonists of PPAR-γ.

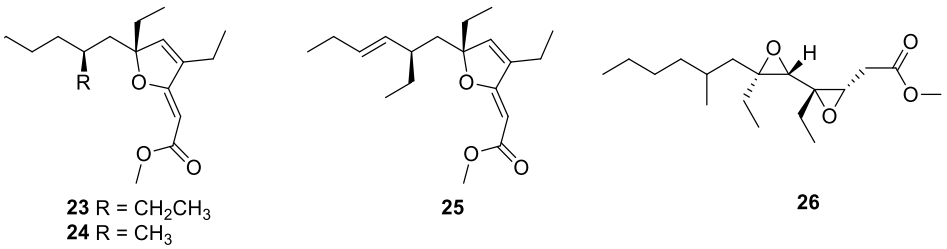

23 R = CH_2CH_3
24 R = CH_3

25

26

Figure 9. Structures of compounds **23-26**.

Only a minimal fraction of molecules mentioned in the review were reported just as an example of how vast the chemical diversity associated with can be and how the pharmacological screening of such different molecules can give information on possible new pharmacophores to be exploited for the development of synthetic drug candidates.

1.3 Identifying new designed multiple ligands in marine resources for the treatment of multifactorial diseases

From the previous paragraph it has been inferred that there are numerous targets that can be modulated for T2DM management, and, in general, interventions on each of them result in increased insulin sensitivity and reduced blood glucose levels. In addition, AR enzyme has also been described, which, along with other targets, promotes T2DM-associated comorbidities that worsen patients' life expectancy. This background of T2DM highlights how the disease is multifactorial in nature. In fact, the current therapeutic strategy involves a single drug in the early stages, that become ineffective in the advanced stages in which, instead, a combination therapy approach is required. The latter approach can be employed through the simultaneous administration of several drugs or the administration of a single pharmaceutical form that contains multiple active ingredients, due

to improve patient compliance [79]. However, combination therapy is not exempt from drawbacks that limit its versatility: the administration of multiple drugs can exacerbate side effects of the individuals due to drug-drug interactions. These considerations are reflected in the drug discovery process as a shift from the more traditional "one drug - one target" model to “multitarget” approach that could be particularly effective for the treatment of T2DM and could overcome the complications of combination therapy [80]. In this strategy, molecules that are capable of modulating two or more selected biological targets are searched for and/or rationally designed [80, 81]. Again, the marine environment aids the drug discovery process in identifying multitarget molecules due to the structural promiscuity that marine NPs are endowed with. In fact, the intrinsic characteristics of NPs that are often multifunctional molecules allow interactions with multiple biological targets. Even though NPs pharmacokinetics properties, efficacy, and specificity on binding to targets do not facilitate their route in drug discovery, these potential hindering challenges could be overcome. The review based on marine invertebrate-derived NPs with antidiabetic properties published during my PhD was also designed as a tool to collect and identify molecules that are active on multiple fronts in the fight against T2DM [67]. Several examples are given below.

Bioprospecting of the Aegean sponge *Dysidea avara* by Casertano et al. led to the isolation of the already known avarone (**27**), its reduced form avarol (**3**), 3-(methylamino)avarone (**28**) and 4-(methylamino)avarone (**29**, Figure 10). Those compounds were funneled into a screening for the identification of dual-type inhibitor of PTP1B and AR enzyme [82].

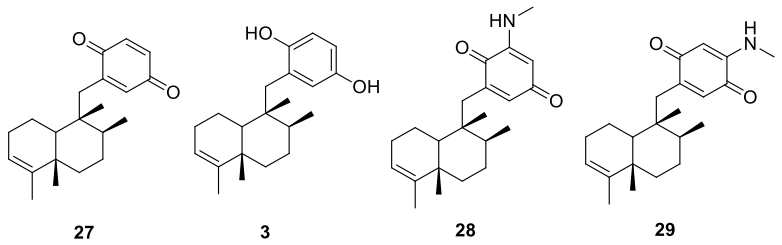

Figure 10. Structures of compound **27**-**29**.

Pharmacological screening on PTPB revealed that avarone (**27**) was the most active compound of the series with an IC_{50} value of 6.7 ± 0.6 μM while 3-(methylamino)avarone (**28**), 4-(methylamino)avarone (**29**) and avarol (**3**) showed IC_{50} values of 15.2 ± 2.1, 21.6 ± 1.0 and 42.2 ± 18 μM, respectively. Further pharmacological investigations on AR of the same compounds highlighed **27** and **3** as strong inhibitor of the enzyme with IC_{50} values of 0.52 ± 0.2 and 0.078 ± 0.02, respectively. The different results reported for avarol is for the different enzymatic assay performed. These results clearly demonstrate the dual inhibitor nature of avarone, whose mechanism of action has been studied: avarone acts as a reversible and competitive inhibitor of PTP1B as and as a non-competitive mixed-type inhibitor of AR, exerting both insulin-mimetic and insulin-sensitizing activity [82]. Moreover, Orhan et al. analyzed in vitro antidiabetic effect of methanol extracts of Dysidea avara which resulted active in the inhibition of α-glucosidase. Therefore, the major compounds of *Dysidea avara*, avarone (**27**) and avarol (**3**), were isolated and tested against α-glucosidase and, notheworthy, they exhibited a strong inhibitory activity of 86.18 ± 1.76% and 78.94 ± 1.38% respectively, at 10 μM [83]. Taken together these results identify the chemotype of avarone, a sesquiterpene quinone characterized by a drimane core, and its reduced analogue, as a

valuable antidiabetic and multitarget scaffold to be further developed through synthetic processes.

Clathriketal (**30**, Figure 11), a tricyclic spiroketal compound isolated from the sponge *Clathria prolifera* showed several interesting antidiabetic properties. Clathriketal is an inhibitor of both α-glucosidase and α-amylase with an IC_{50} value of 0.43 mM and 0.41 mM, respectively. Moreover, this molecule represents the first reported DPP-4 inhibitor from marine invertebrates to date, with the 0.37 mM. The multitarget profile of clathriketal could be useful for simultaneously reducing intestinal glucose absorption and stimulating insulin secretion also highlighting this candidate for further development as multitarget lead [84].

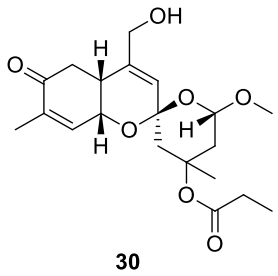

Figure 11. Structure of clathriketal (**30**).

The norterpene cyclic peroxide (−)-muqubilin A (**31**, Figure 12) isolated from the marine sponge *Diacarnus erythraeanus* was validated as a multitarget lead since its capability to activate PPAR-α and PPAR-γ in a low micromolar range (1–10 μM) and also RXRα [85].

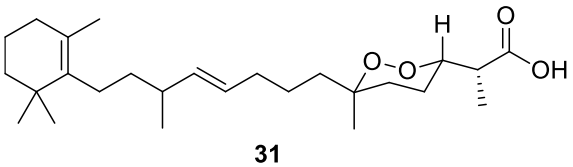

Figure 12. Structure of muqubilin A (**31**).

Hence, marine NPs have arisen as a new and sustainable resource for drug leads to which a high possibility to find new multitarget agents is associated. In this view, marine invertebrates, which are the source of the majority of approved commercial marine-based drugs, offer an excellent opportunity to study diverse and unique compounds endowed with peculiar mechanism of action, not easily accessible from other sources and potentially useful for the treatment of multifactorial diseases such as T2DM and also inflammatory-based diseases [15,86].

CHAPTER 2. Current methodologies for unlocking the potential of marine natural products

2.1 Target-oriented (semi)synthesis (TOS)

As showed in the previous Chapter, marine resources have always been important sources of bioactive molecules, including historical marketed ones, mainly as anticancer drugs. However, such metabolites usually exist in low concentration and, moreover, the supply of marine NPs from nature may also be limited by the difficulties of collecting the organisms/microorganisms and the lack of suitable aquaculture conditions, which could allow the valuable source of these molecules to be bred in laboratories [32,37]. One of the most astonishing strategies to enhance success in marine NPs-drug discovery are the chances offered by synthetic approaches. Probably the most significant contribution of synthetic organic chemistry is the improvement of human health through the production of biologically active compounds and drugs. The development of effective reactions, reagents and techniques, including sustainable and green ones, has enabled the efficient synthesis of an increasing number of natural lead molecules or analogues/derivatives obtained using and/or inspired by a parent NP. As our capabilities have improved, the ability to synthesize complex NPs has also grown, which has become one of the most active areas of a research field at the interface of chemistry and biology [87]. At first, the necessity of these molecules depended entirely on total synthesis; lots of researchers have been involved in the development of new synthetic strategies for the complete chemical synthesis of marine NPs starting from commercially available precursors, also to facilitate the industrial production of the already marketed marine drugs. For example, Ma and co-workers proposed a scalable total synthesis

of Trabectedin (Yondelis®), whose first total synthesis was published by the Corey group in 1996, which consists in 26 steps of reactions starting from a simple building block, Cbz-protected (S)-tyrosine [88]. However, marine NPs are usually difficult to prepare in the laboratory due to their structural complexity; they are often endowed with large and composite structures, with a variety of structural features, most notably the large number of heteroatoms (which often necessitate protecting groups) and stereocenters (which often require difficult stereoselective reactions or separations). It is clear, therefore, that these elaborate synthetic processes are difficult and costly to carry out, and this obviously sometimes prevent an adequate supply to meet the demands for pre-clinical and clinical studies, as well as for industry, thus compromising the marketing of some molecules potentially useful in therapy [87]. Whereas synthetic processes often cannot be applied in the industrial settings, semisynthesis is preferred and involves the use of a structurally richer precursor that allows the number of reaction steps to be cut down. Nevertheless, a semisynthetic process starting from cyanosafracin B, a compound with antibiotic properties obtained by fermentation from the bacteria Pseudomonas fluorescens, has been developed by PharmaMar to synthesise Yondelis in an easier way [42].

Semisynthesis, in addition to being a viable and almost obligatory alternative to total synthesis, can be exploited to chemically manipulate marine metabolites to delineate preliminary structure-activity relationships (SARs) [89]. Therefore, semisyntheses performed by chemical modifications of the already existing functional groups of parent compounds, can generate structural analogues that may have a greater pharmacological activity [90,91]. In this view, for several of the antidiabetic compounds reported in Chapter 1 some modifications to

explore SARs and, eventually, find new and more potent semisynthetic compounds, were carried out by authors.

Sesquiterpene quinones avarol (**3**) and neoavarol (**4**), isolated from *Dysidea sp.* and active against PTP1B, have been subjected to O-acylation and O-methylation of the hydroxy groups on the aromatic system in position 17 and 20 (Figure 13). 17,20-*O*-Diacetylavarol (**32**, IC_{50} = 8.8 μM) and 17,20-O-Diacetylneoavarol (**35**, IC_{50} = 14.0 μM), 17,20-O-dipropionylavarol (**34**, IC_{50} = 8.8 μM) and 17,20-dipropionylneoavarol (**37**, IC_{50} = 9.4 μM) were more active than parents' compound. Pharmacological screening revealed that neoavarol acylated derivatives gained pharmacological activity after derivatization. Furthermore, 20-O-methylation on both avarol and neoavarol gave 20-O-methylavarol (**33**, 0% Inhibition at 25 μM) and 20-O-methylneoavarol (**36**, 50% Inhibition at 31 μM) which were completely inactive [69]. This study suggested that acylation enhances inhibitory activity which resulted higher also increasing carbon chain of acyl group. Those results give more emphasis to the drimane sesquiterpene scaffold as antidiabetic chemotype.

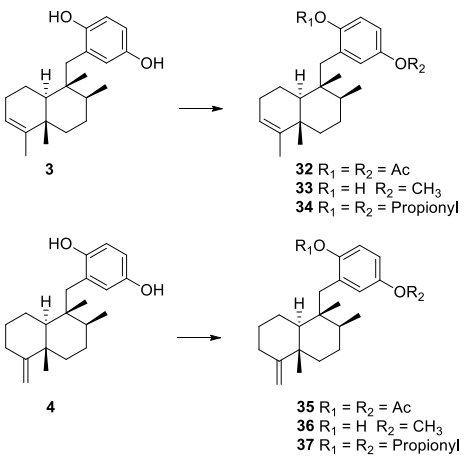

Figure 13. Structures of semisynthetic derivatives of **3** and **4**.

A similar semisynthetic work on the bromodiphenyl ether **12**, isolated from Indonesian marine sponge *Lamellodysidea herbacea*, afforded compound **38**-**42** (Figure 14). The parent compound was identified as PTP1B inhibitor, but its main drawback was cytotoxicity on some human cell lines and, thus, to overcome this issue, modifications of the hydroxy group were performed by Yamazaki and colleagues. Acylated compounds 3,5-dibromo-2-(3',5' -dibromo-2' -methoxyphenoxy)phenyl ethanoate (**39**, IC_{50} = 0.62 μM), 3,5-dibromo-2-(3',5'-dibromo-2'-ethoxyphenoxy)phenyl butanoate (**40**, IC_{50} = 0.68 μM), 3,5-Dibromo-2-(3',5'-dibromo-2'-methoxyphenoxy)phenyl butyrrate (**41**, IC_{50} = 0.69 μM), 3,5-Dibromo-2-(3',5'-dibromo-2'-methoxyphenoxy)phenyl enzoate (**42**, IC_{50} = 0.97 μM) were similar or more potent than natural compound but sill retained cytotoxicity. Indeed, 3,5-dibromo-2-(3',5'-dibromo-2'-ethoxyphenoxy)-1-methoxybenzene (**38**, IC_{50} = 1.7 μM), showed a slightly reduced activity inhibitory against PTP1B but it was proved to be safer for human cells than **12**, confirming that methylation of the hydroxy functionality improves toxicity profile of the parent compound [72].

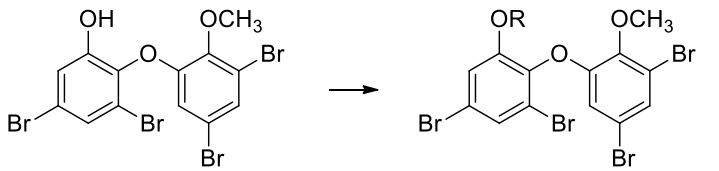

12

38 R = CH3
39 R = Acetyl
40 R = n-Butyryl
41 R = n-Hexanoil
42 R = Benzoyl

Figure 14. Structure of semisynthetic derivatives of compound **12**.

Considering the potential of this polycyclic scaffold for the inhibition of GSK-3β, Hamann and his research developed a library of semisynthetic compounds, using as starting materials both manzamine A and 8-hydroxymanzamine. The effect of polar and heterocyclic substituents on carboline scaffold and modification of the N-heterocyclic system were performed to afford several derivatives. Among them, the hydrogenation of double bond of manzamine A afforded **43** (Figure 15) which showed an IC_{50} of 5.4 μM, higher than its parent compound (IC_{50} = 10.2 μM) [76].

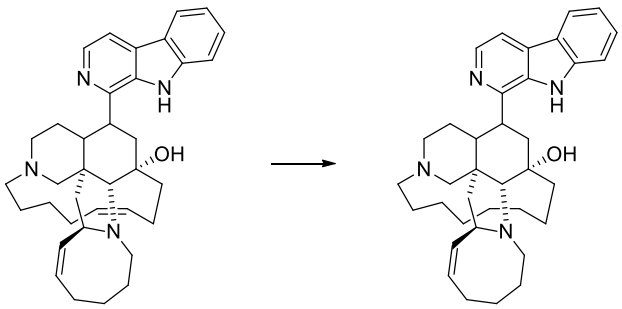

19 **43**

Figure 15. Structures of **19** semisynthetic derivative.

These reported examples highlighted semisynthesis as a validated approach to generate diverse derivatives and analogues, which often outperform their natural counterparts. This method allows precise alterations to the natural scaffolds, unveiling crucial elements responsible of biological effects. Semisynthesis, thus, serves as one of the instruments provided by organic synthesis to elucidate SAR, guiding the creation of optimized derivatives and analogs with enhanced biological properties for drug development. These modified compounds, born of nature diversity and refined by synthesis, yield promising lead compounds. However, it is not always possible to use the semisynthetic approach for obtaining enough of a natural hit of marine origin, even if only to produce analogs

for SAR studies. The applicability of the method depends first on the entire chemical structure of the considered compound but also on its natural availability.

2.2 From the TOS to the Diversity Oriented Synthesis (DOS)

The above-described classic TOS approach in which a single or few compounds of interest are identified and synthesized, although being the oldest and most well-established method, is the least diverse and scalable method. It covers, indeed, only a single or few points (molecules) in chemical space for each synthetic scheme employed. TOS is still a crucial part of the chemist's repertoire when the compound of interest is already known, but it is poorly suited for the discovery of new leads.

The most recent (and currently most promising) attempt to produce large variations (that is, high diversity) in the skeletons of synthetic building blocks is an approach known as diversity-oriented synthesis (DOS). The DOS in a synthetic approach which aims to generate structural diversity in a chemical library covering a bigger chemical space than combinatorial approach. The structural diversity can be achieved in several ways considering the feature to examine in the design of the library: i) building-block diversity, variation in structural moieties around a common skeleton; ii) functional group diversity, variation in the functional groups present; iii) stereochemical diversity, variation in the orientation of potential macromolecule-interacting elements; iv) scaffold diversity, presence of many distinct molecular skeletons [28,29,92]. In this sense, the diversity of chemical libraries should derive from the substitutional, stereochemical or skeletal diversity of its component or also by the combination of these parameters. For example, both building block and functional group diversity can be reached selecting in the properly way the starting material

which should be a polyfunctionalized molecule, which can offer different functional groups that can be transformed through chemoselective reactions, or endowed with a pluripotent functional group which can be converted in several functionalities. The stereochemical diversity can be reached using non-stereoselective reactions which led to the generation of all the possible stereoisomers which should be further separated by chromatographic techniques. Lastly, achieving skeletal diversity necessitates a structural component, named σ-elements, within the scaffold capable of inducing structural rearrangement upon exposure to specific reagents [28,93]. This synthetic approach employes simple building blocks to transform into a diverse set of structurally distinct SMs through further functionalization. These transformations are usually accomplished within five synthetic steps to optimize the efficiency of the entire process. Moreover, synthetic protocols rely on typically high-yielding reactions that usually work effectively with diverse scaffolds and functional groups [93]. DOS libraries are smaller in size compared to combinatorial libraries, but they are endowed with more structural variety exhibiting a wider range of substitution and greater stereochemical variation. Consequently, DOS libraries lead to a more extensive coverage of chemical space which increases possibility to find new lead compounds with new pharmacological activities. In a wider view, DOS approach could be useful to explore the potential of bioactive NPs. In fact, natural metabolites are endowed with peculiar and uncommon scaffold and functional groups which not only cover an enormous chemical space but are also responsible for biological activity. Both terrestrial and marine natural metabolites are considered as *privileged* scaffold since selectively interact with biological systems and macromolecules and, thus, they have been used as inspirational tool for the design of SMs library [94]. Even if the aim of

DOS is to identify new SMs with unveiled pharmacological properties, NPs can inform the design of DOS libraries because of their complex structures which are often characterized by dense substitution and pluripotent functional groups. Moreover, the possibility of discovering new pharmacological properties in the designated SMs remains high thanks to the higher probability in binding structurally similar targets [95].

2.3 Fragment-based drug discovery approach

Fragment-based lead discovery (FBLD), also known as FBDD, is a method used for finding lead compounds where fragments (organic molecules small in size and low in molecular weight) are identified which may bind, also weakly, to the biological target. They be then enlarged, decorated, or combined to produce a lead with a higher affinity. Fragment-based approaches to finding novel bioactive SMs are now firmly established in drug discovery and chemical biology. FBDD can identify relatively simple compounds with low binding affinity due to fewer binding interactions with protein targets. This kind of approach is now firmly established in drug discovery and chemical biology; libraries are based on privileged substructures delineated from known drugs or dugs candidates [26,27]. Particularly, FBDD represent an excellent tool to explore more efficiently the chemical space of NPs, which are endowed as discussed before 3D shapes, sp^3 carbons, and stereocenters richness. These features, while improving the success in drug discovery because flat scaffolds are often associated with adverse biological properties or unfavorable pharmacokinetic profiles [96] pose more demanding challenges for the generation of a wide chemical diversity. In FBDD efforts are being made to include these features into fragment screening libraries, therefore the exploration of biologically relevant chemical space

is rendered more tractable by focusing on fragment-like chemical and providing simpler starting points for subsequent chemical optimization of initial hits [19]. To date, several approaches have been implemented for mapping and navigating into the chemical space offered by nature to explore its different aspects. The approaches providing novel opportunities to synthesize NP-inspired compound libraries involve NP-based fragments, typically small and not complex molecule between 150 and 300 Daltons in size characterized by few functional groups that can be properly transformed for growing bioactive fragments and promoting hit to lead processes [31]. As already mentioned, this approach allows access to areas of chemical space that are less explored from combinatorial chemistry, and consequently help to exploit the use of NPs in drug discovery. In fact, the main limitations in the use of unaltered natural compounds in drug discovery attributable to lack of accessibility and in synthetic intractability. In this context, synthetic tractability is enhanced by the small size and reduced complexity of fragments compared to synthetic challenges to produce larger NPs [31]. Different strategies have been described in literature to develop fragment-based libraries either using NPs or natural product-like compounds for using fragments derived from NPs: i) Fragment-sized NPs, which consist in filtering fragment-sized NPs from an NP library, and with this collection of compounds, chemical modifications or designing of fully synthetic new compounds can be initiated; ii) *in silico* fragmentation, in which fragments are generated in silico from a defined collection of compounds, which will be obtained synthetically or from a commercial library; iii) chemical disassembly of large NPs, in which NPs are chemically manipulated though cleavage reactions for obtaining fragments directly from the structure of the NPs; iv) design of "pseudo NPs", in which NPs are rationally deconstructed into

fragment-like SMs with the objective to identify compounds which resemble portions of considered NPs. In conclusion, fragment-based approach provides many methods to take advantage of NPs chemical diversity, such as chemical disassembly, chemical modifications of low MW NPs, synthesis based on scaffolds occurring in NPs [97].

2.4 Methods for assigning absolute configuration in natural and synthetic small molecules

Despite the above exposed methods aimed at simplifying the complex structures provided by nature, the challenge of determining the absolute configuration trouble both the structural characterization of NPs and synthetic molecules, but to different degrees. The disassembly of NPs also aims at reducing the number of chiral centers, which is often immense, but the need to have efficient and expeditious methods for assigning absolute stereochemistry to fragments remains critical. In fact, all possible stereoisomers of considered fragments are often required to increase stereochemical variability.

The absolute stereochemistry of a chiral organic compound influences its various chemical, physical biological and pharmaceutical properties. Indeed, the need to obtain enantiomerically pure pharmaceuticals and chemicals has increased interest in developing methods for determining the absolute stereochemistry of compounds [98]. X-ray crystallography represents the instrumental method par excellence in the determination of absolute stereochemistry. This technique involves analyzing the diffraction pattern of X-rays passing through a crystal of the considered molecule and provides precise information about the spatial arrangement of atoms determining absolute configuration accurately. However, the use of this method got some limitations related to the specific and expensive

equipment required. Another prominent limitation of X-ray crystallography is its dependence on crystallization. In fact, not all molecules can crystallize easily, or the process could generate inadequate amounts of crystals or poor-quality crystals for conducting an accurate analysis. Moreover, the conditions required for crystallization might force the molecule to adopt a slightly different conformation than its natural state, leading to discrepancies in absolute configuration determination [99]. To address these limitations, organic chemists often prefer other techniques such as chiroptical methods, nuclear magnetic resonance (NMR) spectroscopy, or computational modeling to X-ray crystallography. More recent and innovative approaches are precisely based on the use of NMR spectroscopy. This technique has several advantages, including available spectrometers in most laboratories, small amounts of sample are required, that can then be recovered since the analysis is often conducted in solution. Moreover, this kind of approach could be employed for both liquid and solid samples [100,101]. In general, the application of the NMR-based method can be performed in two different ways, the first of which involves the analysis of the substrate without derivatization, while the second involves the derivatization of the molecule under consideration by reaction with a chiral derivatizing agent (CDA). Through the first approach, the substrate is analyzed in a chiral environment achieved using a chiral solvent or the addition of a chiral solvating agent (CSA) to a standard non-chiral NMR solvent. This approach does not involve the formation of a covalent bond between the substrate and the chiral reagent and, this apparent advantage, is actually the main limitation of the method since no relevant differences could be observed between the chemical shift values of the two enantiomers and, therefore, the two NMR spectra are almost identical. Therefore, the use of

this method is limited to the determination of enantiomeric purity [100–102].

Thus, in determining the absolute configuration of a chiral organic compound, the second approach is mainly used. In fact, the covalent bonding formed between substrate and auxiliary reagent allows the formation of diastereoisomeric derivatives with a suitable conformational rigidity responsible for significant differences in chemical shift values found in different NMR spectra. This method, therefore, requires substrate derivatization for which two options are possible: i) preparation of two derivatives, from the substrate, in the presence of two enantiomers of CDA (double derivatization); ii) preparation of one derivative, starting from the substrate and in the presence of only one enantiomer of CDA (single derivatization) [101,103,104]. In the first case, the ^{1}H NMR spectra of the two diastereoisomers obtained are compared; in the second case, a single spectrum is recorded that can be compared with the spectrum of the same derivative recorded at a lower temperature or with the spectrum of the same derivative following the formation of a complex with a metal salt or with the spectrum of the substrate without derivatization. Therefore, whichever procedure is chosen, two spectra must be obtained and compared. In fact, the assignment of the absolute configuration is based on the analysis of the differences in the chemical shifts ($\Delta\delta$) of the substituents of the asymmetric carbon in the two obtained spectra related to the two derivatives or conformational species. To this end, the auxiliary chiral reagents used have a polar or bulky group, a functional group responsible of the covalent bond with the substrate and a group responsible for the anisotropic effect which selectively influences the chemical shifts of substrate substituents ensuring that the obtained spectra for the two derivatives are different. Chiral auxiliary agents are chosen by considering

the functional groups present on the asymmetric carbon of the molecule to be derivatized. For example, α-methoxyphenylacetic acid (MPA), 9-anthrylmethoxyacetic acid (9-AMA) and methoxytrifluorphenylacetic acid (MTPA, Figure 16) are usually chosen for chiral centers endowed with hydroxy group.

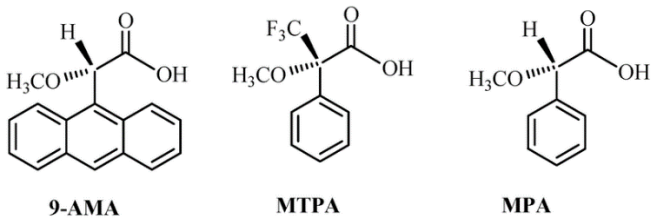

Figure 16. Structures of CDAs for hydroxy group.

In the case of molecules in which only one chiral center is present, two samples of the same molecule are derivatized with one enantiomer of the chiral auxiliary agent and then the other, respectively, to obtain a pair of diasteroisomers. Finally, the ^{1}H NMR spectra of the two obtained molecules will be recorded and the chemical shift values for each hydrogen atom will be compared [100,101,103,105].

The method proposed by Mosher, for example, for the assignment of the configuration of secondary alcohols provides the derivatization of the hydroxy group with both (R)- and (S)-MTPA. This approach is based on the anisotropic effect that the phenyl group of the chiral auxiliary MTPA exerts on the substituents of the secondary aliphatic alcohol. This effect allows a correlation to be made, regarding the spatial position of substituents around the chiral centers, with respect to the phenyl group of the MTPA moiety on the basis of the signs of $\Delta\delta^{SR}$ of the substituents [106]. Therefore, it is possible, for all derivatization methods, correlate the $\Delta\delta$ distribution around the chiral center to an appropriate empiric model which allow to assign the absolute configuration. In the field of the

identification of new marine NPs, organic chemists often have to deal with the determination of the absolute configuration of complex structures endowed with several chiral centers which usually requires a combination of the already described methods.

CHAPTER 3. The phosphoeleganin, a promising antidiabetic and anti-inflammatory lead of marine origin

3.1 An overview on the antidiabetic properties of a phosphorylated metabolite isolated from *Sidnyum elegans*

Polyketides represent a large family of complex natural compounds derived from simple carboxylic acid-derived residues. Widespread in both terrestrial and marine environment, marine polyketides are usually equipped with polyhydroxy and polyoxy substituents in their structures. Phosphoeleganin (**44**, Figure 17) is a linear polyketide composed by a glycine head and a long carbon chain with hydroxy groups and an uncommon phosphate moiety. This compound was isolated from prof. Menna research group afterwards the chemical investigation of the Mediterranean ascidian *Sidnyum elegans* trough a finely standardized isolation protocol [107,108].

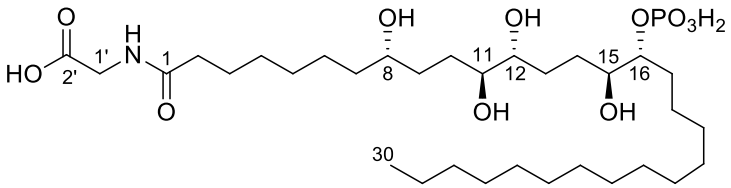

44

Figure 17. Structure of phosphoeleganin (**44**).

Despite the complexity of the planar structure of this metabolite, the most compelling challenge was determining the absolute configuration of the five stereogenic centers which required the combination of several approaches such as chemical degradation of the NPs and synthesis of model molecules for applying UDB Kishi concept [108].

In the view of identifying new multitarget lead for fighting multifactorial diseases, phosphoeleganin (**44**) underwent an extensive pharmacological characterization which revealed the antidiabetic potential of the polyketide. Firstly, in vitro assays were performed highlighting **44** as a dual-type inhibitor of PTP1B and AR with IC_{50} values of 1.3 ± 0.1 μM and 28.7 ± 1.1 μM, respectively. Furthermore, dilution assays demonstrated that **44** acts as a reversible inhibitor of both enzymes [109]. Kinetic studies validated that phosphoeleganin (**44**) acts as a pure non-competitive inhibitor of PTP1B since the analysis of the Lineweaver–Burk plot, indicated that only V_{max} is affected by the presence of the inhibitor (Figure 18) [109].

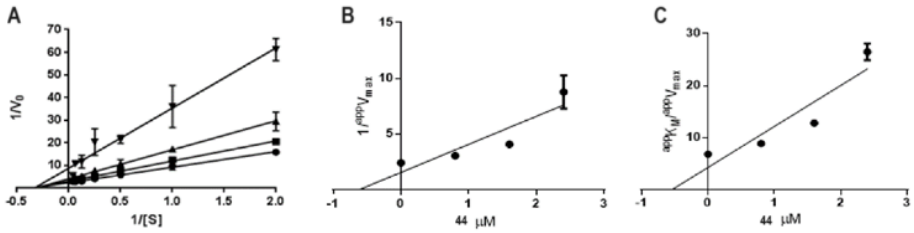

Figure 18. Kinetic characterisation of **44** as a PTP1B inhibitor. (A) PTP1B activity (8 mU) at the indicated *p*-NPP concentrations in the presence of PE at concentrations: 0 (●), 0.8 (■), 1.6 (▲), and 2.4 μM (▼). Data are reported as a Lineweaver–Burk plot. Bars (when not visible, are within the symbols' size) represent the standard deviations of the means from at least three independent measurements. (B) and (C) Secondary plots of the ordinate intercepts ($1/^{app}V_{max}$) and of the slopes ($^{app}K_M/^{app}V_{max}$), respectively, of the primary plot as a function of **44** concentration. Bars (when not visible, are within the symbols' size) represent the standard error of the ordinate intercepts and of the slopes obtained from the data of Panel A.

Moreover, **44** behaves as a mixed inhibitor of AR, being able to affect both V_{max} and K_M (Figure 19). The analysis of the dependence of $appV_{max}$ and $appK_M/appV_{max}$ on the inhibitor concentration allowed the measurement of

K'_i and K_i (Figure 19) whose values indicate the preference of 44 in binding the ES complex instead of the free enzyme [109].

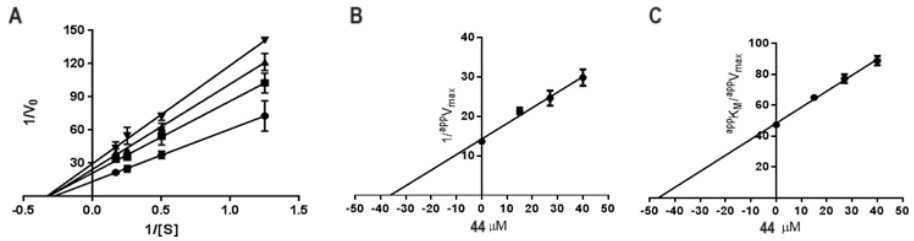

Figure 19. Kinetic characterisation of **44** as an AR inhibitor. Panel (A) AR activity (10 mU) at the indicated L-idose concentrations in the presence of PE at concentrations: 0 (●), 15 (■), 27 (▲), and 40 µM (▼). Data are reported as a Lineweaver–Burk plot. Bars (when not visible, are within the symbols' size) represent the standard deviations of the means from at least three independent measurements. Panels (B) and (C) Secondary plots of the ordinate intercepts ($1/^{app}V_{max}$) and of the slopes ($^{app}K_M/^{app}V_{max}$), respectively, of the primary plot as a function of **44** concentration. Bars (when not visible, are within the symbols' size) represent the standard error of the ordinate intercepts and of the slopes obtained from the data of Panel A.

The dual mechanism of action was further confirmed through *in silico* docking studies that supported the kinetic analyses [109].

Further pharmacological studies involved in vitro assays to study the impact of this natural product on the insulin pathway and confirm antidiabetic effects on cells. Tests on liver cells HepG2 (Figure 20) revealed that phosphoeleganin (**44**) possesses insulin-sensitizing properties: after treatment with the natural compound, phosphorylation levels of the insulin receptor (IR) and protein kinase Akt, a second messenger of the insulin pathway, increased in hormone-stimulated cells, but not in unstimulated cells. In fact, liver cells treated with **44** alone

showed similar phosphorylation levels of both IR and Akt to those evaluated in control cells, confirming that phosphoeleganin (**44**) does not behave as an insulin-mimetic agent [109].

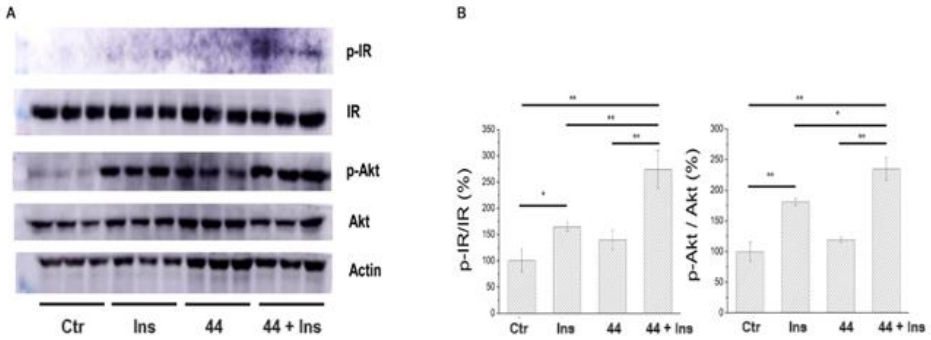

Figure 20. Effect of **44** on the insulin signalling pathway. Panel A: Western blot image; Panel B: quantitation of Western blot carried out using Kodak MI software. Data shown were normalized with respect to the control sample. All tests were carried out in triplicate. Statistical analysis was repeated using ANOVA, followed by Tukey HSD. Data were checked for appropriate normality and homoscedasticity using the Shapiro–Wilk normality test and the Levene's test, respectively. Ctr: control experiment; Ins: cells treated with 10 nM insulin; **44**: cells treated with compound **44** (25 μM); * $p < 0.05$; ** $p < 0.01$.

Moreover, although it has a charged phosphate group, **44** can pass through the plasma membrane and move into the cytoplasm of cells where it inhibits PTP1B, enhancing the insulin signaling pathway. This extended study for the evaluation of the antidiabetic activity of phosphoeleganin (**44**) highlighted the natural metabolite as a dual inhibitor of the PTP1B and AR enzymes, gaining the qualification of the first multitarget antidiabetic lead compound belonging to the family of marine polyketides. Furthermore, it represents the first polyketide-like inhibitor of characterized by a phosphate group. These promising results paved the way to exploit this marine NP as a starting point for the design of a SM

library of both semisynthetic and synthetic molecules to obtain new multitarget drugs capable of overcoming insulin resistance and counteracting the onset of associated complications. To investigate preliminary SARs about **44**, the derivatives **45** and **46** (Figure 21), obtained via oxidative cleavage of the 1,2-*anti* diol system of **44** respecting the overmentioned principle of TOS, were screened against PTP1B and AR enzymes. Interestingly, only **46** showed activity as a reversible mixed-type noncompetitive inhibitor of PTP1B, losing the AR inhibition effect while fragment **45** was inactive on both enzymes. Contrary to the parent compound, compared with which it has a higher IC_{50} value of 6.7 ± 3.3 μM, compound **46** acts as an insulin mimetic agent in murine myoblast C2C12 cells [110].

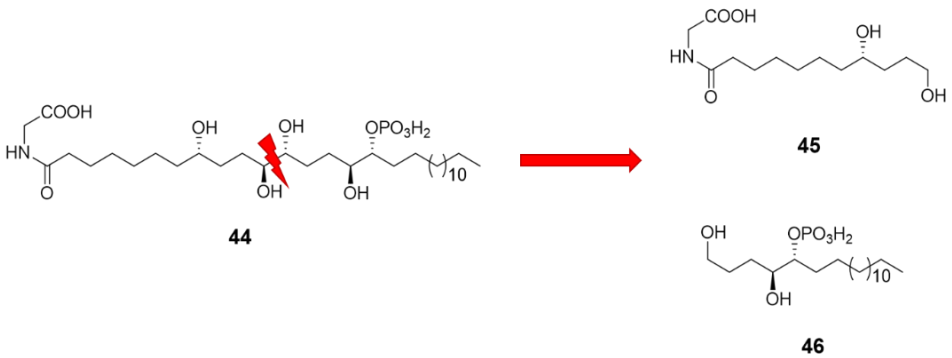

Figure 21. Disassembling of phopshoeleganin (**44**) through TOS approach.

In this view, the synergistic inhibition of PTP1B and AR enzymes would increase insulin sensitivity, thereby decreasing blood glucose levels, and reduce all predisposing factors for the development of diabetes-associated comorbidities. Hence, phosphoeleganin (**44**) and its two degradation fragments **45** and **46** (Figure 21) have been further investigated to in-depth evaluate their insulin sensitizing effect in liver cells for ameliorating

hepatic insulin resistance associated with other diseases besides diabetes such as NAFLD and MAFLD.

3.2 Fighting hepatic insulin resistance for the treatment of NAFLD/MAFLD

Non-alcoholic Fatty Liver Disease (NAFLD) is defined as a chronic liver disease that promotes excessive fat accumulation in liver cells (presence of steatosis in >5% of hepatocytes) in absence of clear pathological causes (excessive alcohol consumption, hepatotoxic medications, toxins, viral infections, genetic diseases). Therefore, the definition of this pathological condition is an exclusion diagnosis [111,112]. NAFLD stands as one of the prevalent causes of chronic liver conditions worldwide and affects about 44% of the adult population, with a prevalence that that can significantly fluctuate across regions, influenced by various factors such as lifestyle, dietary habits, and genetic predisposition. In Western countries, NAFLD impacts about a third of adults and 12% of children [113]. NAFLD includes a spectrum of liver conditions ranging from simple fatty liver (steatosis), where fat accumulates in the liver cells, to a more severe form known as non-alcoholic steatohepatitis (NASH). NASH involves liver inflammation and may progress to fibrosis, cirrhosis, and, in worst cases, liver cancer [114,115]. In 2020, a global panel of experts suggested to update NAFLD as Metabolic Dysfunction–Associated Fatty Liver Disease (MAFLD). The shift in terminology reflects a fundamental change in the clinical basis and diagnostic criteria of the disease. In fact, MAFLD definition expand diagnostic criteria by considering metabolic risk factors such as obesity, insulin resistance, T2DM, dyslipidemia, or other markers of metabolic dysfunction [116,117]. In this view, NAFLD has been reported in over 76% of patients affected by T2DM and in over

90% of severely obese patients undergoing bariatric surgery [118,119]. Insulin resistance resulted as the pathophysiological hallmark not only of T2DM but also of NAFLD/MAFLD, further emphasizing the link between the two diseases [120,121]. Unhealthy lifestyle and dietary habits, characterized by high carbohydrate and lipid intake, together with aging and genetic predisposition, are considered the main causes that promote the development of insulin resistance [52,122]. In a broader view, predisposing factors for NAFLD/MAFLD and for T2DM fall under the metabolic syndrome, which is precisely characterized by insulin resistance, dyslipidemia, abdominal obesity, hypertension, and other predisposing factors for the development of various metabolic-based diseases [123,124]. On this basis, NAFLD/MAFLD are now recognized as the hepatic manifestations of the metabolic syndrome chronic inflammation and, in some cases, could be considered as T2DM comorbidities [125]. Regarding the current therapeutic strategies for managing NAFLD/MAFLD conditions, lifestyle changings represent the cornerstone of non-drug approach. Physical activity and correct dietary style characterized by low refined sugars, saturated fats, and processed foods are fundamental not only for weight management but also for insulin resistance. In this sense, the use of drugs for fighting insulin resistance, dyslipidemia, or inflammation are under investigation for their potential efficacy in treating NAFLD/MALFD since official approved drugs for their treatment were not identified [126,127]. Moreover, addressing associated conditions, such as T2DM, could be critical in the management of NAFLD/MAFLD. In this regard, since insulin resistance is a predisposing factor of both T2DM and NAFLD/MAFLD, molecules capable to counteract this mechanism could be used for liver diseases. As already described in Chapter 1, insulin resistance induces hyperglycemia

due to the altered production of insulin or the inability of insulin-dependent cells, such as hepatocytes, myocytes, and adipocytes, to properly respond to the hormone. In liver, once secreted by pancreatic β-cells, insulin binds to its receptor and induces complex signaling cascades through its substrates (IRSs). Insulin, upon binding to its receptor, triggers the activation of the PI3K/AKT pathway, stimulating hepatic metabolic functions like glycogen synthesis and inhibiting gluconeogenesis, and ERK1/2 pathway, promoting cell growth and differentiation [128]. Despite the benefits provided by some drugs used for the treatment of T2DM, they are far from being able to provide valuable support for the management of NAFLD, for which a combination of drugs as well as a healthy lifestyle is often required [129]. Thus, deeper insights into molecular mechanisms enhancing insulin sensitivity and ameliorating inflammatory responses in the liver are imperative, also to facilitate the discovery of new SMs that could counteract metabolic risk factors. Once again, the sea comes in response to human needs. Noteworthy, omega-3 polyunsaturated fatty acids from marine origins are often used to prevent hepatic steatosis bearing anti-inflammatory action and ameliorating hyperlipidemia [130]. On these bases, identifying new SMs that can control insulin sensitivity and mitigate inflammatory responses in liver cells from marine resources could be useful for developing new therapeutic agents for liver diseases.

3.3 Isolation of phosphoeleganin (44) and oxidative cleavage for the synthesis of 45 and 46

In Chapter 1, molecules endowed with antidiabetic properties were described, and, among them, PTP1B inhibitors were the most abundant [67]. Since the effect of PTP1B inhibition for managing insulin resistance

is already clear [65,131] and considering the pro-inflammatory activity of AR [66,132] phosphoeleganin (**44**) was selected as promising candidates to further in-depth investigation for the treatment of hepatic insulin resistance in NAFLD/MAFLD. Furthermore, the already performed pharmacological studies on HepH2 cells about the effect on insulin pathway that highlighted **44** as an insulin-sensitizing agent paved the way for the next in-depth study. This work was finally facilitated by the possibility to easily reisolate natural product from frozen samples in our laboratories using finely refined and standardized isolation protocols. In addition, spectroscopic characterization was facilitated by comparison of experimentally obtained data with those already reported in the literature. Phosphoeleganin (**44**) was re-isolated following exhaustive extraction and purification procedures of specimens of *S. elegans* available in our laboratories, whose identification and collection were performed by Mr. Arturo Facente, and a voucher of this ascidian is deposited at Department of Pharmacy, University of Naples Federico II, Napoli, Italy. The extraction was performed according to our already reported protocol [107,109] affording three organic extracts with different polarity grade, butanol, ethyl acetate, and water extracts. The butanol soluble material underwent chromatographic separation by MPLC on reversed phase silica gel (C18) using an increasing gradient elution: H_2O/MeOH 9:1 → H_2O/MeOH 7:3 → H_2O/MeOH 1:1 → H_2O/MeOH 3:7 → MeOH 100% → MeOH/$CHCl_3$ 7:3 → MeOH/$CHCl_3$ 1:1 → $CHCl_3$ 100%. Preliminary ^{1}H NMR analysis of the obtained fractions suggested that **44** was the main constituent of the fraction eluted with H_2O/MeOH 3:7 (v/v), according to the literature data. Thus, this fraction was further chromatographed by RP-HPLC on a Synergy RP-MAX 4μm column with H_2O/MeOH 2:8 plus 0.1% of trifluoroacetic acid as mobile phase, yielding **44** (t_R= 20.2 min,

41.6 mg) in a pure state. The identity of PE was confirmed by comparing its NMR and HR-ESIMS data with the reported literature [107].

Then, a sample of phosphoeleganin (**44**), was subjected to an oxidative cleavage following the already used protocol (Scheme 1)[108]. Phosphoeleganin was dissolved in 0.012 M NaIO4 aqueous solution and stirred at room temperature for 3 h. Then the reaction mixture was cooled to 0 °C and an excess amount of $NaBH_4$ was added. The reaction was kept in this condition for 1 h and, after this time, the mixture was partitioned between water and butanol. The butanol soluble material was purified by reverse phase HPLC (Luna C18 3 μm, MeOH/H_2O 8:2 0.1% TFA, 0.5 mL/min) yielding compounds **45** and **46** in pure form. The structural characterization was simplified comparing the experimental spectroscopic data with those reported in literature [108].

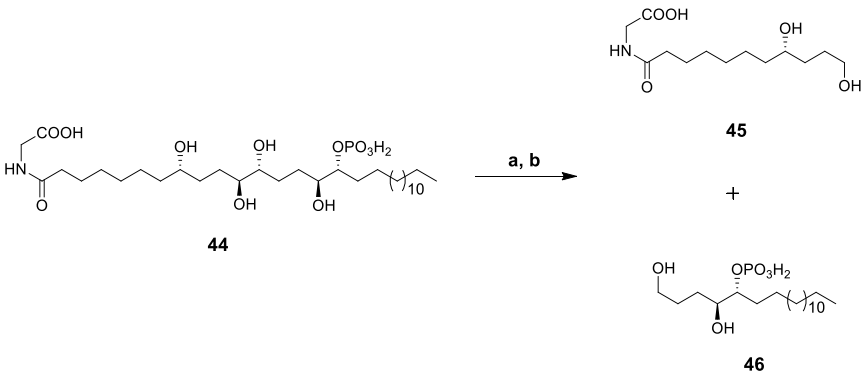

Scheme 1. Reagents and conditions: (**a**) $NaIO_4$, MeOH, rt, 3h. (**b**) NaBH4, 0°C, 1.5 h.

3.4 Pharmacological studies on 44-46

In previous reported experiments the effect on the insulin pathway of the natural metabolite was carried out on HepG2 cells, and, thus, further pharmacological investigations on the same cell line were carried to

expand the knowledge about the role of phosphoeleganin (**44**) and its semisynthetic fragments on hepatic insulin signaling. These in-depth studies have been performed thanks to the active collaboration with prof. Francesco Oriente research group of the university of Naples Federico II. In particular, HepG2 cells were treated with **44**, **45** and **46** (25μM) in presence or absence of insulin. As shown in Figure 22, insulin receptor tyrosine phosphorylation (pINSR) did not significantly change in presence of the marine-derived compounds, while **44** and **45** improve the effect of insulin increasing insulin receptor tyrosine phosphorylation by 10- and 8-fold, respectively. Similarly, treatment of HepG2 cells with **44** and its derivatives did not significantly affect the amount of phosphorylated Akt while an increase of 8.1- and 6.6-fold about Akt phosphorylation could be observed for the treatment with **44** and **45** in presence of insulin, respectively. Contrary to the previous assays, **44** and its derivates did not ameliorate the insulin effect on the ERK1/2 phosphorylation. Total levels of insulin receptor, Akt and ERK1/2 did not change in presence of insulin, **45** or **46** suggesting that these compounds did not act as gene promoters. Finally, the improvement of phosphorylation mediated by **44** and **45** on insulin- stimulated insulin receptor and Akt was statistically significant compared to treatment with insulin alone. These results confirm that phosphoeleganin (**44**) behaves as an insulin-sensitizing agent in Hepg2 cells by positively impacting the phosphorylation levels of insulin receptor and Akt kinase but not ERK1/2 protein. Unexpectedly, the fragment lacking the phosphate group also shows the same activity as the parent compound on the same cell line, thus proving to be an insulin-sensitizing agent with a different mechanism than **44** since it does not affect PTP1B activity.

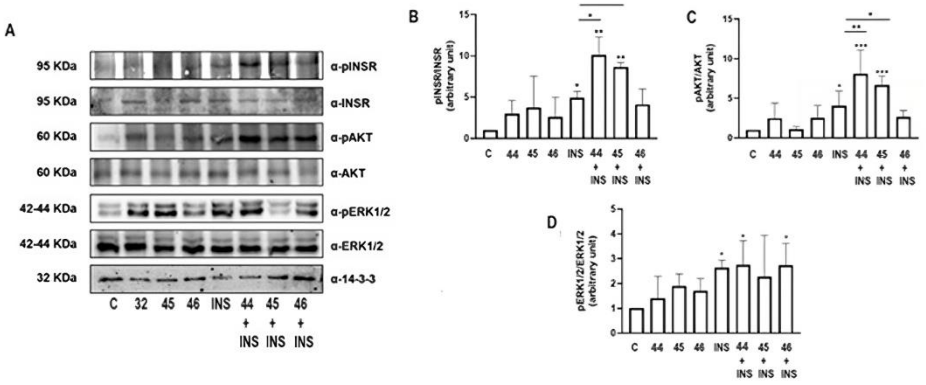

Figure 22. Western-blot on **44**-**46** (A) and effect of **44**, **45** and **46** on insulin receptor (B), AKT (C) and ERK1/2 (D) phosphorylation. HepG2 cells were incubated with **44**, **45**, and **46** (20μM) for 4 hours and then stimulated with insulin (100nM) for 10 minutes. Proteins were separated by SDS-PAGE and blotted with antibodies anti phosphorylated insulin receptor, phosphorylated AKT and phosphorylated ERK1/2. The same filters were blotted with insulin receptor, AKT, ERK1/2 antibodies. 14-3-3 antibody was used for normalization. Bars represent the mean ± SD of three independent experiments. Asterisks denote statistical differences (*$p<0.05$; **$p<0.01$; ***$p<0.001$).

The impact of the marine-derived compounds on gluconeogenesis process was explored by measuring the expression of one of the principal gluconeogenic enzyme, phosphoenolpyruvate carboxykinase. Compounds **44**-**46** alone did not affect phosphoenolpyruvate carboxykinase mRNA levels, as reported in Figure 23A, while, when combined with insulin, compound **45** showed to slightly improve the hormone effect decreasing the levels of the gluconeogenic enzyme by 87%. Investigations continued by focusing on the evaluation of glycogen content in liver cells after the treatment of marine derived compounds alone and in the presence of insulin. The results obtained corroborate with the crucial role of compound **45** in the hepatic insulin pathway since it considerably increased the effect

of insulin in stimulating glycogen synthesis (Figure 23B). Finally, the additive effects of fragment **45** on phosphoenolpyruvate carboxykinase mRNA levels and glycogen content were statistically relevant compared to treatment with insulin alone. Furthermore, these obtained results confirmed that the natural compound **44** exerts the insulin-sensitizing effect via PTP1B inhibition, the mechanism thanks to which fragment **45** exerts its effects in improving hepatic insulin sensitivity has been explored though other experiments.

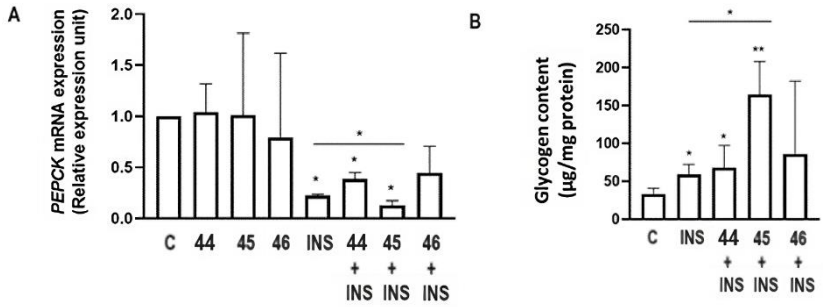

Figure 23. Effect of **44**, **45** and **46** on phosphoenolpyruvate carboxykinase expression and glycogen content. (**A**) HepG2 cells were incubated with **44**, **45** and **46** (20µM) and insulin (100nM) for 4 hours. phosphoenolpyruvate carboxykinase mRNA levels were evaluated by real-time RT-PCR analysis. Data were normalized by the amount of *beta-ACTIN*, used as internal control. Bars represent the mean ± SD of three independent experiments, each performed in triplicate. (**B**) HepG2 cells were incubated with **44**, **45** and **46** (20µM) and insulin (100nM) for 6 hours. Glycogen content was measured as described in methods. Asterisks denote statistical differences (*p<0.05; **p<0.01).

To identify the mechanism by which compound **45** exerts the insulin-sensitizing effect, considering its inability to inhibit the PTP1B enzyme [110], further pharmacological assays will be conducted by investigating

the connection that exists between hepatic insulin resistance and inflammatory processes.

3.5 Materials and method

3.5.1 Isolation of phosphoeleganin (44)

Specimens of *S. elegans* collected at Pozzuoli (Naples, Italy, April 2019) were available in Department of Pharmacy, University of Naples Federico II. They were frozen immediately after collection and kept frozen until extraction. A fresh thawed sample (23.1 g of dry weight after extraction) were extracted according to a previously reported procedure [33]. The butanol soluble material (492.8 mg) was chromatographed by MPLC over a C18 column following a gradient elution $H_2O \rightarrow MeOH \rightarrow CHCl_3$. The fraction eluted with MeOH/H_2O 7:3 (v/v) was further purified by HPLC on reversed phase (column Synergi RP-MAX 4 μm 250 mm x 4.6 mm, MeOH/H_2O 8:2 + 0.1% of TFA) and afforded compound **44** (tR = 20.5 min, 42.1 mg) in pure form as a colourless oil. All data agree with those reported in the literature [108].

3.5.2 Semisynthesis of compounds 45 and 46

Compounds **45** and **46** were obtained by carrying out the procedure that is reported in our previous work [REF]. Phosphoeleganin (10 mg) was dissolved in 1.5 mL of 0.012 M $NaIO_4$ aqueous solution and stirred at room temperature for 3 h. Then the reaction solution was cooled to 0°C, an excess amount of $NaBH_4$ (5 mg) was added and kept in this condition for 1 h. The reaction solution was partitioned between water and butanol. The butanol extract was separated by reverse phase HPLC (Luna C18 3 μm, MeOH/H_2O 8:2 0.1% TFA, 0.5 mL/min) yielding compounds **45** and **46** in pure form.

Compound **45** ^{1}H NMR (700 MHz, CD_3OD): δ 2.25 (*t*, 7.6, H-2), 1.64 (overlapped, 2H, H-3), 1.36, (overlapped, 2H, H-4), 1.34 (overlapped, 2H, H-5), 1.34 (overlapped, 2H, H-6), 1.46 (overlapped, 1H, H-7a), 1.41 (overlapped, 1H, H-7b), 3.54 (m, 1H, H-8), 1.54 (overlapped, 1H, H-9a), 1.40 (overlapped, 1H, H-9b), 1.67 (overlapped, 1H, H-10a), 1.56 (overlapped, 1H, H-10b), 3.56 (overlapped, 1H, H-11), 3.92 (s, 2H, H-2'). HRESIMS *m/z* 274.1644 $[M-H]^-$ (calcd. for $C_{13}H_{24}NO_5$ 274.1649). ^{1}H NMR and HR-ESIMS spectrum are reported in Chapter 7.

Compund **46** ^{1}H NMR (700 MHz, CD_3OD): δ 3.58 (m, 2H, H-1), 1.78 (m, 1H H-2a), 1.56 (overlapped, 1H H-2b), 1.65 (overlapped, 1H, H-3a), 1.47 (overlapped, 1H, H-3b), 3.68, (dt,9.4, 3.0, 3.0, 1H, H4), 4.16 (m, 1H, H-5), 1.65 (overlapped, 1H, H-6a), 1.55 (overlapped, 1H, H-6b), 1.55 (overlapped, 1H, H-7a), 1.39 (overlapped, 1H, H-7b), 1.29 (overlapped, 2H, H-8/H-17), 1.28 (overlapped, 2H, H-18), 1.31 (overlapped, 2H, H-19), 0.89 (t,7.6, 3H, H-20); HRESIMS *m/z* 395.2578 $[M-H]^-$ (calcd. for $C_{19}H_{40}O_6P$ 395.2557). ^{1}H NMR and HR-ESIMS spectrum are reported in Chapter 7.

3.5.3 Pharmacological assays on 44-46

Cell culture procedures and cell proliferation

HepG2 hepatocarcinoma cells were purchased from the American Type Culture Collection (ATCC, Manassas, VA, USA). HepG2 were cultured at 37°C in a humidified 95% air and 5% CO_2 atmosphere (all vol./vol.) and grown in Dulbecco's modified Eagle's medium (DMEM) supplemented with 10% fetal calf serum, 2% L-glutamine, 10,000 units/ml penicillin, 10,000µg/ml streptomycin. After overnight starvation, cells

were incubated for 4 hours with **44**-**46** (25µM) and then stimulated with insulin (100nM) for the indicated times.

Western blot analysis

Total cell lysates were obtained and separated by SDS-PAGE. Briefly, cells were solubilized with lysis buffer containing 50mM HEPES, 150mM NaCl, 10mM EDTA, 10mM $Na_4P_2O_7$, 2mM sodium orthovanadate, 50mM NaF, 1mM phenylmethylsulfonyl fluoride, 10µg/ml aprotinin, 10µg/ml leupeptin, pH 7.4, and 1% (v/v) Triton X-100. Lysates were clarified by centrifugation at 14000 rpm for 20 minutes at 4°C. The protein concentrations in the cell lysates were measured using a Bio-Rad DC (detergent compatible) assay. Proteins (50µg) were resolved by dodecyl sulfate-polyacrylamide gel electrophoresis (SDS-PAGE), transferred onto PVDF membrane, and blocked with 5% BSA in Tris-buffered saline containing 1% tween 20. Membranes were incubated with specific primary antibodies: INSR (1:1000, Catalog #: 3025, Cell Signaling Technology, Beverly, MA, USA). pINSR (1:1000, Catalog #: 3021, Cell Signaling Technology, Beverly, MA, USA); AKT (1:1000, Catalog #: 06-558, Upstate Biotech New York, NY, USA); pAKT (1:1000, Catalog #: 4058, Cell Signaling Technology, Beverly, MA, USA); ERK1/2 (1:1000, Catalog #: sc-514302, Santa Cruz Biotechnology, Dallas, TX, USA); pERK1/2 (1:1000, Catalog #: 9101, Cell Signaling Technology, Beverly, MA, USA); 14-3-3 (1:1000, Catalog #: sc-732, Santa Cruz Biotechnology, Dallas, TX, USA). Secondary antibodies were all diluted 1:1000 and were anti-rabbit (Catalog #: 170-6515, Bio-Rad, Hercules, CA), anti-mouse (Catalog #: 170-6516, Bio-Rad, Hercules, CA).

Real-Time RT-PCR analysis

Total cellular RNA was isolated from HepG2 cells by Qiazol reagent lysis (QIAGEN Sciences, Germany), according to manufacturer instructions. 1µg of cell RNA was reversely-transcribed using Superscript III Reverse Transcriptase (Life Technologies Carlsbad, CA, USA). PCR reactions were analyzed using IQTM SYBR Green Supermix (Bio-Rad, Hercules, CA). Reactions were performed using Platinum SYBR Green qPCR Super-UDG using an iCycler IQ multicolor Real Time PCR Detection System (Biorad, CA) running a total of 40 cycles. All reactions were performed in triplicate and expression data were normalized to the geometric mean of housekeeping gene beta-ACTIN analyzed using the $2^{-\Delta CT}$ or $2^{-\Delta\Delta CT}$ methods [133].

Determination of glycogen content

Glycogen was isolated from HepG2 cells homogenized in 0.1% SDS, saturated with Na_2SO_4 for 30' at 37°C followed by EtOH precipitation. Glycogen content was determined as described in literature [134].

Statistical procedures

Data were analyzed with the GraphPad Prism 8.0 (GraphPad Inc., San Diego, CA, USA). Multiple comparisons among more groups were made using the ANOVA test with Tukey correction (for normally distributed data). *p* values equal or less than 0.05 were considered statistically significant.

CHAPTER 4. Merging FBDD and DOS to explore the antidiabetic chemical space of phosphoeleganin

4.1 Design of a NP-fragments library

As previously discussed (Chapter 2), FBDD and DOS are formidable strategies in the field of organic chemistry, as they offer systematic methods for unlocking the latent power of marine-derived compounds. FBDD exploits small molecular fragments, while DOS, with its emphasis on creating libraries of diverse compounds, explores the chemical diversity of scaffolds[27,135]. Particularly, FBDD approach offers several advantages in exploiting larger molecules such as those derived from the marine environment, which can serve as guide compounds for rational fragment synthesis. Fragments hold an edge over marine NPs due to their size and complexity. They are smaller and less complex, facilitating optimization process by growing fragments structure with properly functional groups and chemical architectures. Moreover, the cost-effectiveness of fragments cannot be underrated. These smaller compounds are usually easier to synthesize compared to the larger, complex molecules offered by marine environment. These more affordable synthetic protocols contribute significantly to the feasibility and scalability of drug development efforts [97,136,137]. FBDD applied to bioactive marine NPs involves breaking down their complex structures into smaller and simpler fragments for drug development. The fragmentation can be performed following several strategies which include employing chemical cleavage or designing fragments inspired to the bioactive parent compound, usually aided by computational tools [97]. DOS can aid in developing libraries of fragments inspired by bioactive

NPs. This method is based on the creation of fragment-like SMs with diverse structural features, such as enabling exploration of chemical space provided from nature [30,92]. Stereostructural diversity within DOS-generated SMs amplifies their potential bioactivity by enhancing the specificity in the interactions with biological targets. Interestingly, the inclusion of sp^3 centers increases binding affinity and reduces off-target effects, contributing to favorable pharmacokinetic profiles, critical for clinical translation [138]. DOS approach can be considered a valuable strategy to synthesize structurally and stereochemically diverse fragments inspired by bioactive marine NPs. Together, these methodologies open new horizons in unveiling the therapeutic potential of marine NPs by systematically exploring the chemical space, delineating structure-activity relationships and facilitating the development of new drug candidates. The first publication conceptually merging DOS and FBDD appeared in 2011 in which Hung et al. [139] the application of DOS for the generation of a 3D fragment collection for the identification of novel binders for challenging biological targets. The synergistic combination of these two strategies enables the discovery of unique (semi)synthetic lead compounds inspired by bioactive marine metabolites. Recent applications of DOS, however, exemplify how this methodology can be utilized to address significant challenges currently faced within the field of FBDD.

Combining the FBDD and DOS approaches, we investigated the potential of phosphoeleganin (**44**) as a dual inhibitor of PTP1B and AR. This synergistic strategy allowed both to investigate the essential structural requirements for the inhibitory effects on both enzymes, delineating SARs related to the natural product and to obtain a library of (semi)synthetic fragments to be further functionalized for structural optimization. In addition to the fragments **45** and **46** (Figure 17) obtained by oxidative

cleavage of **44** several smaller derivatives inspired to the most functionalized part of the natural molecule, have been designed and synthesized, thus creating a first fragments library to be screened. It is worth noting that synthesis of NP-derived fragments, although they are far less complex structurally than the guiding NP itself, often still require considerable synthetic effort and the development of novel, efficient synthesis methodologies. This has been the case of phosphoeleganin (**44**) inspired fragments where, due to the number of chiral carbons present in its structure, we included in the library also a high rate of stereochemical diversity. However, their syntheses have never met the level of difficulty that would be encountered in the total multi-step synthesis of a natural product such as phosphoeleganin (**44**).

4.2 Synthesis of compound 47a-50b

The C5-C20 most functionalized part of the parent compound guided the rational design of a focused library of SMs-like fragments **47a-50b** (Figure 24). Following the principles of DOS, a library of SMs based on a tetradecane-5,8,9-triol scaffold was developed, modifying the stereochemistry of the *anti*-1,2-diol core. Moreover, diol core was then functionalized by the introduction of a phosphate group through a reaction that resulted in obtaining both regioisomers. The variability obtained from both stereodiversity and regiodiversity enriched the chemical space of the library efficiently, so that the role of the spatial arrangement of substituents in the inhibition of PTP1B and AR enzymes could be investigated. Furthermore, the semisynthetic phosphorylated fragment and the synthetic SM endowed with the favorable stereochemistry *S*,*S*,*R* and the phosphate moiety in the same position of the natural metabolite were identified as PTP1B inhibitors.

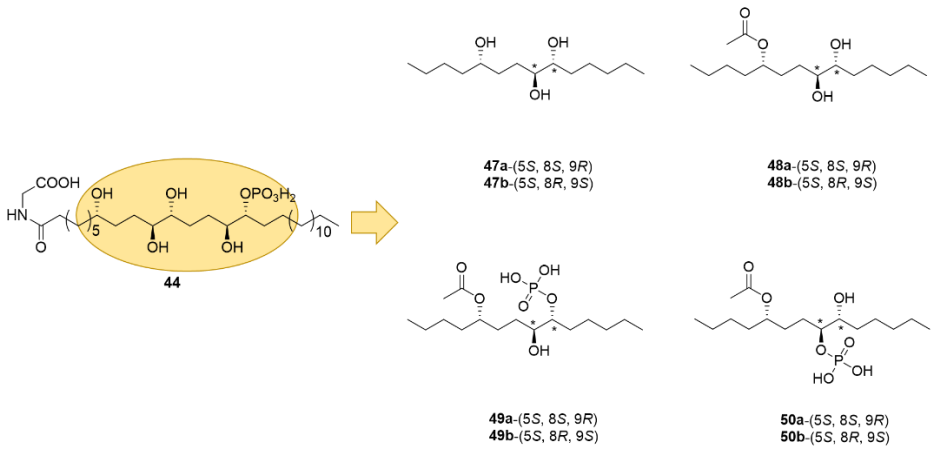

Figure 24. Semisynthetic fragments **45**-**46** and designed fragment-like small molecules **47a**-**50b**.

The synthetic protocol consisted in several efficient, cheap and easy to perform reactions. Initially, triols **47a** and **47b** were separately dissolved in 2,2-dimethoxypropane alongside a small amount of p-toluenesulfonic acid, and the resultant mixtures were stirred magnetically overnight. After this time, both mixtures were neutralized with a saturated $NaHCO_3$ solution, and after removing the solvent, acetonide intermediate **51a** and **51b** were obtained in pure form for the next synthetic step. Those compounds **51a** and **51b** were then treated directly with acetic anhydride in pyridine as a solvent and both mixtures were left to stir at room temperature overnight. Once completed, the mixtures were cooled, treated with MeOH, and the solvent was then removed under vacuum. This procedure efficiently produced compounds **52a** and **52b** in high yield, which underwent hydrolysis of the acetonide group using acidic conditions, resulting in the pure form of compound **48a** and **48b**.

Following this, the acetylated polyols **48a** and **48b** were transformed into phosphate monoesters using a phosphorylation method which consist in a efficient one-pot method. Previous phosphorylation protocols often faced

challenges such as the formation of side products like pyrophosphates or the necessity of employing excessive substrates or phosphorylation reagents. This reaction has been extensively studied due to the significant impact of introducing a phosphate group on chemical scaffold, affecting both pharmacokinetic and pharmacodynamic properties. An advancement in achieving better results was made through a one-pot method that increased the yield of phosphate monoesters while eliminating the production of pyrophosphates [140].

This innovative method provided the reaction between commercially available tetrabutylammonium dihydrogen phosphate and trichloroacetonitrile to generate an activated phosphate resembling a mixed anhydride, known as the trichloroacetimidate. Lira et al. proposed a mechanism in which this intermediate undergoes nucleophilic attack by the alcohol's hydroxyl group, resulting in the desired phosphate monoester and trichloroacetamide. As showed in Scheme 2, compound **48a** and **48b** were separately dissolved in acetonitrile, and trichloroacetonitrile was separately introduced to both mixtures. Subsequently, tetrabutylammonium dihydrogen phosphate in acetonitrile was slowly added in both mixtures which were stirred at room temperature for 2 hours. After solvent evaporation under nitrogen, the raw materials were purified via HPLC using a reversed phase with a MeOH/H_2O 75:25 mixture with 0.1% TFA, collecting two fractions composed of compounds **49a**/**49a** and **49b/50b**. Further purification through HPLC (MeOH/H_2O 6:4 + 0.1% TFA) yielded the two phosphorylated compounds **49a/49a** and **49b**/**50b** in their pure forms.

All compounds were extensively characterized using NMR spectroscopy and HRESI mass spectrometry to definitively establish their structures and distinguish between structural isomers.

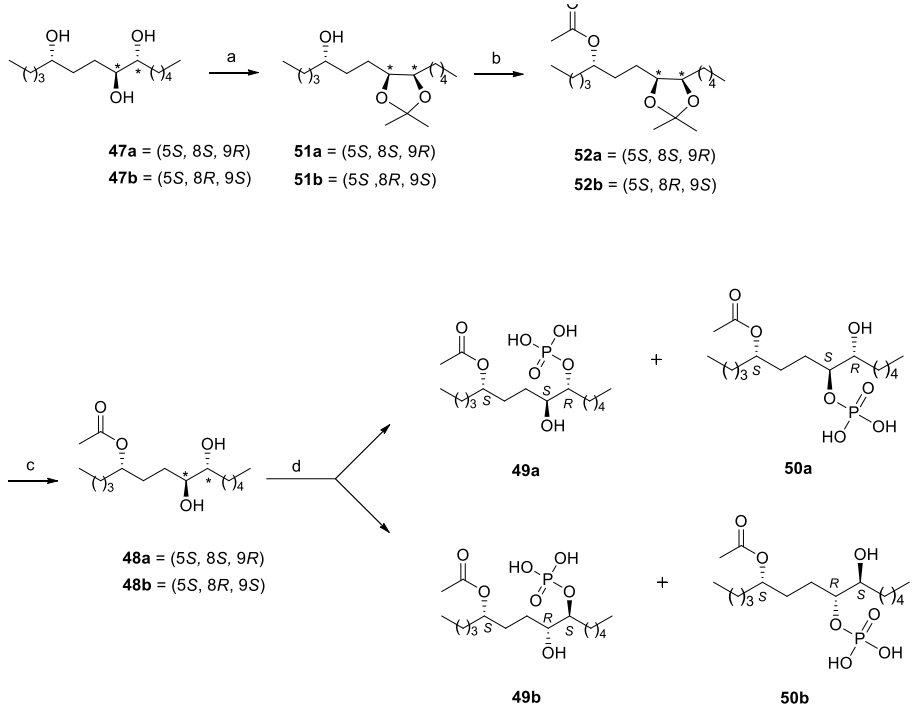

Scheme 2. Reagents and conditions: (**a**) 2,2-dimethoxypropane, p-toluenesulfonic acid, rt, overnight. (**b**) Ac_2O, pyridine, rt, overnight. (**c**) HCl 1%, MeOH/H_2O 9:1, rt, overnight. (**d**) (1) Cl_3CCN; (2) $(n\text{-}Bu)_4NH_2PO_4$, CH_3CN, rt, 2h. The symbol * represents relative configuration.

4.3 Pharmacological screening of compounds 45-46 and 47a-50b

Semisynthetic fragments **45** and **46** and compounds **47a-50b** have been funneled in a pharmacological screening to evaluate the inhibitory activity on PTP1B and AR thanks to the active collaboration with the research groups of Proff. Paolo Paoli and Antonella Del Corso of the Universities of Florence and Pisa, respectively. Preliminary screening of **45-46** and **47a-50b** showed that all compounds were inactive on AR while compounds **46** and **49b** were the most potent inhibitors of PTP1B in the series (Figure 25). While natural metabolite phosphoeleganin (**44**) exerted

a significant inhibition of AR enzyme, both semisynthetic and synthetic derivatives lost this activity. These findings align with prior in silico docking analysis of **44** in the AR active site, which highlighted interactions involving both the polar functionalized portion and aliphatic portion of the molecule . Despite attempts to introduce an acetyl group in synthetic fragments to facilitate the presence of a carbonyl group linked to AR inhibition, this modification wasn't sufficient to maintain the inhibitory activity which seems to be ensured by the entire molecule. All these results encourage the design of fragments which necessitate the inclusion of both glycine and polar groups alongside an adequate aliphatic chain. Concerning the screening on PTP1B, preliminary results (Figure 25) revealed that compounds endowed with a phosphate group (**46**, **49a**, **49b**, **49a**, and **50b**) showed inhibitory effect. The phosphate-lacking fragment **45** did not show any inhibitory effect on PTP1B, thus, confirming that its insulin sensitizing activity, discussed in the previous Chapter, should be imposable to another unexplored mechanism of action.

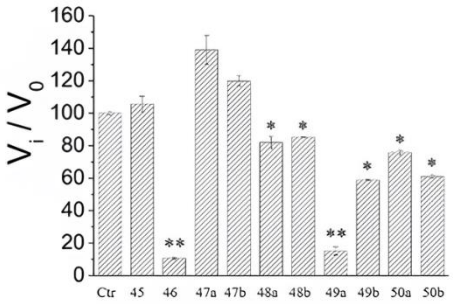

Figure 25. Preliminary screening assay on PTP1B. All assays were started by diluting an aliquot of PTP1B in the assay solution containing substrate alone (control test) or substrate and an aliquot of each compound (20 μM, final concentration). After 30 minutes, the reactions were stopped by adding a concentrated KOH solution. The enzyme activity was determined by measuring

the amount of *p*-nitrophenol that was released in each sample using a spectrophotometer. Data obtained were normalized respect to control sample. Data showed in the figure represent the mean value ± SD (n = 3).

Among these, compounds **46** and **49a** displayed the most potent activity, with IC_{50} values of 6.7 ± 3.3 μM and 16.0 ± 2.0 μM, respectively (Figure 26). However, these compounds were less potent than phosphoeleganin (**44**), underscoring the significance of the aliphatic chain possessed by natural product in fortifying the interaction with the enzyme. The IC_{50} values of **46** and **49a** outlined the crucial role of a phosphate group for PTP1B inhibition also in terms of its spatial orientation and position along the carbon chain. In fact, differences in stereochemistry and position of the phosphate moiety strongly affected inhibitory potency, as seen in comparisons between **49a**/**49b** and **50a**/**50b**.

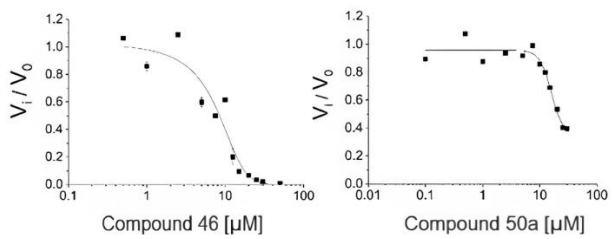

Figure 26. Determination of the IC_{50} values with compounds **46** and **49a**. An aliquot of PTP1B enzyme was diluted in the presence of increasing concentration of the compounds. The activity of PTP1B was determined by measuring the absorbance of the sample at 400 nm, using a spectrophotometer. Data obtained were normalized respect to the control sample and analysed using a non-linear fitting software. Data showed in the figure represent the mean value ± SD (n = 3).

4.3.1 Pharmacological characterization of compound 46 and 49a

Further characterization of compounds **46** and **49a** has continued to glean deeper insights into the features underlying PTP1B inhibition. Kinetic analyses were performed analyzing the dependence of Km and Vmax on the concentration of the inhibitor and all the obtained data were evaluated through Linewaver-Burke plot.

Concerning the inhibitory mechanism of **46** on PTP1B, the dependency of K_M and V_{max} on the inhibitor concentration (Figure 27A/B) was studied. It has been evidenced that the increase of inhibitor concentration was associated with a decrease of V_{max} value and an increase of K_M. Furthermore, Lineweaver-Burk plot (Figure 27C) shows that experimental points described straight lines that intersect one each other in the left panel.

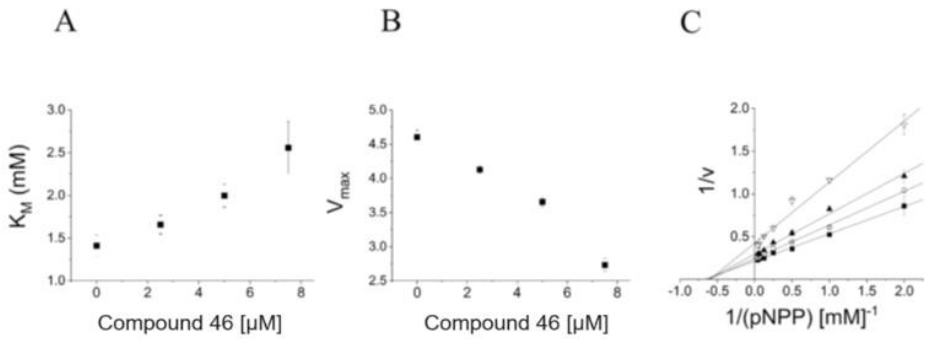

Figure 27. Kinetic characterization of **46** as PTP1B inhibitor. The concentrations of compound **46** used were 0 (■), 2.5 (○), 5 (▲) and 7.5 (▽). Dependence of main kinetic parameters K_M (A) and V_{max} (B) from the concentration of compound **46**. Lineweaver-Burk plot (C). Bars represent the standard deviations of the means from at least three independent measurements (if not present, they are within the symbol's size).

Moreover, a similar analysis was carried out with compound **49a** (Figure 28). As the previous analysis, the increase of concentration of **49a** resulted

in an increase in K_M and a decrease in V_{max}. According with this hypothesis, the Lineweaver-Burk plot describes straight lines that intersect one to each other in a point in the left side of the graphic.

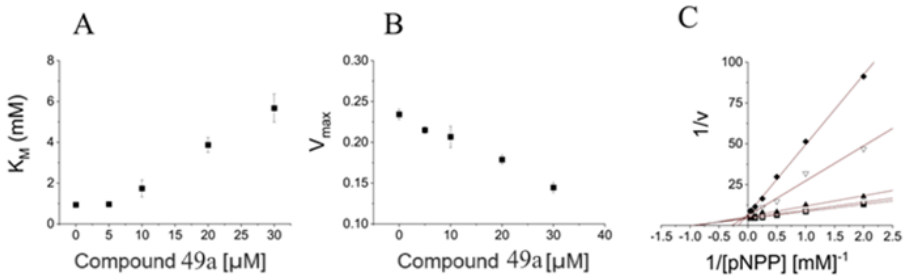

Figure 28. Kinetic characterization of **49a** as PTP1B inhibitor. The concentrations of compound **3** used were 0 (■), 5 (○), 10 (▲), 20 (▽) and 30 (◆) μM. Dependence of K_M (A) and V_{max} (B) from the inhibitor concentration. Lineweaver-Burk graph (C). Bars represent the standard deviations of the means from at least three independent measurements (if not present, they are within the symbol's size).

Taken together, results of kinetic analysis revealed that both compounds **46** and **49a** act as mixed-type non-competitive inhibitors, whose mechanism of action is described in Figure 29.

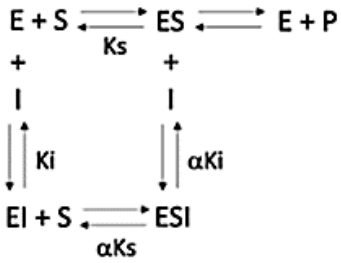

Figure 29. The mechanism of action of a linear mixed-type inhibitor. E, free enzyme; S, substrate; ES, enzyme-substrate complex; EI, enzyme-inhibitor complex; ESI the enzyme-substrate-inhibitory ternary complex; Ks, dissociation constant of the enzyme-substrate complex; Ki, dissociation constant of EI

complex; αKs and αKi, dissociation constant of enzyme-substrate-inhibitor complex (α>1)

Finally, by analysing the behaviour of K_M/V_{max} (Figure 30A) and $1/V_{max}$ (Figure 30B) with respect to the compound **46** concentration, we calculated both the values of Ki (6.6 ± 0.8 μM), Ki' (9.4 ± 0.6 μM) and of α (1.4 ± 0.2). Similarly, the values of K_i (3.3 ± 0.4 μM), of K_i' (5.4 ± 0.2 μM) and α (1.6 ± 0.1) with respect to the compound **49a** concentration, were calculated (Figure 30C).

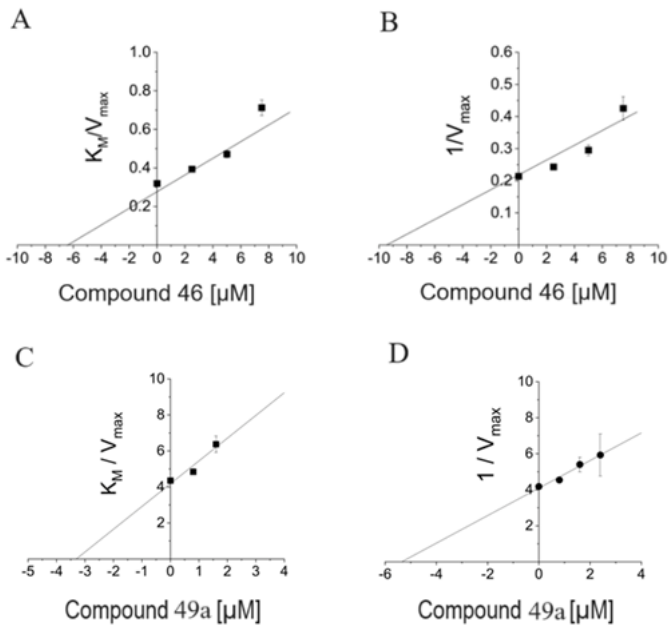

Figure 30. Secondary plots. K_M/V_{max} (A and C) and $1/V_{max}$ (B and D) versus **46** and **49a** concentration, respectively. The intercept of straight line with the "x" axis in Panel A and C, represents the Ki value, while the intercept of straight line with the "x" axis in Panel B and D represents the Ki' value (Ki' = αKi).

To enrich our knowledge about mechanism of action of compound **46** and **49a**, a dilution assay test to evaluate whether these compounds act as reversible or non-reversible inhibitors was performed. After incubation of PTP1B with both compounds, the enzyme recovered its activity almost completely upon dilution in the assay buffer suggesting that both compounds behave as reversible inhibitors of PTP1B (Figure 31).

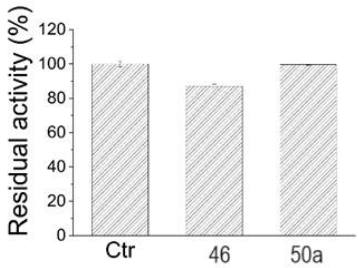

Figure 31. Dilution assay. To evaluate the mechanism of action of the compounds, a reversibility assay was carried out. The PTP1B was incubated in the presence of the saturating concentration of each compound (50 μM) for 30 minutes at 37°C. Then, an aliquot of enzyme was diluted 1000 folds in the assay buffer to evaluate the residual activity of the enzyme. Tests were carried out in triplicate. Data represent the mean value ± SD.

The discovery of new reversible and non-competitive inhibitors is notable since this kind of inhibition reduces toxicity associated with prolonged or irreversible enzyme inhibition and minimizes interference with other enzymatic isoforms involved in physiological processes, reducing also side effects.

More pharmacological assays were performed due to study the ability of compound **46** and **49a** in improving glucose homeostasis. The effect of both compounds on insulin signalling pathway was evaluated in murine myoblast C2C12 cells. The treatment of C2C12 cells with compound **49a**

did not interfere with insulin signalling pathway; in contrast of phosphorylated fragment **46** did it (Figure 32). Further experiments were performed on compound **46** to investigate the mechanism of action. The C2C12 cells treated with **46** in absence of insulin, the phosphorylation levels of both insulin receptor (IR) and kinase Akt increased with respect to control cells. However, the phosphorylated fragment was demonstrated to be unable to increase insulin sensitivity when administered in combination with the hormone. The hypothesis that could explain this phenomenon relies in post-translational modifications of the enzyme. In fact, phosphorylation of PTP1B can alter the overall structure of the enzyme, thus impairing the formation of the enzyme-inhibitor complex.

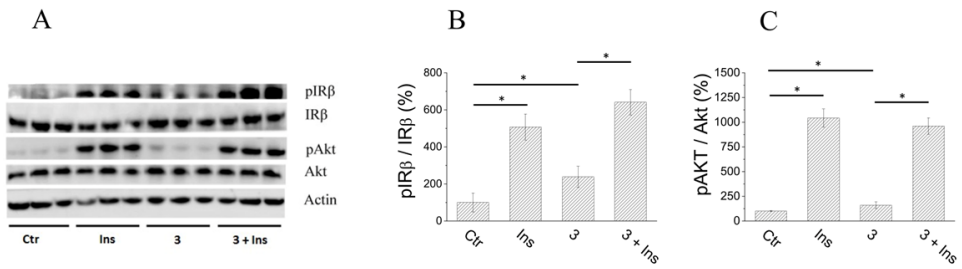

Figure 32. Effect of compound **46** on insulin signalling pathway. C2C12 cells were incubated with compound **46** (20 µM final concentration) for 30 minutes, in the presence or not of insulin (10 nM). After that, cells were lysed, and cellular extracts were analysed to evaluate the phosphorylation status of IR and Akt. (A), western blot image; (B, C), quantitation of western blot carried out using Kodak MI software. Data were normalized respect to control sample. All tests were carried out in triplicate. Ctr: control experiment; Ins: cells treated with 10 nM insulin; **46**: cells treated with compound **46** (20 µM); **46**+Ins, cells treated with insulin and compound 3*$p < 0.05$.

Further pharmacological assays were performed to verify its ability to improve glucose uptake. Interestingly, C2C12 cells treated with **46** alone embed more glucose than insulin-stimulated ones, while cells stimulated with the combination of **46** and insulin showed intracellular glucose levels like those present in the cells treated with the hormone alone (Figure 33). Taken together, these results corroborated with the insulin mimetic behavior of compound **46**.

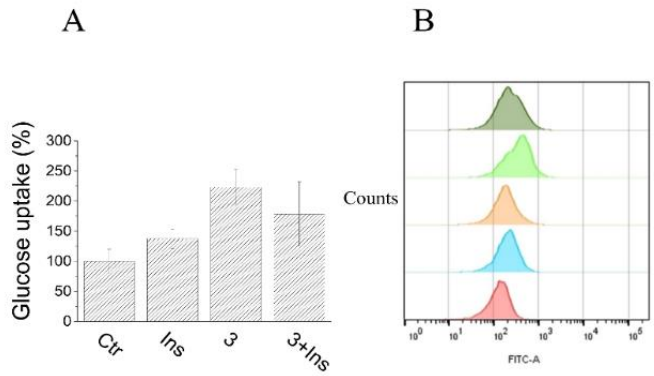

Figure 33. Glucose uptake assay. C2C12 cells were treated with 10 nM insulin, 20 µM compound **46** or **46**-insulin combination and then incubated in the presence of 2-NBDG for 3 h. After that, the glucose uptake was evaluated by flow cytometry analysis. Each test was performed out in quadruplicate. For each test, 10000 events at least were analyzed. (A), quantification of the mean fluorescence values of C2C12 cells. Data represent the mean value ± SD (n = 4). Statistical analysis was performed using Unpaired *t*-student test. * $p < 0.05$, ** $p < 0.01$. (B), representative cell fluorescence distribution obtained by analyzing data with the FlowJo software. Red, cells autofluorescence; light blue, control cells; orange, C2C12 cells stimulated with 10 nM insulin; green, C2C12 cells stimulated with 20 µM **46**; dark green, C2C12 cells stimulated with **46**-insulin combination.

4.3.2 Docking of compound 46 and 49a

The computational docking analysis provides crucial insights into how compounds **46** and **49a** interact with PTP1B. In the most favorable pose of synthetic compound **49a** (Figure 34A), it engages various regions on the enzyme's surface. Specifically, the phosphate of **49a** strongly interacts with the side chain of Arg221 located within the PTP1B active site, while the contiguous hydroxyl group forms a hydrogen bond with the side chain of Asp181, contributing to obstructing the enzyme's active site in its "closed conformation." The positioning of the phosphate group in the middle of the aliphatic chain appears to be the primary factor favoring this interaction. The active site, since the presence of the Arg221, is positively charged so the aliphatic chain of **49a** cannot enter and, consequently, this limitation promotes interactions between the aliphatic chain of **49a** with specific residues within the active site (Tyr46, Ala49, Phe182) and the hydroxyl group with Asp181, while enabling the phosphate group to penetrate deeper into the PTP1B active site. In an alternative configuration (Figure 34B), the aliphatic chain of **49a** seems embedded within a hydrophobic zone formed by the side chains of Asn42, Arg45, Leu88, Pro89, Asn90, and Leu119, while the phosphate group forms hydrogen bonds with the carbonyl group of Lys41 and Asn44 residues. Despite being distanced from the active site, these residues are in proximity to the YRD motif (residues 46-48), crucial for the enzyme's full catalytic activity. Hence, the interaction of **49b** in this region could potentially disrupt the positioning of essential residues, affecting the enzyme's catalytic process.

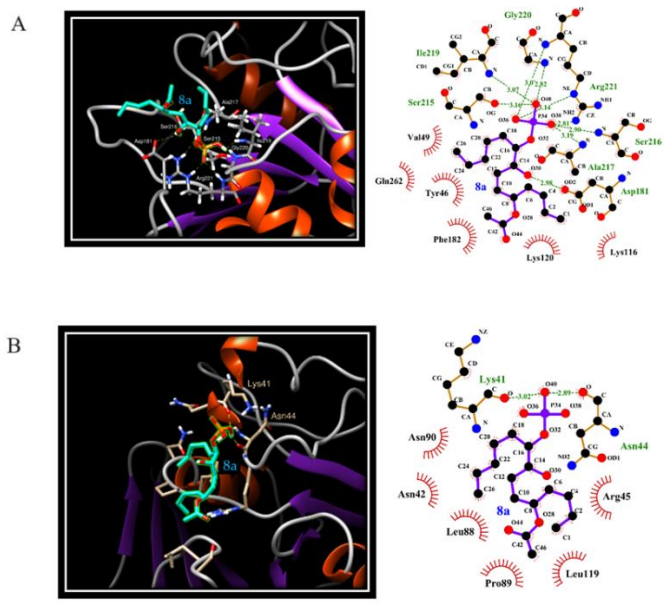

Figure 34. Visualization of the interaction between compound **49a** and the active site of PTP1B (A). Interaction of compound **49a** with the region lining the active site of PTP1B enzyme (B).

Compound **46** possesses a longer side chain than **49a** and a phosphate group located at the molecule's end. Notable, the most favorable interaction pattern reveals compound that compound **46** interact with PTP1B active site (Figure 35A). Specifically, its aliphatic chain interacts with a hydrophobic region formed by the side chains of Lys41, Asn42, Asn44, Leu88, Pro89, and Lys120, while its phosphate group interacts through hydrogen bonds with the side chain of Arg45 and Tyr46. The latter residue resides in a surface loop between the α1 helix and β1 strand and plays a direct role in substrate binding. Furthermore, in an alternate positioning (Figure 35B), the phosphate moiety of compound **46** aligns with the second aryl binding site, forming hydrogen bonds with the

carbonyl group of Arg24 and nitrogen atoms of the Arg254 side chain. Concurrently, the terminal hydroxyl group of compound **49a** engages in hydrogen bonding with the side chain of Gln262, a crucial residue governing the positioning of the nucleophilic water molecule involved in catalytic cysteinyl-phosphate intermediate hydrolysis. These findings collectively confirm that both compounds **49a** and **46** can penetrate the active site or interact with various sites on the enzyme's surface, supporting their mechanism of action as mixed-type non-competitive inhibition.

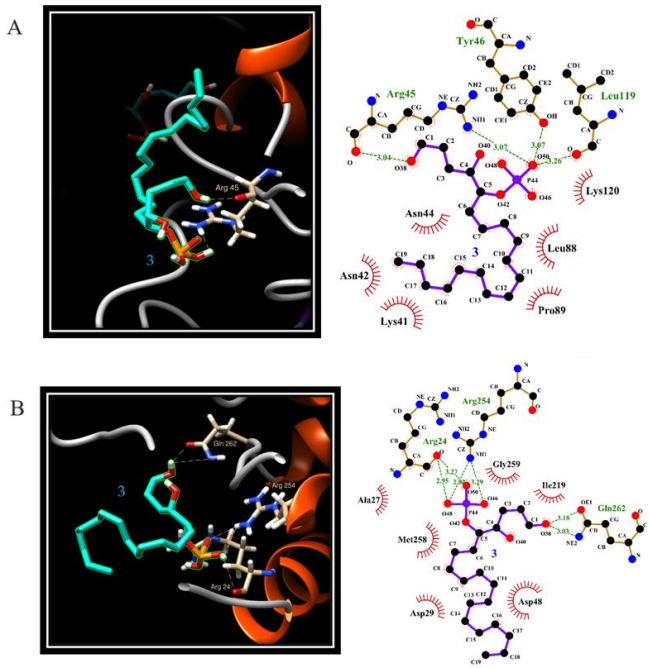

Figure 35. (A) Interaction of compound **46** with the region lining the active site of PTP1B. (B) Interaction of compound **46** within the second aryl binding site of PTP1B enzyme.

4.4 Conclusions

A multidisciplinary work was conducted exploiting phosphoeleganin (**44**) as a starting point for the development of new inhibitors. In particular, the synthesis of fragments **45**-**46** and fragments-like SMs **47a**-**50b** highlighted the structural requirements for both PTP1B and AR inhibition. First, all compounds, both semisynthetic and synthetic are inactive on AR, emphasizing the importance of the whole structure of the marine NP **44** in inhibiting the enzyme. We suppose that the glycine head and the suitable alkyl chain are essential for the pharmacological activity. Regarding PTP1B, the semisynthetic fragment **46** equipped with the phosphate group turned out as a potent inhibitor of the enzyme, exerting a reversible and mixed-type non-competitive inhibition mechanism. In addition, studies on C2C12 cells revealed the insulin mimetic activity of the compound. In contrast, among the synthetic SMs, only compounds endowed with phosphate maintained the activity on the enzyme PTP1B. Compound **49a**, characterized by the same stereochemistry as the C7-C14 segment of phosphoeleganin (**44**), is the most potent derivative in the series highlighting the importance of the correct orientation of the phosphate group in space as well as its position along the alkyl chain, as outlined by the less potent regioisomer **50a**. The extensive pharmacological characterization of **49a** revealed that it acts as a reversible and mixed-type non-competitive inhibitor. However, this result cannot be supported by further studies since compound **49a** did not improve the insulin signaling pathway in vitro. This preliminary investigation outline the phosphorylate polyketide-like scaffold as a promising chemotype for PTP1B inhibition.

4.5 Material and methods

4.5.1 Synthesis of compounds 47a-50b

*Synthesis of compounds **47a** and **47b***

Compounds **47a** (120 mg) and **47b** (115 mg) were obtained by carrying out the synthetic protocol reported in literature [108]. Compound **47a**: white powder; HRESIMS:m/z 269.2101 $[M+Na]^+$ (calcd. for $C_{14}H_{30}O_3Na$ m/z 269.2087). The NMR data of compound **47a** agree with literature data [108]. Compound **47b**: white powder; HRESIMS: m/z 269.2103 $[M + Na]^+$ (calcd. for $C_{14}H_{30}O_3Na$ m/z 269.2087). The NMR data of compound **47b** agree with literature data [108].

*Synthesis of compounds **51a** and **51b***

110 mg (0.445 mmol) of the triol **47a** were dissolved in 15.0 mL of 2,2-dimethoxypropane and a catalytic amount of p-toluenesulfonic acid was added in one portion. The reaction mixture was stirred overnight at room temperature. Then, a saturated $NaHCO_3$ solution quenched the reaction and the desired product **51a** was extracted with EtOAc for three times. The organic layer was dried over anhydrous Na_2SO4, filtered and concentrated under reduced pressure to obtain a colourless oil (120.0 mg, 94%). The obtained product was used for the next reaction step without any purification. Compound **51a** ^1H NMR (700 MHz, CD_3OD): ^1H NMR (CD_3OD): 0.93 (3H, t, J = 7.6 Hz); 1.44 (2H, H-2); 1.44-1.43 (2H, overlapped, H-3); 1.42-1.46 (2H, overlapped, H-4); 3.53 (1H, m, H-5); 1.34 (1H, m, H-6a); 1.68 (1H, m, H-6b); 1.34 (1H, m, H-7a); 1.61 (1H, H-7b); 4.02 (1H, m, H-8); 4.05 (1H, m, H-9); 1.47-1.48 (2H, overlapped, H-10); 1.34 (1H, overlapped, H-11a); 1.54 (1H, m, H-11b); 1.34 (2H, overlapped, H-12); 1.34 (2H, overlapped, H-13); 0.91 (3H, t, J = 7.6 Hz, H-14); 1.30 (3H, s, CH_3, H-1'); 1.39 (3H, s, CH_3, H-3'); ^{13}C NMR

(CD_3OD): 14.1 (CH_3, C-1); 23.5 (CH_2, C-2); 28.7 (CH_2, C-3); 37.9 (CH_2, C-4); 73.9 (CH, C-5); 34.9 (CH_2, C-6); 27.5 (CH_2, C-7); 79.0 (CH, C-8); 79.5 (CH, C-9); 30.4 (CH_2, C-10); 26.4 (CH_2, C-11); 44.8 (CH_2, C-12); 23.7 (CH_2, C-13); 14.1 (CH_2, C-14); 108.5 (C, C-2'); 28.5 (CH_3, C-1'); 25.7 (CH_3, C-3'); HRESIMS: m/z 287.2597 $[M+H]^+$ (calcd. for $C_{17}H_{35}O_3$ m/z 287.2581).

The same procedure used for **51a** was adopted to obtain **51b** (114.7 mg, 94%) starting from 105 mg (0.426 mmol) of **47b**. The obtained product was used for the next reaction step without any purification. The NMR data of compound **51b** agree with literature data [REF]. HRESIMS: m/z 287.2597 $[M + H]^+$ (calcd. for $C_{17}H_{35}O_3$ m/z 287.2581). Compound **51b** ^1H NMR (700 MHz, CD_3OD) values: 0.92 (3H, t, J = 7.6 Hz); 1.44 (2H, H-2); 1.44-1.43 (2H, overlapped, H-3); 1.42-1.46 (2H, overlapped, H-4); 3.53 (1H, m, H-5); 1.34 (1H, m, H-6a); 1.68 (1H, m, H-6b); 1.34 (1H, m, H-7a); 1.61 (1H, H-7b); 4.01 (1H, m, H-8); 4.03 (1H, m, H-9); 1.47-1.48 (2H, overlapped, H-10); 1.34 (1H, overlapped, H-11a); 1.54 (1H, m, H-11b); 1.34 (2H, overlapped, H-12); 1.33 (2H, overlapped, H-13); 0.89 (3H, t, J = 7.5 Hz, H-14); 1.30 (3H, s, CH_3, H-1'); 1.39 (3H, s, CH_3, H-3'); ^{13}C NMR (CD_3OD): 14.1 (CH_3, C-1); 23.5 (CH_2, C-2); 28.7 (CH_2, C-3); 37.6 (CH_2, C-4); 73.9 (CH, C-5); 34.9 (CH_2, C-6); 27.6 (CH_2, C-7); 79.1 (CH, C-8); 79.5 (CH, C-9); 30.5 (CH_2, C-10); 26.5 (CH_2, C-11); 44.8 (CH_2, C-12); 23.6 (CH_2, C-13); 14.1 (CH_2, C-14); 109.5 (C, C-2'); 28.5 (CH_3, C-1'); 25.7 (CH_3, C-3').

*Synthesis of compounds **52a** and **52b***

65 mg (0.226 mmol) of the acetonide **51a** was dissolved in 10.0 mL of pyridine, treated with an excess of acetic anhydride and the resultant mixture was stirred for 18h at room temperature. During this time, the

reaction was monitored by TLC until the starting material was disappeared. Then, the excess of acetic anhydride was removed by cooling the reaction mixture at 0°C in an ice-bath and adding ~25 mL of MeOH. The solvent removal in vacuo afforded compound **52a** (72.0 mg, 97%) as a colourless oil that was subjected to hydrolysis reaction without any purification. Compound **52a** ^{1}H NMR (700 MHz, CD_3OD): 0.93 (3H, H-1); 1.44 (2H, H-2); 1.44-1.43 (2H, H-3); 1.42-1.46 (2H, H-4); 3.53 (1H, H-5); 1.34-1.68 (2H, H-6); 1.34-1.61 (2H, H-7); 4.02 (1H, H-8); 4.05 (1H, H-9); 1.47-1.48 (2H, H-10); 1.34-1.54 (2H, H-11); 1.34 (2H, H-12); 1.34 (2H, H-13); 0.91 (3H, H-14); 1.30 (3H, CH3, H-1'); 1.39 (3H, CH3, H-3'); 13C NMR (CD_3OD): 14.1 (CH_3, C-1); 23.5 (CH_2, C-2); 28.7 (CH_2, C-3); 37.9 (CH_2, C-4); 73.9 (CH, C-5); 34.9 (CH_2, C-6); 27.5 (CH_2, C-7); 79.0 (CH, C-8); 79.5 (CH, C-9); 30.4 (CH_2, C-10); 26.4 (CH2, C-11); 44.8 (CH_2, C-12); 23.7 (CH_2, C-13); 14.1 (CH_2, C-14); 108.5 (C, C-2'); 28.5 (CH_3, C-1'); 25.7 (CH_3, C-3').

The same procedure used for **52a** was adopted to obtain **52b** (66.5 mg, 97%) starting from 60 mg (0.209 mmol) of **51b**. Compound **52b** ^{1}H NMR (CD_3OD, 700 MHz): 0.93 (3H, H-1); 1.44 (2H, H-2); 1.44-1.43 (2H, H-3); 1.42-1.46 (2H, H-4); 3.53 (1H, H-5); 1.34-1.68 (2H, H-6); 1.34-1.61 (2H, H-7); 4.02 (1H, H-8); 4.05 (1H, H-9); 1.47-1.48 (2H, H-10); 1.34-1.54 (2H, H-11); 1.34 (2H, H-12); 1.34 (2H, H-13); 0.91 (3H, H-14); 1.30 (3H, CH3, H-1'); 1.39 (3H, CH3, H-3'); 13C NMR (CD3OD): 14.1 (CH3, C-1); 23.5 (CH_2, C-2); 28.7 (CH_2, C-3); 37.9 (CH_2, C-4); 73.9 (CH, C-5); 34.9 (CH_2, C-6); 27.5 (CH_2, C-7); 79.0 (CH, C-8); 79.5 (CH, C-9); 30.4 (CH_2, C-10); 26.4 (CH_2, C-11); 44.8 (CH_2, C-12); 23.7 (CH_2, C-13); 14.1 (CH_2, C-14); 108.5 (C, C-2'); 28.5 (CH_3, C-1'); 25.7 (CH_3, C-3').

*Synthesis of compounds **48a** and **48b***

70 mg of **52a** (0.213 mmol) were dissolved in 20 mL of MeOH/H_2O (9:1) and 160 µL of HCl 37% (p/p) were added dropwise to the mixture. The reaction mixture was kept at 4°C for 36 h before removing the solvent by rotary evaporator. The raw material was purified by HPLC on C18 reversed phase (Luna 5 µm C18 column 250 mm x 4.6 mm, MeOH/H_2O 7:3 as mobile phase, flow rate 1 mL/min) to yield the acetylated compound **52a** as a white powder (60.2 mg, 98%). Compound **48a** ^{1}H NMR (700 MHz, CD_3OD) values: 0.91 (3H, t, J = 7.6 Hz, H-1); 1.33 (2H, overlapped, H-2); 1.44 (1H, overlapped, H-3a); 1.28 (1H, m, H-3b); 1.56 (2H, overlapped, H-4); 4.82 (1H, m, H-5); 1.83 (1H, m, H-6a); 1.52 (1H, overlapped, H-6b); 1.68 (1H, m, H-7a); 1.31 (1H, overlapped, H-7b); 3.29 (1H, m, H-8); 3.33 (1H, m, H-9); 1.62 (1H, overlapped, H-10a); 1.35 (1H, overlapped, H-10b); 1.54 (1H, m, H-11a); 1.34 (1H, overlapped, H-11b); 1.33 (2H, overlapped, H-12); 1.34 (2H, overlapped, H-13); 0.91 (3H, t, J = 7.6 Hz, H-14); ^{13}C NMR (CD_3OD): 14.1 (CH_3, C-1); 23.5 (CH_2, C-2); 28.4 (CH_2, C-3); 34.7 (CH_2, C-4); 76.0 (CH, C-5); 31.5 (CH_2, C-6); 29.4 (CH_2, C-7); 79.5 (CH, C-8); 79.6 (CH, C-9); 33.5 (CH_2, C-10); 26.5 (CH_2, C-11); 44.7 (CH_2, C-12); 23.5 (CH_2, C-13); 14.1 (CH_3, C-14); 173.7 ($\underline{C}OCH_3$); HRESIMS: m/z 311.2194 $[M+Na]^+$ (calcd. for $C_{16}H_{44}O_4Na$ m/z 311.2193)

The same procedure used for **48a** was adopted to obtain **48b** (56.0 mg, 98%) starting from 65 mg (0.198 mmol) of **52b**. Compound **48b** ^{1}H NMR (700 MHz, CD_3OD) values: 0.91 (3H, t, J =7.0 Hz , H-1); 1.33 (2H, overlapped, H-2); 1.34 (2H, overlapped, H-3); 1.58 (2H, overlapped, H-4); 4.82 (2H, m, H-5); 1.60 (2H, overlapped, H-6); 1.39 (1H, overlapped, H-7a); 1.61 (1H, overlapped, H-7b); 3.35 (1H, m, H-8); 3.36 (1H, m, H-9); 1.36 (1H, overlapped, H-10a); 1.56 (1H, overlapped, H-10b); 1.34 (1H, overlapped, H-11a); 1.54 (1H, overlapped, H-11b); 1.34 (2H, overlapped,

H-12); 1.35 (2H, overlapped, H-13); 0.91 (3H, t, J =7.0 Hz, H-14); 2.06 (3H, s, COC$\underline{H}_3$) ^{13}C NMR (CD_3OD): 14.4 (CH_3, C-1); 23.7 (CH_2, C-2); 44.8 (CH_2, C-3); 34.8 (CH_2, C-4); 75.9.0 (CH, C-5); 33.8 (CH_2, C-6); 28.9 (CH_2, C-7); 75.3 (CH, C-8); 75.4 (CH, C-9); 33.5 (CH_2, C-10); 26.7 (CH_2, C-11); 44.8 (CH_2, C-12); 23.6 (CH_2, C-13); 14.3 (CH_3, C-14); 172.9 ($\underline{C}OCH_3$); HRESIMS: m/z 311.2191 $[M+Na]^+$ (calcd. for $C_{16}H_{44}O_4Na$ m/z 311.2193).

*Synthesis of compounds **49a** and **50a***

58 mg (0.201 mmol) of compound **48a** were dissolved in 12.0 mL of acetonitrile and treated with 60 µL (0.601 mmol) of trichloroacetonitrile, following by dropwise addition of 136.0 mg (0.402 mmol) of tetrabutylammonium dihydrogenphosphate, previously solubilized in 4.0 mL of acetonitrile. The reaction was kept under magnetic stirring at room temperature for 2 h and the solvent removal in vacuo afforded a raw material which was first purified by HPLC on reversed phase (Synergy 4 µm Max-RP column 250 mm x 4.6 mm, MeOH:H_2O 75:25 + 0.1% TFA as mobile phase, flow rate 1 mL/min). The collected fraction which contained the mixture of the two isomeric phosphorylated compounds **49a** and **50a** (24.4 mg, 44%) was further purified by HPLC on reversed phase (Synergy 4 µm Fusion column 250 mm x 4.6 mm and MeOH/H_2O 6:4 + 0.1% TFA as mobile phase, flow rate 1 mL/min) affording compound **49a** (14.8 mg, tR = 27.4 min) and **50a** (9.6 mg, tR = 28.8 min) in pure form as colorless oil. Compound **49a** ^{1}H NMR (700 MHz, CD_3OD): 0.91 (3H, t, J = 6.9 Hz, H-1); 1.31 (2H, overlapped, H-2); 1.28 (1H, overlapped, H-3a); 1.37 (1H, overlapped, H-3b); 1.55 (2H, overlapped, H-4); 4.87 (1H, m, H-5); 1.60 (1H, overlapped, H-6a); 1.82 (1H, overlapped, H-6b); 1.38 (1H, overlapped, H-7a); 1.61 (1H, overlapped, H-7b); 3.67 (1H, ddd, H-8); 4.11

(1H, overlapped, H-9); 1.60 (1H, overlapped H-10a); 1.68 (1H, overlapped, H-10b); 1.41 (1H, overlapped, H-11a); 1.48 (1H, overlapped, H-11b); 1.33 (2H, overlapped, H-12); 1.36 (2H, overlapped, H-13); 0.91 (3H, t, J =6.9 Hz, H-14); 2.02 (3H, s, $COC\underline{H_3}$); ^{13}C NMR (CD_3OD): 14.1 (CH_3, C-1); 23.4 (CH_2, C-2); 28.6 (CH_2, C-3); 34.8 (CH_2, C-4); 76.0 (CH, C-5); 31.6(CH_2, C-6); 29.3(CH_2, C-7); 74.0 (CH,C-8); 82.9 (CH, C-9); 31.5 (CH_2, C-10); 25.6 (CH_2, C-11); 44.8 (CH_2, C-12); 23.4 (CH_2, C-13); 14.1 (CH_3, C-14); 173.6 ($\underline{C}OCH_3$); 20.9 ($CO\underline{C}H_3$). HRESIMS: m/z 367.1882 $[M-H]^-$ (calcd. for $C_{16}H_{44}O_7P$ m/z 367.1880).

Compound **50a** ^1H NMR (700 MHz, CD_3OD): 0.91 (3H, t, J =6.9 Hz, H-1); 1.34 (2H, overlapped, H-2); 1.28 (1H, overlapped, H-3a); 1.44 (1H, overlapped, H-3b); 1.57 (2H, overlapped, H-4); 4.88 (1H, m, H-5); 1.61 (1H, overlapped, H-6a); 1.86 (1H, overlapped, H-6b); 1.65 (1H, overlapped, H-7a); 1.69 (1H, overlapped, H-7b); 4.15 (1H, ddd, H-8); 3.63 (1H, overlapped, H-9); 1.40 (1H, overlapped H-10a); 1.56 (1H, overlapped, H-10b); 1.33 (1H, overlapped, H-11a); 1.56 (1H, overlapped, H-11b); 1.33 (2H, overlapped, H-12); 1.34 (2H, overlapped, H-13); 0.91 (3H, t, J =6.9 Hz, H-14); 2.02 (3H, s, $COC\underline{H_3}$) ; ^{13}C NMR (CD_3OD): 14.1 (CH_3, C-1); 23.4 (CH_2, C-2); 28.4 (CH_2, C-3); 34.6 (CH_2, C-4); 76.0 (CH, C-5); 30.7 (CH_2, C-6); 27.3 (CH_2, C-7); 82.4 (CH, C-8); 73.8 (CH, C-9); 33.5 (CH_2, C-10); 26.4 (CH_2, C-11); 44.7 (CH_2, C-12); 23.3 (CH_2, C-13); 14.1 (CH_3, C-14); 173.7 ($\underline{C}OCH_3$); 20.9 ($CO\underline{C}H_3$). HRESIMS: m/z 367.1871 $[M-H]^-$ (calcd. for $C_{16}H_{44}O_7P$ m/z 367.1880).

*Synthesis of compounds **49b** and **50b***

The same procedure used for **49a** and **50a** was adopted to obtain the mixture **49b**/**50b** (21.0 mg, 44%) starting from 50 mg (0.173 mmol) of compound **48b**. The mixture was purified by HPLC on reversed phase

(Synergy 4 μm Fusion column 250 mm x 4.6 mm and MeOH/H_2O 6:4 + 0.1% TFA as mobile phase, flow rate 1 mL/min) affording **49b** (13.4 mg, tR = 26.9 min) and **50b** (7.6 mg, tR = 27.6 min). Compound **49b** ^{1}H NMR (700 MHz, CD_3OD): ^{1}H NMR (CD_3OD): 0.91 (3H, t, J =7.0 Hz, H-1); 1.30 (2H, overlapped, H-2); 1.28 (1H, overlapped, H-3a); 1.30 (1H, overlapped, H-3b); 1.56 (2H, overlapped, H-4); 4.90 (1H, m, H-5); 1.65 (1H, overlapped, H-6a); 1.75 (1H, m, H-6b); 1.64 (1H, overlapped, H-7a); 1.66 (1H, overlapped, H-7b); 4.16 (1H, m, H-8); 3.66 (1H, m, H-9); 1.44 (1H, overlapped H-10a); 1.56 (1H, overlapped, H-10b); 1.33 (1H, overlapped, H-11a); 1.55 (1H, overlapped, H-11b); 1.33 (2H, overlapped, H-12); 1.34 (2H, overlapped, H-13); 0.91 (3H, t, J =7.1 Hz, H-14); 2.02 (3H, s, COC$\underline{H}_3$); ^{13}C NMR (CD_3OD): 14.0 (CH_3, C-1); 23.5 (CH_2, C-2); 28.5 (CH_2, C-3); 34.8 (CH_2, C-4); 75.1 (CH, C-5); 31.2 (CH_2, C-6); 27.1 (CH_2, C-7); 82.6 (CH,C-8); 73.4 (CH, C-9); 33.4 (CH_2, C-10); 26.5 (CH_2, C-11); 44.6 (CH_2, C-12); 23.4 (CH_2, C-13); 14.0 (CH_3, C-14); 173.1 ($\underline{C}OCH_3$); 20.8 ($CO\underline{C}H_3$). HRESIMS: m/z 367.1848 $[M-H]^-$ (calcd. for $C_{16}H_{44}O_7P$ m/z 367.1880); Compound **50b** ^{1}H NMR (700 MHz, CD_3OD): 0.91 (3H, t, J =7.0, H-1); 1.34 (2H, overlapped, H-2); 1.30 (1H, overlapped, H-3a); 1.33 (1H, overlapped, H-3b); 1.56 (2H, overlapped, H-4); 4.94 (1H, m, H-5); 1.71 (1H, overlapped, H-6a); 1.76 (1H, overlapped, H-6b); 1.71 (1H, overlapped, H-7a); 1.57 (1H, overlapped, H-7b); 3.71 (1H, m, H-8); 4.17 (1H, m, H-9); 1.39 (1H, overlapped H-10a); 1.52 (1H, overlapped, H-10b); 1.33 (1H, overlapped, H-11a); 1.53 (1H, overlapped, H-11b); 1.30 (2H, overlapped, H-12); 1.34 (2H, overlapped, H-13); 0.90 (3H, t, J =7.0 , H-14); 2.02 (3H, s, COC$\underline{H}_3$) ; ^{13}C NMR (CD_3OD): 14.0 (CH_3, C-1); 23.2 (CH_2, C-2); 28.3 (CH_2, C-3); 34.8 (CH_2, C-4); 74.9 (CH, C-5); 30.4 (CH_2, C-6); 26.4 (CH_2, C-7); 73.9 (CH,C-8); 81.7 (CH, C-9); 33.4 (CH_2, C-10); 26.4 (CH_2, C-11); 44.7 (CH_2, C-12); 23.3 (CH_2, C-13);

14.0 (CH_3, C-14); 172.7 ($\underline{C}OCH_3$); 20.8 ($CO\underline{C}H_3$). HRESIMS: m/z 367.1901 $[M-H]^-$ (calcd. for $C_{16}H_{44}O_7P$ m/z 367.1880).

4.5.2 Pharmacological assays on 47a-50b

Enzymatic Assays with PTP1B

An aliquot of human recombinant PTP1B (1–302) was added in the assay buffer (0.075 M β,β-dimethylglutarate pH 7.0 containing 1 mM EDTA, 0.1 mM DTT and a *p*-nitrophenylphosphate (p-NPP) (Chemcruz, Santa Cruz Biotechnology (Santa Cruz, CA, USA)). The reactions were performed at 37 °C in a final volume of 1 mL. After 30 min of incubation, the reactions were stopped adding 2 mL of 0.1 M KOH in each sample. The released amount of *p*-nitrophenol was determined by measuring the absorbance at 400 nm in a 1 cm pathlength cuvette [141].

AR Enzymatic Assay

The human recombinant AR, purified to electrophoretic homogeneity, was used as target enzyme. AR activity was determined at 37 °C as previously described by evaluating the decrease in absorbance at 340 nm linked to NADPH oxidation using a Biochrom Libra S60 spectrophotometer. 0.8 mM L-idose was used as substrate in the conditions described above, in the presence of 10 mU of enzyme and of a final concentration of DMSO of 0.7% (*v*/*v*). The standard assay mixture contained 0.25 M sodium phosphate buffer pH 6.8, 0.18 mM NADPH, 0.42 M ammonium sulfate, 0.5 mM EDTA and 4.7 mM D,L-glyceraldehyde. One unit of enzyme

activity is the amount that catalyses the conversion of 1 µmol of substrate/min in the above assay conditions [142] .

Determination of the IC_{50} Values and Reversibility Assay with PTP1B

The IC_{50} value of compounds against PTP1B was determined by measuring the hydrolysis rate of the enzyme in the presence of a fixed substrate concentration (2.5 mM p-NPP) and increasing inhibitor concentrations (generally 14–16 different concentrations). Each test was carried out in triplicate. Experimental data were normalized respect to control samples and then fitted using a non-linear fitting software, using the following equation:

$$\frac{V_i}{V_0} = \frac{Max - Min}{1 + \left(\frac{x}{IC_{50}}\right)^{slope}} + Min$$

where the Vi/V_0 value represents the relative activity calculated in presence of each inhibitor concentration; the maximum and minimum value of the activity are represented by "*Max*" and "*Min*", respectively; "*x*" is the concentration of the inhibitor; IC_{50} is the inhibitor concentration able to decrease the enzymatic activity up to 50%; "*slope*" represents the slope of the curve in the transition zone.

A dilution test was performed to verify if the compound behaves as reversible or irreversible inhibitor of PTP1B. An aliquot of the enzyme was diluted with different concentration of inhibitor and the samples incubated at 37 °C for 1 h. After this time, an aliquot of these samples was diluted 500 times in the assay buffer containing 2.5 mM p-NPP, to evaluate whether the enzyme is able to recover its activity since the final concentration of inhibitor is now far away from its IC_{50} value. Control test

was carried out diluting the enzyme with an equal volume of deionized water. All tests were performed in triplicate. Obtained data were normalized respect to the control experiment and reported in the figures as mean value +/− S.D.

Determination of the Mechanism of Inhibition on PTP1B

The inhibitory mechanism of tested compounds was determined evaluating the dependence between the main kinetics parameters (K_M and V_{max}) and the inhibitors concentrations. K_M and V_{max} values were calculated measuring the hydrolysis amount of PTP1B in the absence/presence of different inhibitor concentrations, while increasing substrate content. The obtained data were fitted using Michaelis-Menten equation and a non-linear fitting software. Then, data were analysed using the double reciprocal plot (Lineweaver-Burk method).

Cell Cultures

Murine myoblasts (C2C12) and human liver cells were purchased from the American Type Culture Collection (ATCC, Manassas, VA, USA). C2C12 cells were routinely cultured in Dulbecco's Modified Eagle's Medium (DMEM)-high glucose (4500 mg/L) supplemented with 10% Foetal Bovine Serum (FBS, Euroclone, Milan, Italy), 2 mM glutamine, 100 U/mL penicillin, and 100 μg/mL streptomycin (Sigma-Aldrich, St. Louis, MO, USA). Cells were incubated at 37 °C in humidified atmosphere with 5% CO_2. Myoblast differentiation was induced by adding differentiation medium (DMEM containing 2% horse serum) to 80% confluent myoblasts and incubating them for five days.

Insulin Signaling Pathway Analysis

C2C12 cells were plated on P35 dishes, grown until 80% confluence, and then incubated in the presence of differentiation medium (DMEM-high glucose (4500 mg/L) supplemented with 2% Horse serum (HS, Euroclone), 2 mM glutamine, 100 U/mL penicillin, and 100 μg/mL streptomycin) for 4 days. Then, cell plates were washed with PBS and cells stimulated with 10 nM insulin, compound **46** or insulin-compound **46** association for 30 min. After cell plates were washed with cold PBS solution and lysed using 1X Leammli sample buffer. Samples were store at 4 °C for 15 min and then protein solutions were collected and boiled for 5 min. Proteins were analysed by SDS-PAGE and then transferred on a PVDF membrane by western blot. Phosphorylation status of insulin receptor and the kinase Akt was evaluated using specific antibodies (pIR β subunit, Y1162/1163 (sc-25103-R) and β-actin, clone C-4 (sc-47778) were from Santa Cruz Biotechnology (Santa Cruz, CA, USA); IR β subunit, clone CT-3 (MABS65) was from Merck-Millipore (Burlington, MA, USA). Akt (9272S) and p-Akt (9271S) antibodies were from Cell Signalling Technology (Danvers, MA, USA). Secondary antibodies were from Santa Cruz Biotechnology (Santa Cruz, CA, USA). Detection was performed using Clarity western ECL substrates (Bio-Rad Laboratories, Inc.).

Glucose Uptake Assay

To evaluate glucose uptake, C2C12 cells were grown until 80% confluence and then incubated in starvation medium for 24 h. After this time, cells were stimulated with 10 nM insulin (Humalog Lispro, Eli Lilly), 20 μM compound **46** or **46**-insulin association for 30 min and then incubated in the presence of 40 μM of 2-NBDG (Invitrogen) for 3 h. Then,

cells were washed with PBS, tripsinized, pelleted by centrifugation (1000× *g* for 5 min), then suspended in 500 µL of PBS. The amount of 2-NBDG uploaded by cells was determined analysing cells by using a flow cytometer apparatus (FACSCanto II, BD Biosciences, San Jose, CA, USA). For each sample 1×10^4 events were acquired. Data obtained were then analysed with FlowJo software. Cells autofluorescence values were determined before sample analysis and subtracted to each sample.

Statistical Analysis

The results were expressed as mean ± SD. The differences between the experimental and control groups were compared using one way ANOVA followed by Tukey's HSD test for pairwise comparison. All statistical analyses were performed using OriginPro 8.0 2021 software. The *p* value < 0.05 was considered statistically significant. * $p < 0.05$; ** $p < 0.01$.

CHAPTER 5. Targeting human 15-lipoxygenase-1 with phosphoeleganin and its analogues

5.1 Human 15-lipoxygenase-1 (15-LOX-1): an emerging target for drug discovery

Lipoxygenases (LOXs) are a heterogeneous family of enzymes capable of oxidizing polyunsaturated fatty acids (PUFAs), such as arachidonic acid, linoleic acid and linolenic acid, into corresponding hydroperoxide derivatives that serves as lipid mediators responsible for metabolic variations during several physiopathological conditions. Lipoxygenases catalyze the insertion of molecular oxygen into PUFAs, at specific carbon positions, forming hydroperoxyeicosatetraenoic acids (HpETEs) which are further metabolized to further metabolized into 15S-hydroxyeicosatetraenoic acid (HETEs). The position of oxygen insertion changes among different isoforms of lipoxygenases, leading to the formation of different HPETE products. Then, several products of LOX pathway are subsequently converted to a large array of bioactive lipid mediators, which include leukotrienes, lipoxins, hepoxilins, eoxins, resolvins, protectins and others, usually involved in inflammatory process [143,144]. Traditionally, lipoxygenases have been classified based on the site of hydroperoxide group insertion into 5-LOX, 8-LOX, 11-LOX, 12-LOX, and 15-LOX, and on their location. However, the different LOX isoforms can have affinity for analogous substrates or high structural similarity and can be grouped together in a single class. This is the case with leukocytic 12-LOXs and reticulocyte 15-LOXs, enclosed in a large set (12/15-LOX) that also includes human 15-lipoxygenase-1 [145,146].

15-LOX-1 is presently a focal target in drug discovery due to the involvement of its products in several inflammation-based pathologies including asthma, chronic obstructive pulmonary disease (COPD), cancer, neurodegenerative diseases like Alzheimer's and Parkinson's diseases and hearth stroke [147,148]. In animal models, intradermal injection of 15S-HETE induces inflammatory-based symptoms, while 12S-HETE boosts the expression of pro-inflammatory cytokines and chemokines like IL-6 and TNF-α in macrophages. Moreover, a study demonstrated that the depletion of 12/15-LOX significantly reduce the risk of development of autoimmune T1DM in non-obese mice. In addition, preliminary studies demonstrate the involvement of both 12- and 15-LOX in the development of diabetes comorbidities such as retinopathy, nephropathy and neuropathy [149,150]. Probably, 15-LOX-1 acts with two different mechanistic pathways depending on the district in which the enzyme is located. Increased levels of 15-LOX-1 have been observed in the bronchial mucosa of patients affected of asthma and COPD. In fact, the enzyme is primarily expressed in airway district such as epithelial cells, eosinophils, and alveolar macrophages, contributing to the production of lipid mediator, including eoxins and other PUFAs metabolites. Generation of the inflammatory lipid-like mediators is followed by the production of proinflammatory cytokines that coordinate the inflammatory response [151]. Widely expressed in the central nervous system (CNS), 15-LOX-1 plays a pivotal role in the progression of neurodegenerative diseases. In fact, while in the airway 15-LOX-1 causes inflammation, in the CNS it can also promote apoptosis [152,153]. While the therapeutic potential of targeting 15-LOX-1 is promising, its precise role in other diseases remains under investigation. Nonetheless, its involvement in inflammatory pathways and lipid mediator production makes it an attractive target for

drug development in inflammatory and neurodegenerative diseases and cancer. Advancements in the understanding of the molecular mechanisms involving 15-LOX-1 have opened new avenues in drug discovery, emphasizing the modulation of its activity and metabolite production. In this view, inhibiting or modulating 15-LOX-1 could a promising strategy in managing inflammatory diseases, neurodegenerative disorders, and some cancer types [154]. Continuing the research into the molecular mechanisms associated with 15-LOX-1 will pave the way for novel therapeutic strategies aimed at managing inflammatory diseases and related disorders.

5.2 Targeting 15-LOX-1 with marine natural products

Several researchers demonstrated that targeting 15-LOX-1 with marine NPs may be a valuable approach not only to identify new classes of inhibitors but also to discover new mechanisms of inhibition [155]. First marine-derived 15-LOX-1 inhibitors discovered were polybrominated ethers **51**-**56** isolated from the sponge *Dysidea sp.* collected in Indo-Pacific Ocean. Compounds **51**-**55** exerted a strong inhibitory activity against 15-LOX with IC_{50} of 15, 2.5, 7.4, 7.4 and 1.3 μM, respectively while compound **56** promoted the 100% inhibition of the enzyme at 40 μM [156]. Two sesterpenes, isolated from the sponges *Jaspis splendens* and *Subea sp*., (-)-jaspic acid (**57**), (-)-subersic acid (**58**) and jaspaquinol (**59,** Figure 36), were classified as potent inhibitors of 15-LOX showing IC_{50} of 1.4 μM and 15 μM, respectively. However, compounds **57** was not selective against this enzyme isoform since they were capable to inhibit also human 12-LOX with IC_{50} of 0.7 ± 0.1. Similarly, puupehenone (**60**) and 21-chloropuupehenone (**61**, Figure 36), isolated from *Hyrtios sp.* were found out as potent but nonselective inhibitors of both human 12-

lipoxygenase (12-LOX) with an IC_{50} of 8.3 ± 1.7 and 0.7 ± 0.1 μM, respectively and 15-LOX with IC_{50} of 0.76 ± 0.1 and 0.8 ± 0.1 μM, respectively [155].

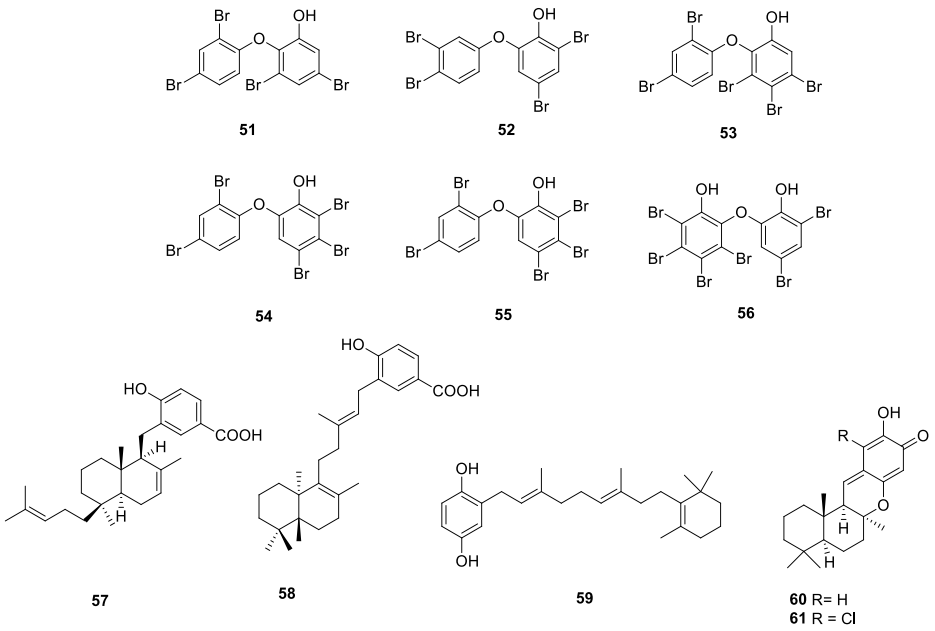

Figure 36. Structures of compounds **51**-**61**.

The bioprospecting of the marine sponge *Psammocinia sp*. led to the identification of chromarols A-E (**62**-**66**, Figure 37) as potent and selective inhibitors of human 15-LOX with IC_{50} values ranging from 0.6 to 4.0 μM. Moreover, from the same sample some meroterpenoids with non-selective inhibitory effect on 15-LOX were isolated [157].

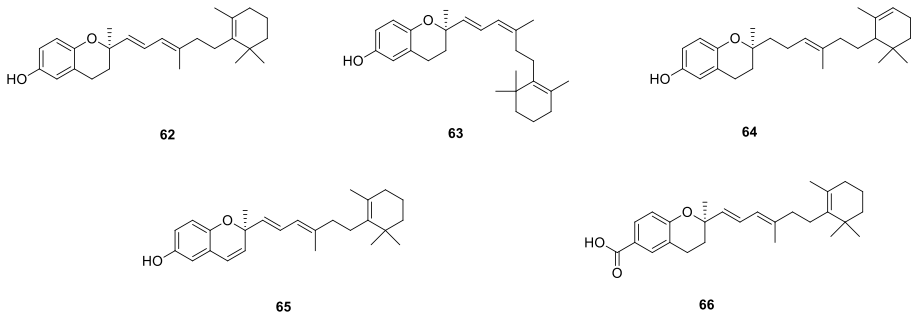

Figure 37. Structures of compounds **62**-**66**.

Among the few examples, a recent study concerns the evaluation of the activity of compounds isolated from a Red Sea brown alga, *Sargassum Cinereum.* Among them, aryl cresols (**67** and **68**, Figure 38) and 1-O-arachidonyl-3-O-(α-D-glucopyranosyl)glycerol (**69**, Figure 38) exhibited potent inhibitory activity against the 5-LOX enzyme and less inhibitory activity against the 15-LOX enzyme with IC_{50} values 25.3 ± 0.4 μM, 23.6 ± 0.3 μM and 6.7 ± 0.3 μM, respectively [158].

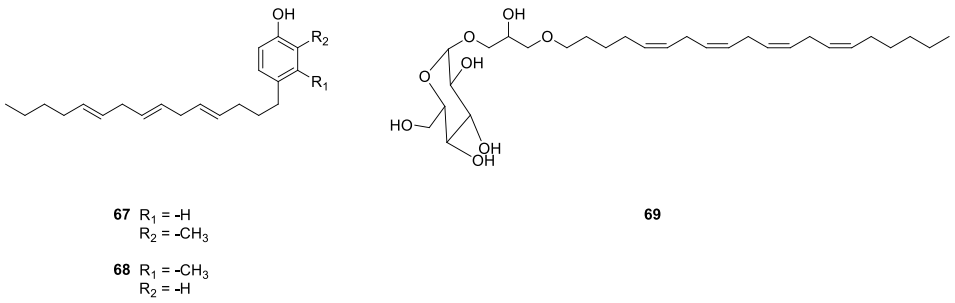

Figure 38. Structures of compounds **67**-**69**.

As can be observed from the examples of marine metabolites active on 15-LOX-1 reported, many inhibitors have a planar structure guaranteed by an aromatic or heteroaromatic scaffold. Many of the best-known inhibitors of the enzyme, including those of synthetic origin, belong to the class of

phenols which is associated with antioxidant and iron-chelating properties [159]. To increase the knowledge about aliphatic and chiral compounds, we decided to explore phosphoeleganin (**44**) chemical space for the inhibition of 15-LOX-1.

5.3 Pharmacological evaluation of phosphoeleganin (44) and its derivatives on 15-LOX-1

Based on the above, we have recognized in the structure of phosphoeleganin (**44**) many promising structural elements for a 15-LOX-1 inhibiting activity, such as a long aliphatic chain, hydroxy and phosphate groups, glycine head and several chiral centers. The interest in evaluating this marine metabolite also arose from the structural similarity with the substrates of 15-LOX, arachidonic acid and oleic acid. On this basis, compound **44** has been tested in collaboration with the research group of dr. Eleftheriadis for its modulation of 15-LOX-1 activity. The semisynthetic fragments **45** and **46,** which include the glycine and the phosphate warhead, respectively, and both contain the chiral substituted aliphatic, were screened, too. The 15-LOX-1 activity studies were performed using an established UV absorbance assay in a 96-well format, following the enzymatic product (234 nm) after its conversion from linoleic acid [160].

This screening revealed that phoshpoeleganin (**44**) exerted more than 70% of inhibition of 15-LOX-1 with an IC_{50} of 12.4 ± 1.2 μM at 50 μM (Figure 39B). It is noteworthy that, based on the latter result, phosphoeleganin (**44**) proves to be an interesting and promising multitarget agent, capable of interacting with as many as three targets involved in multifactorial diseases; moreover, it is the first and only marine phosphorylated polyketide inhibitor of the 15-LOX-1 enzyme, to date.

Interestingly, only phosphate-containing fragment **46** provided more than 70% of inhibition like the natural product at concentrations of 50 μM with a lower IC_{50} value of 4.6 ± 1.5 μM (Figure 39C), highlighting the phosphate motif as a key structural requirement for ensuring pharmacological activity (unpublished results).

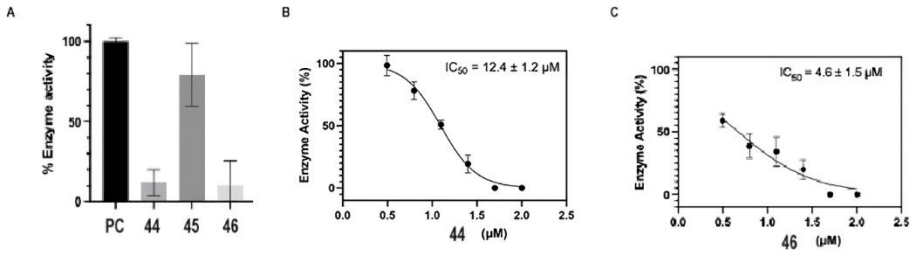

Figure 39. Preliminary screening assay of **44-46** on h-15-LOX-1 (**A**). All assays were started by diluting an aliquot of h-15-LOX-1 in the assay solution containing substrate alone (control test) or substrate and an aliquot of each compound (50 μM, final concentration). The enzyme activity was determined by measuring the amount of 13S-hydroperoxy-9Z,11E-octadecadienoic acid (13(S)-HpODE) converted from linoleic acid in each sample using a spectrophotometer at 234nm. Determination of the IC_{50} values with compounds **44** and **46** (**B**). An aliquot of h-15-LOX-1 enzyme was diluted in the presence of increasing concentration of the compounds. The activity of h-15-LOX-1 was determined by measuring the absorbance of the sample at 254 nm, using a spectrophotometer.

5.4 Generating regiochemical and stereochemical diversity within a phosphorylated fragments library: synthesis of compounds 71-72

Acknowledged the importance of phosphate group in the inhibition of 15-LOX-1, we have decided to create a new chemical library of fragment-like SMs endowed with phosphate group. The library, which included the previously mentioned compounds **49a-50b**, aims to increase is characterized by both regiochemical and stereochemical diversity of

phosphorylated fragments in order to investigate the influence of phosphate group position along the aliphatic chain of tetradecan-5,8,9-triol scaffold and its spatial orientation. In this view, new derivatives in which the phosphate group was introduced on the isolated hydroxyl group were synthesized, starting from the (5*S*,8*S*,9*R*)-tetradecan-5,8,9-triol. The synthetic protocol was developed involving the same reactions used in the previous one for the synthesis of **47a-50b** derivatives (Scheme 3) [110] and involves the synthesis of acetonide as the protecting group followed by the introduction of the phosphate group through the method proposed by Lira and coworkers [140]. (5*S*,8*S*,9*R*)-tetradecan-5,8,9-triol (**47a**) was treated with 2,2-dimethoxypropane and a catalytic amount of p-toluensolfonic acid as previously described in Chapter 2 to obtain compound **51a** in pure form and quantitative yield. Then, the acetonide derivative **51a** was dissolved in acetonitrile and treated with trichloroacetonitrile, followed by dropwise addition of a solution of tetrabutylammonium dihydrogen phosphate ($(n\text{-}Bu)_4NH_2PO_4$) in acetonitrile. The reaction was kept under magnetic stirring at room temperature for 16 h and, after the solvent removal *in vacuo*, compound **70** was obtained. At this point, the acetonide derivative **70** was directly hydrolyzed in acidic conditions (HCl 1%). The reaction mixture was kept at 4°C for 36 h before removing the solvent by rotary evaporator. The raw material was purified by HPLC on reversed phase (Luna 5 μm C-18 column 250 mm x 4.6 mm and MeOH/H_2O 75:25 + 0.1% TFA as mobile phase, flow rate 1 mL/min) to isolate the phosphorylated product **71** in pure form and excellent yield as a colorless oil. Finally, the phosphorylated product **71** was dissolved in pyridine and treated with an excess of acetic anhydride. The reaction mixture was stirred for 18h at ambient temperature and then, the excess of acetic anhydride was removed by

cooling the reaction mixture at 0°C in an ice-bath and adding of MeOH to the mixture. The solvent removal in vacuo afforded the raw material which was purified by HPLC on reverse phase (Luna 5 μm C18 column 205 mm x 4.6 mm and MeOH/H_2O 9:1 + 0.2% TFA as mobile phase, flow rate 1 mL/min) to afford 72 in pure form as a colourless oil.

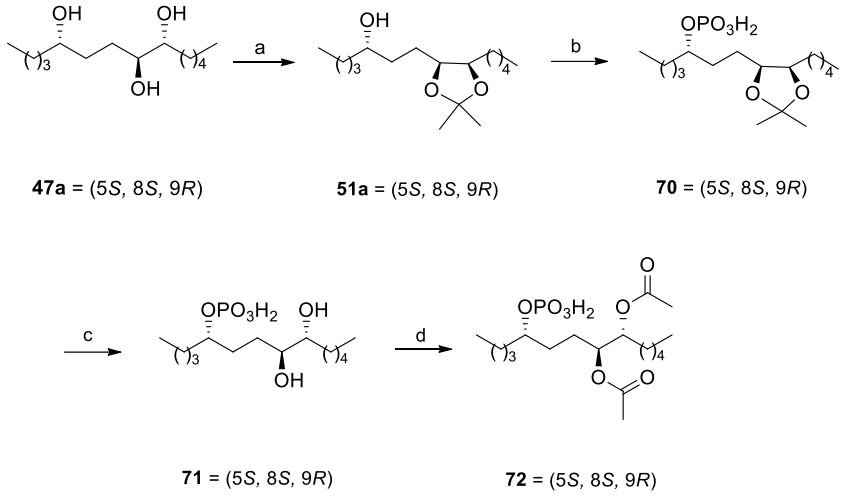

Scheme 3. Reagents and conditions: (**a**) 2,2-dimethoxypropane, *p*-toluenesulfonic acid, r.t. overnight. (**b**) (1) Cl_3CCN; (2) $(n\text{-}Bu)_4NH_2PO_4$, CH_3CN, r.t. overnight. (**c**) (1) HCl 1%, MeOH/H_2O 9:1, r.t. overnight; (**d**) (1) Ac_2O, pyridine, r.t.18 h

Then, library will be further enriched with the diasteroisomers of compounds **71-72**, starting from (5*R*,8*S*,9*R*)-tetradecan-5,8,9-triol and adopting the overmentioned synthetic protocol.

5.5 Materials and methods

*Synthesis of compound **71***

55 mg (0.192 mmol) of **6** were dissolved in 12.0 mL of acetonitrile and treated with 57 μL (0.57 mmol) of trichloroacetonitrile, following by dropwise addition of 130 mg (0.384 mmol) of tetrabutylammonium dihydrogenphosphate, previously solubilized in 4.0 mL of acetonitrile. The reaction was kept under magnetic stirring at room temperature for 16 h and the solvent removal in vacuo afforded compound **70** which was directly hydrolyzed. The raw material was dissolved in 10 mL of MeOH/H_2O (9:1) and 150 μL of HCl 37% (p/p) were added dropwise to the mixture. The reaction mixture was kept at 4°C for 36 h before removing the solvent by rotary evaporator. The organic layer was purified by HPLC on reversed phase (Luna 5 μm C-18 column 250 mm x 4.6 mm and MeOH/H_2O 75:25 + 0.1% TFA as mobile phase, flow rate 1 mL/min) to isolate the phosphorylated product **71** in a pure form as a colorless oil (21.9 mg, tR = 12.1 min). ^{1}H NMR (700 MHz, CD_3OD): 0.91 (3H, overlapped, H-1); 1.36 (2H, overlapped, H-2); 1.38 (1H, overlapped, H-3a); 1.34 (1H, overlapped, H-3b); 1.64 (1H, overlapped, H-4); 4.29 (1H, m, H-5); 1.89 (1H, overlapped, H-6a); 1.62 (1H, overlapped, H-6b); 1.78 (1H, m, H-7a); 1.41 (1H, overlapped, H-7b); 3.35 (1H, overlapped, H-8); 3.38 (1H, m, H-9); 1.61 (1H, overlapped, H-10a); 1.36 (1H, overlapped, H-10b); 1.36 (2H, overlapped, H-11); 1.55 (2H, overlapped, H-12a); 1.44 (1H, overlapped, H-12b); 1.35 (2H, overlapped, H-13); 0.91 (3H, overlapped, H-14). ^{13}C NMR (145 MHz, CD_3OD): 14.2 (CH_3, C-1); 23.5 (CH_3, C-2); 28.1 (CH_2, C-3); 35.9 (CH_2, C-4); 79.9 (CH, C-5); 44.5 (CH_2, C-6); 29.0 (CH_2, C-7); 75.9 (CH, C-8); 75.7 (CH, C-9); 44.9 (CH_2, C-10); 23.9 (CH_2, C-11); 26.5 (CH_2, C-12); 23.6 (CH_2, C-13); 14.0 (CH_3, C-14); 172.1 (C, C-1'); 20.7 (CH_3, C-2'), 172.2 (C, C-3'), 20.7 (CH_3, C-4').

*Synthesis of compound **72***

11.9 mg (0.036 mmol) of the phosphorylated product **17** was dissolved in 3.0 mL of pyridine, treated with an excess of acetic anhydride and the resultant mixture was stirred for 18h at room temperature. During this time, the reaction was monitored by TLC until the starting material was disappeared. Then, the excess of acetic anhydride was removed by cooling the reaction mixture at 0°C in an ice-bath and adding ~15 mL of MeOH. The solvent removal in vacuo afforded compound the raw material which was purified by HPLC on reverse phase (Luna 5 μm C18 column 205 mm x 4.6 mm and MeOH/H_2O 9:1 + 0.2% TFA as mobile phase, flow rate 1 mL/min) to afford a colourless oil (14.5 mg, 98%, tR = 3.92 min). ^{1}H NMR (700 MHz, CD_3OD): 0.93 (3H, overlapped, H-1); 1.36 (2H, overlapped, H-2); 1.38 (2H, overlapped, H-3); 1.64 (1H, overlapped, H-4a); 1.60 (1H, overlapped, H-4b); 4.24 (1H, m, H-5); 1.68 (1H, overlapped, H-6a); 1.56 (1H, overlapped, H-6b); 1.80 (1H, m, H-7a); 1.66 (1H, overlapped, H-7b); 4.94 (1H, overlapped, H-8); 5.00 (1H, m, H-9); 1.58 (2H, overlapped, H-10); 1.36 (1H, overlapped, H-11a); 1.28 (1H, overlapped, H-11b); 1.29 (1H, overlapped, H-12a); 1.33 (1H, overlapped, H-12b); 1.35 (2H, overlapped, H-13); 0.91 (3H, overlapped, H-14); 2.03 (6H, s, H-2', H-3'). ^{13}C NMR (145 MHz, CD_3OD): 14.1 (CH_3, C-1); 23.6 (CH_3, C-2); 27.8 (CH_2, C-3); 35.9 (CH_2, C-4); 79.1 (CH, C-5); 44.1 (CH_2, C-6); 25.6 (CH_2, C-7); 75.4 (CH, C-8); 75.0 (CH, C-9); 29.9 (CH_2, C-10); 26.1 (CH_2, C-11); 44.4 (CH_2, C-12); 23.6 (CH_2, C-13); 14.0 (CH_3, C-14); 172.1 (C, C-1'); 20.7 (CH_3, C-2'), 172.2 (C, C-3'), 20.7 (CH_3, C-4').

CHAPTER 6. Synthesis of a second-generation library inspired to phosphoeleganin

6.1 Design and synthesis of compounds 73a-75b

A new small library of fragments was designed, based on the principles of FBDD and DOS, to better investigate the structural requirements necessary to guarantee the antidiabetic and anti-inflammatory properties that phosphoeleganin (**44**) is endowed with. To this aim, also the SARs of bioactive fragments belonged to the first-generation library have been taken in consideration. In particular, the phosphate moiety appears to be an essential structural motif for both PTP1B and 15-LOX-1 inhibition. Furthermore, considering the importance of the entire structure of **44** in the inhibition of the AR enzyme [109], the approach envisages the introduction of glycine head at the end of the alkyl chain into the new SMs. To further simplify the new molecules from those synthesized previously **49a-50b**, one chiral center has been removed resulting in only two chiral centers corresponding to the *anti*-1,2-monophosphotylated diol system also present within the natural model **44**. Moreover, both the relevance of the length of the linear aliphatic scaffold and the position of the diol system along the chain will be investigated. Following, the principles of DOS, a versatile and easy to perform protocol have been developed to generate both pairs of stereoisomers of the 1,2-*anti* diols to investigate the importance of the correct spatial arrangement of the substituents. To achieve this aim, monounsaturated acids equipped with a double bond in Z configuration that are commercially available or easily obtainable by oxidation of the corresponding aldehyde or by hydrolysis of the corresponding methyl ester were used as building blocks. Carboxylic acids with 10, 18 and 22 carbon atoms with a Z-configuration double bond at

different positions were chosen to provide SARs on this structural motif. Moreover, the carboxylic acid moiety is necessary for the introduction of the glycine head. Furthermore, in accordance with the natural model and bioactive phosphorylated fragments, the phosphate group will then be introduced onto the diol system. Once the enantiopure compounds **73a-75b** (Figure 40) are obtained, the same phosphorylation reaction used previously will also be conducted on these substrates to, thus, obtain the two regioisomers in which the phosphate is inserted onto both hydroxyl groups of the *anti*-1,2-diol system. In this way, the importance of the position of the phosphate group in ensuring the desired pharmacological activity can be verified.

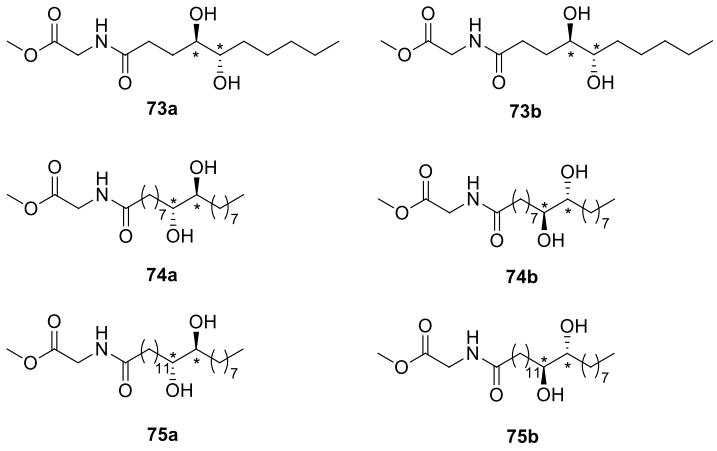

Figure 40. Structures of *anti*-1,2-diols **73a-75b**

The synthetic protocol adopted for the synthesis of diols **73a** and **73b** involved the use of *Z*-4-decenal as starting materials (Scheme 4). Specifically, *Z*-4-decenal was added slowly and dropwise to a 10% sodium hydroxide aqueous solution at rt and under electromagnetic stirring. After 3 hours, the reaction mixture is filtered and subsequently acidified with a

1N HCl solution. The resulting aqueous phase was extracted three times with ethyl acetate, and, subsequently, the solvent was removed under vacuum to obtain *Z*-4-decenoic acid in a form sufficiently pure for the next reaction step. An aliquot of *Z*-4-decenoic acid is dissolved in dry dichloromethane and glycine methyl ester and 4-dimethylaminopyridine (4-DMAP) were added to the resulting reaction mixture under stirring at room temperature. After 30 minutes, the coupling EDC hydrochloride was added to the reaction mixture and the resulting reaction mixture was kept at room temperature and under stirring overnight. Afterwards, the reaction was interrupted with the addition of a 1N HCl solution and then extracted three times with dichloromethane to obtain, after the removal of the solvent under vacuum, compound **76** in pure form and in quantitative yield. Finally, compound **76** was solubilized in a 9:1 acetone/H_2O mixture at room temperature and then solution of OsO_4 (1%) was then added to the reaction mixture, together with NMO. After 24 hours, the reaction was quenched with a saturated aqueous solution of NH_4Cl and then extracted with ethyl acetate to provide an enantiomeric mixture of **73a/b** in quantitative yield. The enantiomeric mixture was subsequently chromatographed using a 5 μm Lux cellulose-1 chiral column using a 95:5 (v/v) hexane/isopropanol mixture as mobile phase to obtain, in pure form, diols **73a** and **73b**.

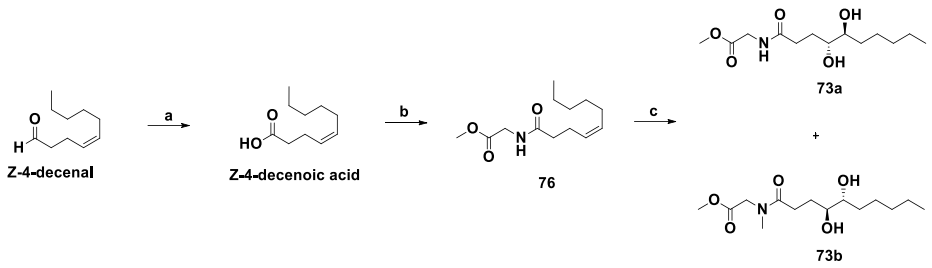

Scheme 4. Reagents and conditions: (**a**) Ag_2O, NaOH (10%), H_2O, rt, 3h. (**b**) Glycine-OMe, EDC, 4-DMAP, DCM, rt, overnight. (**c**) OsO4 1%, Acetone/H2O 9:1, rt, overnight.

The synthetic protocol adopted for the synthesis of diols **74a** and **74b** involved oleic acid as starting material (Scheme 5). Starting from an aliquot of oleic acid, the synthesis of compound **77** was carried out through the same procedure used to obtain compound **76**. Similarly, starting from compound **77**, the enantiomeric mixture of diols **74a**/**b** is obtained using the same procedure used to obtain the enantiomeric mixture of diols **73a/b**. To simplify the chromatographic separation of the racemic mixture, mixture **74a**/**b** were derivatized in the corresponding acetonide to make the molecule more rigid. In particular, 2,2-dimethoxypropane was added in large excess to the enantiomeric mixture, together with a spatula tip of p-toluenesulfonic acid. The reaction was left under electromagnetic stirring and at room temperature overnight. After this time, a saturated aqueous solution of $NaHCO_3$ was added to the reaction mixture and the partition with ethyl acetate was subsequently carried out. After the solvent removal in *vacuo*, the acetonide of the racemic mixture **78a/b** was obtained. The mixture, then, was subjected to chiral chromatographic separation to obtain the enantiopure compound **78a** and **78b**. At this point, the two acetonide derivatives were separately treated with 1% HCl solution obtaining diols **74a** and **74b**.

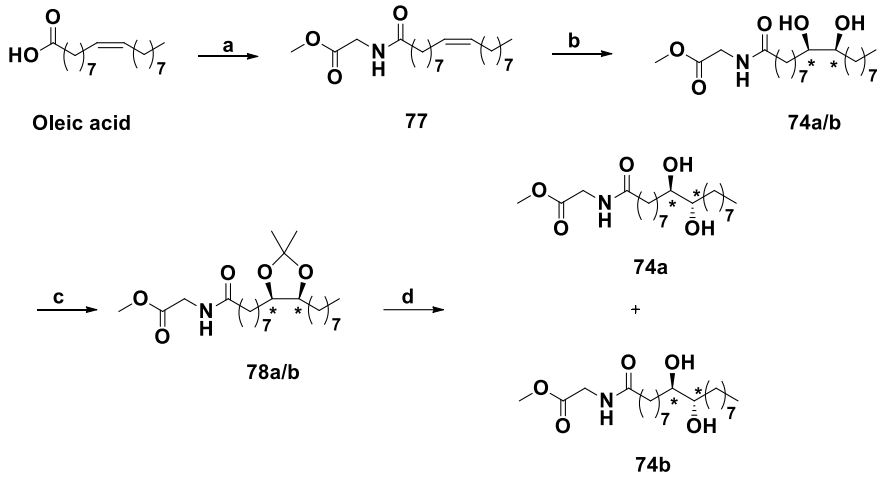

Scheme 5. Reagents and conditions: (**a**) Glycine-OMe, EDC, 4-DMAP, DCM, rt, overnight. (**b**) OsO4 1%, NMO, Acetone/H_2O 9:1, rt, overnight. (**c**) 2,2-dimethoxypropane, p-toluenesulfonic acid, rt, overnight. (**d**) 1% HCl, MeOH/H_2O 9:1, rt, overnight.

The synthetic protocol adopted for the synthesis of diols **75a** and **75b** involves the use of methyl erucate as starting material (Scheme 6).

In particular, an aliquot of methyl erucate is dissolved in THF under stirring and subsequently, a 25% aqueous solution of NaOH is added to the reaction. The resulting mixture was kept under reflux stirring throughout the night, after which it is partitioned between NH_4Cl and ethyl acetate to afford erucic acid in quantitative yield. Starting from an aliquot of erucic acid, the synthesis of compound **79** was carried out through the same procedure used to obtain compound **76**. Similarly, starting from compound **79**, the enantiomeric mixture of diols **75a** and **75b** was afforded using the same procedure used to obtain the enantiomeric mixture of diols **73a-73b**. To simplify the chromatographic separation of the racemic

mixture, the compounds of diol nature were derivatized in the corresponding acetonide, following the procedure previously described for diols **74a/b**. The acetonide of the racemic mixture **80a/b** was then subjected to chiral chromatographic separation and the enantiopure compounds **80a** and **80b** were separately treated with 1% HCl solution obtaining compounds **75a** and **75b**.

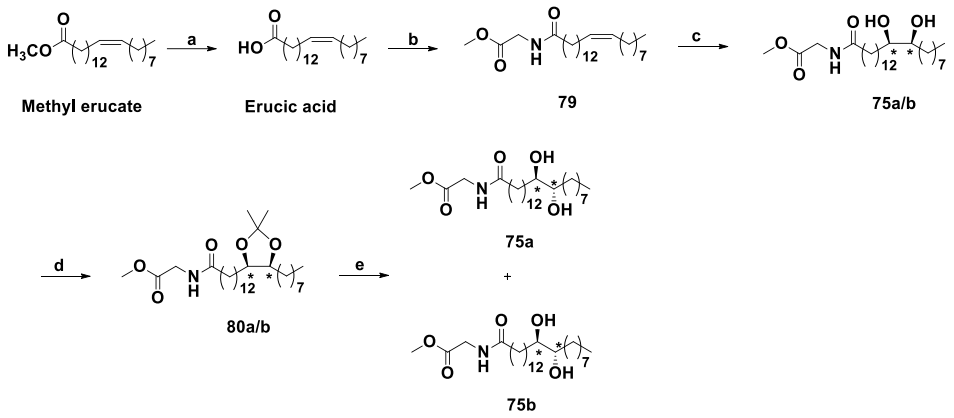

Scheme 6. Reagents and conditions: (**a**) THF, NaOH 25%, reflux, overnight. (**b**) Glycine-OMe, EDC, 4-DMAP, DCM, rt, overnight. (**c**) OsO4 1%, NMO, Acetone/H_2O 9:1, rt, overnight. (**d**) 2,2-dimethoxypropane, p-toluenesulfonic acid, rt, overnight; (**e**) HCl 1%, MeOH/H_2O 9:1, rt, overnight.

6.2 Determination of the absolute configurations of diols 73a-75b

The double derivatization method proposed by *Riguera* research group for the assignment of the configuration of sec-1,*n*-diols [104]was applied for the previously synthesized diols **73a**-**75b**. Precisely, 1,2-*anti*-diol are obtained from the reaction of *Z*-double bond of each chosen starting materials with osmium tetroxide since the reaction is both stereoselective and stereospecific. Therefore, we made a slight modification of the

standard method since the preparation of the esters of the other diol of the enantiomeric pair was not necessary because of the stereoselective nature of reaction used to obtain the 1,2-diol system. At this point, from the configuration of the derivatized diol, the configuration of the other can be deduced. Each enantiomer of the pair was esterified separately with both (*R*)- and (*S*)-MPA, and then ^{1}H NMR spectra of the obtained diasteroisomers were recorded. It can be observed that the MPA affects the chemical shift value of each proton differently depending on the tridimensional structure of the diol and the absolute stereochemistry of the auxiliary reagent used. Consequently, the observed $\Delta\delta^{RS}$ are the result of the additive shielding/deshielding effect imparted by the substituents of the introduced chiral agent. In our case, we proceed with the structural characterization of the bis esters thus assigning the chemical shift value to each proton of the derivatives and the calculation of $\Delta\delta^{RS}$ was performed. After the evaluation of $\Delta\delta^{RS}$ between the bis esters it is possible to apply the models developed by *Riguera* (Figure 41) in which the ligands of the stereogenic center are distributed with positive values on one side and the one with negative values on the opposite side. In this way, the absolute stereochemistry for each chiral carbon can be defined.

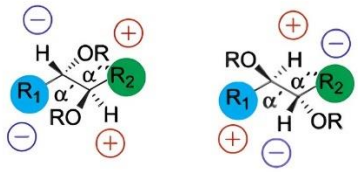

Figura 41. Proposed models for the assignment of the absolute configuration of anti-1,2-diols.

6.2.1 Structural characterization of diols 73a-73b

Following the approach proposed by Riguera's group, the diol **73b** was subjected to double derivatization with (*R*)- and (*S*)-MPA. Specifically, two aliquots of the selected diol were separately solubilized in dichloromethane, and (*R*)-MPA and (*S*)-MPA were added to the mixture, followed by DMAP and EDC. The reaction was kept at rt and under stirring overnight to obtain diester-(*R*)-MPA and diester-(S)-MPA of **73b** (Scheme 7).

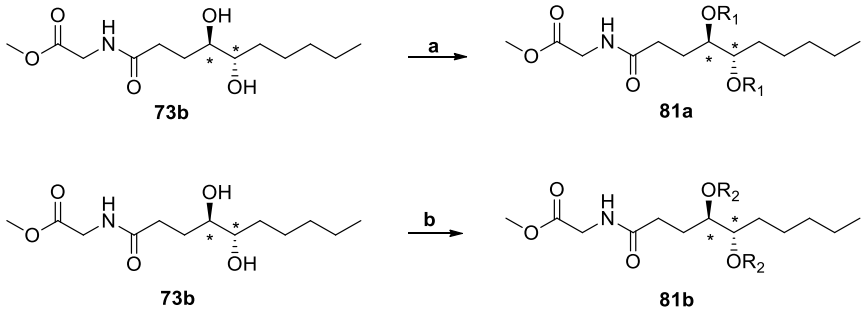

Scheme 7. Reagents and conditions: (**a**) EDC, DMAP, (*R*)-MPA, CH_2Cl_2, rt. overnight, R_1 = (*R*)-MPA; (**b**) EDC, DMAP, (*S*)-MPA, CH_2Cl_2, rt. overnight, R_2= (*S*)-MPA.

The (*R*)- and (*S*)-MPA derivatives **81a-81b** were purified by HPLC, and mono and bi-dimensional NMR spectra were recorded to fully characterize them (Table 2 and Table 3). Based Riguera's method, the proton chemical shift differences $\Delta\delta^{RS}$ (δ_H-81a-δ_H-81b) in the obtained **81a-81b** compounds were calculated (Figure 42).

Table 2. ^{1}H (700 MHz) and ^{13}C NMR (125 MHz) data of compound **81b** recorded in chloroform-d.[a]

81a		
Pos.	**δ_H**	**δ_c[b]**
1	-	171.1
2a	1.46, ovl, 1H	30.1
2b	1.35, ovl, 1H	
3a	1.77, m, 1H	22.5
3b	1.35, ovl, 1H	
4	4.70, dt, 1H	73.6
5	5.23, m, 1H	73.7
6	1.52, ovl, 2H	29.7
7	1.24, ovl, 2H	24.5
8	1.44, ovl, 2H	21.9
9	1.25, ovl, 2H	21.9
10	0.85, t (*J*=7Hz), 3H	13.5
1'a	3.86, dd (*J*=5.5Hz, 18.5Hz), 1H	40.1
1'b	3.75, dd (*J*=5.5Hz, 18.5Hz), 1H	
2'	-	170.2
-NH	6.50, brt	5.02
-OCH_3	3.75, s, 3H	51.9

[a]δ_H and δ_C values are referred to the deuterated solvent chloroform-d (δH= 7.26 ppm and δC = 77.0 ppm). [b]δ_C values for compound **81a** were assigned by HSQC correlation analysis.

Table X. ^{1}H (700 MHz) and ^{13}C NMR (125 MHz) data of compound **81b** recorded in chloroform-d.[a]

81b		
Pos.	**δ_H**	**δ_c[b]**
1	-	171.4
2a **2b**	2.17, m, 1H 2.13, ovl, 1H	31.7
3a **3b**	1.95, m, 1H 1.86, ovl, 1H	25.5
4	5.08, dt, 1H	73.6
5	4.80, dt, 1H	74.3
6a **6b**	1.13, m, 1H 1.08, m, 1H	28.1
7a **7b**	0.65, m, 1H 0.57, m, 1H	23.7
8a **8b**	0.84, m, 1H 0.78, m, 1H	30.8
9	0.94, m, 2H	21.9
10	0.68, t (*J*=7.5Hz)	13.4
1'	4.0, dd (*J*=2.0Hz, 5.0 Hz), 2H	40.9
2'	-	169.9
-NH	5.94, brt, 1H	5.94
-OCH_3	3.76, s, 3H	52.0

[a]δ_H and δ_C values are referred to the deuterated solvent chloroform-d (δH= 7.26 ppm and δC = 77.0 ppm). [b]δ_C values for compound **81b** were assigned by HSQC correlation analysis.

By distributing the substituents around the chiral center according to the models proposed by Riguera's method previously mentioned, it is possible to define the correct orientation of the hydroxyl groups and, subsequently, the descriptor of each chiral Cα center. The calculated $\Delta\delta^{RS}$ values then made it possible to apply the model proposed by Riguera and define the absolute stereochemistry of compound **73b**. Specifically, compound **73b** has absolute configuration 4*S*,5*R* and, consequently, compound **73a** 4*R*,5*S* (Figure 42).

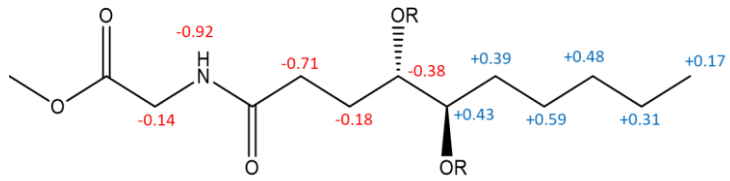

Figure 42. $\Delta\delta^{RS}$ sign distribution patterns for the MPA esters of the pairs **81a/81b**.

6.2.2 Structural characterization of diols 74a-74b

According with the approach used for the previous pair of diols, the diol **74a** was subjected to double derivatization with (*R*)- and (*S*)-MPA (Scheme 8).

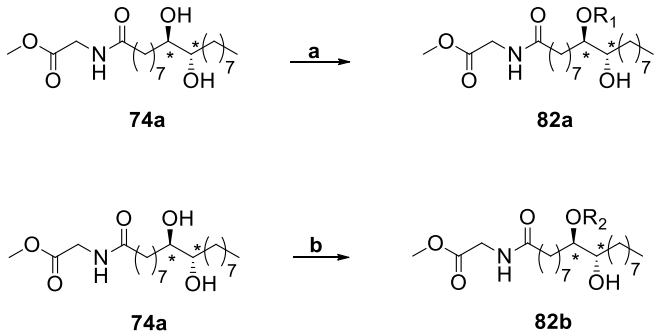

Scheme 8. Reagents and conditions: (**a**) EDC, DMAP, (*R*)-MPA, CH_2Cl_2, rt. overnight, R_1= (*R*)-MPA; (**b**) EDC, DMAP, (*S*)-MPA, CH_2Cl_2, rt. overnight, R_2= (*S*)-MPA

Similarly to the previous case, the (*R*)- and (*S*)-MPA derivatives obtained **82a**-**82b** were purified by HPLC. Mono and bi-dimensional NMR spectra were recorded for their complete characterization (Tables 4 and 5) and the proton chemical shift differences $\Delta\delta^{RS}$ (δ_H-**82a**-δ_H-**82b**) were calculated (Figure 43).

Table 4. ^{1}H (700 MHz) and ^{13}C NMR (125 MHz) data of compound **82a** recorded in chloroform-d.[a]

	82a	
Pos.	**δ_H**	**δ_c[b]**
1	-	172.9
2	2.19, t (*J*=8.0 Hz), 2H	36.0
3	1.55, ovl, 2H	25.1
4	1.11, m, 2H	28.6
5a	0.92, ovl, 1H	28.4
5b	0.84, ovl, 1H	
6a	0.86, ovl, 1H	28.5
6a	0.79, ovl, 1H	
7a	0.64, m, 1H	24.0
7b	0.56, m, 1H	
8a	1.12, ovl, 1H	27.5
8b	1.06, ovl, 1H	
9	4.75, ovl, 1H	74.4
10	5.12, m, 1H	74.3
11	1.48, ovl, 2H	30.0
12	1.24, ovl, 2H	28.8

13	1.22, ovl, 2H	25.0
14	1.24, ovl, 2H	28.7
15	1.26, ovl, 2H	24.9
16	1.23, ovl, 2H	31.5
17	1.29, ovl, 2H	22.3
18	0.88, t, (*J*=7.5 Hz), 3H	13.8
1'	4.06, d (*J*=5.0 Hz), 2H	40.7
2'	-	170.4
-NH	5.95, brt	-
-OCH_3	3.77, s, 3H	51.8

[a]The δ_H and δ_C values are referred to the deuterated solvent chloroform-d (δ_H= 7.26 ppm and δ_C = 77.0 ppm). [b]The δ_C values for compound **82a** were assigned by HSQC correlation analysis.

Table 5. ^{1}H (700 MHz) and ^{13}C NMR (125 MHz) data of compound **82b** recorded in chloroform-d.[a]

82b		
Pos.	**δ_H**	**δ_c[b]**
1	-	172.9
2	2.23, t (*J*=7.5 Hz), 2H	35.8
3	1.63, ovl, 2H	25.1
4	1.29, ovl, 2H	28.5
5	1.23. ovl, 2H	24.9
6	1.24, ovl, 2H	28.7
7	1.26, ovl, 2H	25.1

8	1.47 ovl, 2H	29.8
9	5.13, m, 1H	74.2
10	4.73, ovl, 1H	74.6
11a	1.10, ovl, 1H	27.5
11b	1.05, ovl, 1H	
12a	0.62, m, 1H	24.1
12b	0.54, m, 1H	
13a	0.89, ovl, 1H	28.6
13b	0.79, m, 1H	
14a	0.91, ovl, 1H	28.6
14b	0.83, ovl, 1H	
15	1.06, m, 2H	28.3
16	1.16, q, 2H	31.5
17	1.26, ovl, 2H	22.0
18	0.88, t, (*J*=7.5 Hz), 3H	13.8
1'	4.06, d (*J*=5.0 Hz), 2H	40.7
2'	-	170.1
-NH	6.01, brt	-
-OCH_3	3.76, s, 3H	51.8

[a]The δ_H and δ_C values are referred to the deuterated solvent chloroform-d (δ_H= 7.26 ppm and δ_C = 77.0 ppm). [b]The δ_C values for compound **82b** were assigned by HSQC correlation analysis.

The calculated $\Delta\delta^{RS}$ values allowed to apply the model proposed by Riguera and define the absolute stereochemistry of compound **74b**. Specifically, compound **74b** has absolute configuration 9*S*,10*R* and, consequently, compound **74a** 9*R*,10*S* (Figure 43).

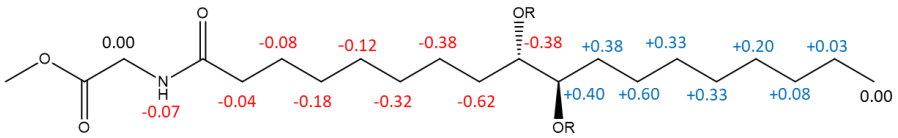

Figure 43. $\Delta\delta^{RS}$ sign distribution patterns for the MPA esters of the pairs **82a/82b**.

6.2.3 Structural characterization of diols 75a-75b

Concerning the characterization of the absolute stereochemistry of diols **75a-75b**, we assumed that it was not necessary to resort to double derivatization with MPA. In fact, these diols are structurally similar to compounds **74a** and **74b**, showing just slight differences regarding the carbon chain length and the position of the diol system. The structural similarity between the pair **74a**/**74b** and **75a**/**75b** can also be appreciated in the conditions for chromatographic separation of the corresponding acetonide derivatives, which are almost superimposable. Precisely, in both cases the enantiomeric pairs were eluted using the same chiral column and mobile phase. On this basis, we decided to assume that diols **75a** and **75b** possess the same absolute stereochemistry as diols **74a** and **74b**, respectively.

6.3 Materials and methods

Synthesis of Z-decenoic acid

The first synthetic step involves the preparation *in situ* of Z-4-decenoic acid from Z-4-decenal. To an aqueous solution of NaOH (10%), 765 mg of Ag_2O were added at room temperature, and then 500 μL (2.74 mol) of

Z-4-decenal were added dropwise to the reaction mixture, which was kept under electromagnetic stirring at the same temperature for 3 hours.
The reaction mixture was then filtered and, subsequently, acidified with a 1N HCl solution. The aqueous phase was extracted three times with ethyl acetate, and then the resulting organic layer was dried with sodium sulfate, filtered, and the solvent is removed under vacuum to Z-4-decenoic acid (400 mg, 85 % yield) in a sufficiently pure form for the next reaction step.

*Synthesis of compound **76***

An aliquot of 120 mg of the Z-4-decenoic acid was dissolved in 10 mL of dry dichloromethane, and 130 mg (1.05 mmol) of glycine methyl ester were added to the resulting reaction mixture at room temperature. Then, 260 mg (2.11 mmol) of 4-DMAP and, after 30 minutes, 200 mg (1.05 mmol) of 3-(3- dimethylaminopropyl) carbodimine (EDC) chlorohydrate were added to the reaction mixture. The resulting reaction mixture is kept at room temperature and under stirring overnight. After that, the reaction was quenched by the addition of 20 ml of an aqueous solution of HCl 1N and then extracted three times with dichloromethane to obtain, after removal of the solvent under vacuum, compound **76** (150mg) as yellowish oil, in pure form and in quantitative yield.
Compound **76** ^{1}H NMR ($CDCl_3$, 400 MHz) values: δ 6.34 (bs, 1H), 5.33 (m, 2H), 3.97 (m, 2H), 3.68 (s, 3H), 2.44 (m, 2H), 2.24 (m, 2H), 1.97 (m, 2H), 1.97 (m, 2H), 1.30-1.21 (ovl, 6H), 0.82 (t, J = 7 Hz, 3H). ^{13}C NMR ($CDCl_3$, 125 MHz): δ 172.8, 170.5, 131.6, 127.4, 53.3, 41.1, 36.1, 31.4, 29.3, 27.1, 23.2, 22.5, 14.0.

*Synthesis of diols **73a-73b***

At this point, 100 mg of compound **76** were dissolved in a 9:1 acetone/H_2O mixture at room temperature. A 1 % solution of OsO4 (5 mol%) together with 64.2 mg (0.550 mmol) of N-methylmorpholine oxide (NMO) were then added to the reaction mixture which was kept under stirring. After 24 h, the reaction was stopped with a saturated aqueous solution of NH_4Cl and then extracted with ethyl acetate to provide in quantitative yield an enantiomeric mixture of **73a-73b** (105 mg). A portion of 15 mg of the enantiomeric mixture was subsequently chromatographed using a Lux cellulose-1 5 µm chiral column using 95:5 (v/v) hexane/isopropanol as the mobile phase to obtain, in pure form, the diols **73a** (7.5 mg t_R=35.6 min) and **73b** (6.2 mg, t_R =37.2 min) as white solid.

Compound **73a** ^{1}H NMR (CD_3OD, 700 MHz): δ 3.93 (s, 2H), 3.71 (s, 3H), 3.38 (ovl, 2H), 2.46 (m, 1H), 2.35 (q, 1H), 1.96 (m, 1H), 1.66 – 1.53 (ovl, 4H), 1.37 – 1.29 (ovl, 6H), 0.89 (t, *J* = 7 Hz, 3H). ^{13}C NMR ($CDCl_3$, 125 MHz): δ 171.9, 171.8, 73.4, 75.7, 75.2, 52.5, 41.8, 33.8, 33.15, 33.1, 29.3, 26.6, 23.7, 14.4.

Compound **73b** ^{1}H NMR (CD_3OD, 700 MHz): δ 3.93 (s, 2H), 3.71 (s, 3H), 3.38 (ovl, 2H), 2.46 (m, 1H), 2.35 (q, 1H), 1.96 (m, 1H), 1.66 – 1.53 (ovl, 4H), 1.37 – 1.29 (ovl, 6H), 0.89 (t, *J* = 7 Hz, 3H). ^{13}C NMR ($CDCl_3$, 125 MHz): δ 171.9, 171.8, 73.4, 75.7, 75.2, 52.5, 41.8, 33.8, 33.15, 33.1, 29.3, 26.6, 23.7, 14.4.

Synthesis of compound 77

The synthetic scheme adopted for the synthesis of diols **74a** and **74b** involves using oleic acid as the starting material. 300 mg of oleic acid (1.06 mmol) were used for the synthesis of compound **77**, of which 380 mg is obtained in quantitative yield as a white solid, through the same procedure used to obtain compound **76**.

Compound **77** ^{1}H NMR (CDCl3, 400 MHz): δ 6.77 (bs, 1H), 5.26 (m, 2H), 3.96 (m, 2H), 3.68 (s, 3H), 2.22 (m, 2H), 1.93 (m, 2H), 1.97 (m, 2H), 1.58 (m, 2H), 1.44-1.15 (ovl, 18H), 0.82 (t, J = 7 Hz, 3H). 13C NMR (CDCl3, 125 MHz): δ 174.1, 170.1, 129.7, 129.5, 52.05, 41.0, 35.9, 31.7, 29.5, 29.4, 29.3, 29.1, 29.07, 29.0, 28.9, 27.0, 26.9, 25.5, 22.4, 12.9.

*Synthesis of enantiomeric mixture **74a/b***

Similarly, starting with 150 mg of compound **77**, the enantiomeric mixture of diols **74a** and **74b** (150 mg, quantitative yield) was obtained using the same procedure used to obtain the enantiomeric mixture of diols **73a** and **73b**. The diol compounds are subsequently derivatized into the corresponding acetonide by the addition of 400 µL of 2,2-dimethoxypropane (excess) and a spatula tip of p-toluenesulfonic acid, to 15 mg of the enantiomeric mixture of the **74a** and **74b** diols.

*Synthesis of compounds **78a** and **78b***

The reaction was left under electromagnetic stirring at room temperature overnight. After that, the reaction was stopped by the addition of a saturated solution of sodium bicarbonate ($NaHCO_3$) and, subsequently, it is extracted with ethyl acetate to obtain, after the removal of the solvent under vacuum, the acetonide of racemic compound **78** (16.2 mg) in pure form as colorless oil and in quantitative yield. The enantiomeric mixture **78a/b** was subsequently chromatographed using a Lux i-Amylose-3 3 µm chiral column using an 85:15 (v/v) acetonitrile:H_2O mixture as the mobile phase and a flow rate of 0.5 ml/min to obtain the two enantiomeric pure acetonide derivatives (6.7 mg, **78a** t_R=15.8 min; 7.0 mg, **78b** t_R=17.2 min). Compound **78a** ^{1}H NMR ($CDCl_3$, 700 MHz): δ 5.98 (bs, 1H); 4.05 (d, J = 5 Hz, 2H); 4.01 (ovl, 2H), 3.76 (s, 3H); 2.23 (t, J = 7.5 Hz, 2H); 1.64 (m,

2H); 1.57 (m, 2H); 1.48 (ovl, 4H); 1.42 (s, 3H); 1.33 (ovl, 3H); 1.36 – 1.25 (ovl, 22H); 0.88 (t, *J* = 7.0 Hz, 3H). ^{13}C NMR (CDCl3, 125 MHz): *δ* 173.22, 170.6, 107.2, 78.10, 78.05, 54.4, 41.2, 36.4, 31.9, 29.7, 29.68, 29.66, 29.5, 29.3, 29.2, 28.7, 26.26, 26.2, 26.06, 25.5, 22.7, 14.1

Compound **78b** ^{1}H NMR ($CDCl_3$, 700 MHz): *δ* 5.94 (bs, 1H); 4.05 (d, *J* = 5 Hz, 2H); 4.01 (ovl, 2H), 3.76 (s, 3H); 2.23 (t, *J* = 7.5 Hz, 2H); 1.64 (m, 2H); 1.57 (m, 2H); 1.48 (ovl, 4H); 1.42 (s, 3H); 1.33 (ovl, 3H); 1.36 – 1.25 (ovl, 22H); 0.87 (t, *J* = 7.0 Hz, 3H). ^{13}C NMR (CDCl3, 125 MHz): *δ* 173.22, 170.6, 107.2, 78.10, 78.05, 54.4, 41.2, 36.4, 31.9, 29.7, 29.68, 29.66, 29.5, 29.3, 29.2, 28.7, 26.26, 26.2, 26.06, 25.5, 22.7, 14.1

*Synthesis of diols **74a** and **74b***

At this point, the two acetonide derivatives are separately treated with 2 ml of MeOH:H_2O=9:1 solution to which few drops of HCl 1% aqueous solution was added. The reaction was kept at room temperature overnight and then the solvent was removed under vacuum by addition of methanol to prevent the acid concentration to afford compounds **74a** (7.2 mg) and **75b** (7.4 mg) in pure form.

Compound **74a** ^{1}H NMR ($CDCl_3$, 700 MHz): *δ* 5.85 (bs, 1H), 3.98 (d, *J* = 5 Hz, 2H), 3.94 (m, 2H), 3.69 (s, 3H), 2.12 (t, *J* = 8 Hz 2H), 1.58 (m, 2H), 1.44-1.41 (ovl, 4H), 1.30-1.19 (ovl, 18H), 0.82 (t, *J* = 7 Hz, 3H). ^{13}C NMR ($CDCl_3$, 125 MHz): *δ* 173.3, 170.6, 107.2, 78.1, 78.05, 52.7, 41.2, 36.4, 31.9, 29.7, 29.68, 29.65, 29.5, 29.3, 29.3, 28.7, 26.25, 26.2, 26.1, 25.5, 22.7, 14.1.

Compound **74b** ^{1}H NMR ($CDCl_3$, 700 MHz): *δ* 5.85 (bs, 1H), 3.98 (d, *J* = 5 Hz, 2H), 3.94 (m, 2H), 3.69 (s, 3H), 2.12 (t, *J* = 8 Hz 2H), 1.58 (m, 2H), 1.44-1.41 (ovl, 4H), 1.30-1.19 (ovl, 18H), 0.82 (t, *J* = 7 Hz, 3H). ^{13}C NMR ($CDCl_3$, 125 MHz): *δ* 173.3, 170.6, 107.2, 78.1, 78.05, 52.7, 41.2, 36.4,

31.9, 29.7, 29.68, 29.65, 29.5, 29.3, 29.3, 28.7, 26.25, 26.2, 26.1, 25.5, 22.7, 14.1.

Synthesis of methyl erucate

The synthesis of diols **75a** and **75b** was carried out from methyl erucate. 2 g of methyl erucate is dissolved in 15 ml of THF under electromagnetic stirring. Then, 5 ml of aqueous solution NaOH 25% was added to the reaction mixture, keeping the reaction under electromagnetic stirring, refluxing overnight. After that, the reaction was quenched by the addition of an aqueous solution of NH_4Cl and then, extracted with ethyl acetate. The solvent removal in vacuo afforded erucic acid in quantitative yield (1.8 g). The obtained spectroscopic data agreed with those reported in literature.

*Synthesis of compound **79***

Starting with 500 mg of erucic acid (1.40 mmol), the synthesis of compound **79** (600 mg, quantitative yield) was carried out through the same procedure used to obtain compound **76**. Compound **79** ^{1}H NMR ($CDCl_3$, 400 MHz): δ 6.09 (bs, 1H), 5.44 (m, 2H), 4.03 (d, J = 5 Hz, 2H), 3.74 (s, 3H), 2.22 (t, J = 7 Hz 2H), 1.99 (q, 4H), 1.62 (m, 2H), 1.30-1.24 (ovl, 44H), 0.86 (t, J = 7 Hz, 3H). ^{13}C NMR ($CDCl_3$, 125 MHz): δ 173.4, 170.65, 129.9, 129.8, 53.3, 41.2, 36.4, 31.9, 29.78, 29.77, 29.6, 29.56, 29.52, 29.48, 29.34, 29.44, 29.25, 27.2, 25.6, 24.8, 22.7, 14.1.

*Synthesis of enantiomeric mixture **75a/b***

Continuing, starting with 500 mg of compound **79**, the enantiomeric mixture of diols **75a** and **75b** (520 mg, quantitative yield) was obtained using the same procedure used to obtain the enantiomeric mixture of diols **73a** and **73b**.

*Synthesis of compounds **80a** and **80b***

An aliquot of 81.5 mg of the enantiomeric mixture was subsequently derivatized into the corresponding acetonide by the addition of 700 µL (excess) of 2,2-dimethoxypropane and a spatula tip of p-toluenesulfonic acid. The reaction was stirred overnight, and, after that, the reaction was quenched by the addition of a saturated solution of $NaHCO_3$ and, subsequently, extracted with ethyl acetate to obtain, after the removal of the solvent under vacuum, the acetonide of racemic mixture **80a/b** (82 mg) in pure form and with a quantitative yield. The mixture **80** was subsequently chromatographed using a Lux i-Amylose-3 3 µm chiral column using a 9:1 (v/v) acetonitrile:H_2O mixture as the mobile phase and a flow rate of 0.5 ml/min to obtain the two acetonide derivatives (**80a** t_R =24.9 min ; **80b** t_R = 26.0 min).

Compound **80a** ^{1}H NMR ($CDCl_3$, 700 MHz): δ 5.94 (bs, 1H), 4.05 (d, *J* = 5 Hz, 2H); 4.01 (m, 2H); 3.76 (s, 3H); 2.23 (t, *J* = 7 Hz, 2H); 1.64 (q, 2H); 1.48 (m, 4H); 1.33 (s, 3H); 1.30-1.24 (ovl, 33H); 0.86 (t, *J* = 7 Hz, 3H). ^{13}C NMR ($CDCl_3$, 125 MHz): δ 173.3, 170.6, 107.22, 78.12, 52.4, 41.8, 36.4, 31.9, 29.75, 29.7, 29.6, 29.55, 29.50, 29.45, 29.3, 29.27, 29.25, 28.7, 26.2, 26.1, 25.6, 22.7, 14.1.

Compound **80b** ^{1}H NMR ($CDCl_3$, 700 MHz): δ 5.94 (bs, 1H), 4.05 (d, *J* = 5 Hz, 2H); 4.01 (m, 2H); 3.76 (s, 3H); 2.23 (t, *J* = 7 Hz, 2H); 1.64 (q, 2H); 1.48 (m, 4H); 1.33 (s, 3H); 1.30-1.24 (ovl, 33H); 0.86 (t, *J* = 7 Hz, 3H). ^{13}C NMR ($CDCl_3$, 125 MHz): δ 173.3, 170.6, 107.22, 78.12, 52.4, 41.8, 36.4, 31.9, 29.75, 29.7, 29.6, 29.55, 29.50, 29.45, 29.3, 29.27, 29.25, 28.7, 26.2, 26.1, 25.6, 22.7, 14.1.

*Synthesis of diols **75a** and **75b***

At this point, the two acetonide derivatives are separately treated with 2 ml of MeOH:H_2O=9:1 to which few drops of aqueous solution of HCl 1% were added. The reaction was kept at room temperature overnight and then concentrated. This yields compounds **75a** (6.2 mg) and **75b** (5.9 mg) in pure form.

Compound **75a** ^{1}H NMR ($CDCl_3$, 700 MHz): δ 6.00 (bs, 1H), 4.05 (d, J = 5 Hz, 2H), 3.76 (s, 3H), 3.60 (m, 2H), 2.23 (t, J = 7 Hz 2H), 1.63 (q, 2H), 1.42(m, 2H), 1.28-1.25 (ovl, 34H), 0.87 (t, J = 7 Hz, 3H).

Compound **75b** ^{1}H NMR ($CDCl_3$, 700 MHz): δ 6.00 (bs, 1H), 4.05 (d, J = 5 Hz, 2H), 3.76 (s, 3H), 3.60 (m, 2H), 2.23 (t, J = 7 Hz 2H), 1.63 (q, 2H), 1.42(m, 2H), 1.28-1.25 (ovl, 34H), 0.87 (t, J = 7 Hz, 3H).

*Synthesis of bis-esters **81a-81b** and **82a-82b***

The esterification reaction was carried out on compounds **73a** (2 mg) and **74b** (2 mg) separately dissolved in 1 ml of dry CH_2Cl_2. Then, 3.3 eq of EDC chlorohydrate, a spatula tip of 4-dimethylaminopyridine (4-DMAP) and 3.3 eq of (R)-MPA were added to each solution. Each reaction mixture is kept under stirring at room temperature overnight.

Then, following solvent evaporation, HPLC purification is performed using Luna C18 column using a 75:25 (v/v) methanol/H_2O mixture as the mobile phase to obtain compound **81a** in pure form (t_R=15.2). Instead, methanol/H_2O 9:1 (v/v) mixture was used as mobile phase to afford compound **82a** in pure form (t_R=7.9). The same procedure was adopted to obtain the (S)-MPA esters in pure form (compound **81b** tR = 14.3 min; compound **22b** t_R = 8.8 min). The NMR values recorded for both *R*- and *S*-MPA derivatives are reported in Tables 2-5.

CONCLUDING REMARKS

The research project I worked on pave the way for new scenarios in the development of new marine-derived antidiabetic agents. The preliminary and promising results have been obtained thanks to the active collaborations with national and international research groups that made this work multidisciplinary. In particular, my contribution has led to the expansion of knowledge regarding the pharmacological activities of phosphoeleganin (**44**). From the already known dual activities on PTP1B and AR enzymes that contribute to making this molecule an insulin-sensitizing agent, further studies on HepG2 liver cell lines have confirmed and deepened the insulin-sensitizing behavior of the natural metabolite. Moreover, phosphoeleganin (**44**) was identified as a potent inhibitor of 15-LOX-1 with an IC_{50} in the micromolar range. The framing of the marine-derived lead compound as a multitarget agent endowed with both antidiabetic and anti-inflammatory properties has aroused our interest in the development of synthetic analogues. In order to obtain molecules with high pharmacological potential, the principles of FBDD and DOS were applied to produce small libraries of fragments of the natural molecule that could simultaneously have enough structural and stereochemical variability to enable SARs elaboration. A first-generation library of fragments was developed by oxidative cleavage of phosphoeleganin (**44**) and by the design and synthesis of polyketide-like SMs that resemble the phosphate group-containing portion of the molecule. In the latter case, adhering to the principles of DOS, efficient reactions were used to achieve as much variability as possible in terms of regiochemical and stereochemical diversity of compounds. Pharmacological results afforded interesting findings. First, phosphorylated fragment **46** turned out as a

potent inhibitor of PTP1B enzyme exerting a reversible and mixed-type non-competitive mechanism of action. In addition, assays performed on C2C12 muscle cells framed it as an insulin mimetic agent. Moreover, although fragment **46** lost the AR inhibition activity, it was identified as 15-LOX-1 inhibitor, recovering the multitarget action. Similarly, the phosphorylated SM **49a** proved to be an inhibitor of PTP1B acting with a reversible and mixed-type mechanism of action. Interestingly, fragment **45** endowed with the glycine head was inactive on PTP1B, AR and 15-LOX-1 but affected positively the hepatic insulin signaling, and thus more in-depth studies will be performed to identify its mechanism of action. These promising results provided insight into the structural motifs for the inhibition of the three selected targets. In particular, the entirety of the structure of phosphoeleganin (**44**) appears to be a crucial requirement in the inhibition of the AR enzyme. Our hypothesis is that glycine is probably involved in the inhibition as well as the long aliphatic chain with which the natural compound is equipped. Furthermore, only fragments **46** and **49a** are active on PTP1B, outlining the importance of the correct spatial orientation of the phosphate group, as well as its position along the alkyl carbon chain. In the end, the preliminary screening of phosphoeleganin (**44**) and its derivatives **45** and **46** on 15-LOX-1 highlight the phosphorylated polyketide scaffold as a promising chemotype to further explore for its anti-inflammatory properties. On these bases, the development second-generation library has begun starting from the synthesis of enantiomerically pure *anti*-1,2-diols that will be further functionalized by the insertion of the phosphate moiety. Concluding, in the current genomic era, in which tens of thousands of potential drug targets have been identified, the need of molecules both for studying disease and as starting points for making drugs has become even more prominent. The

exploration of biologically relevant chemical space offered by marine NPs is, thus, rendered more feasible by focusing on fragment-like chemical space. This study, therefore, confirms the fundamental and everlasting role that NPs can play in medicinal chemistry following the latest approaches for drug discovery.

CHAPTER 7. Spectroscopic data

^{1}H NMR of compound **44** in CD_3OD

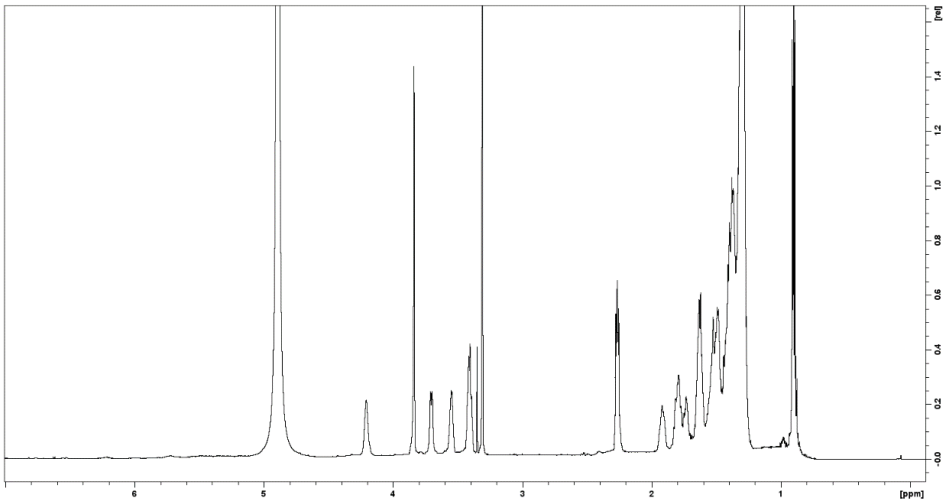

HR-ESIMS spectrum of compound **44**

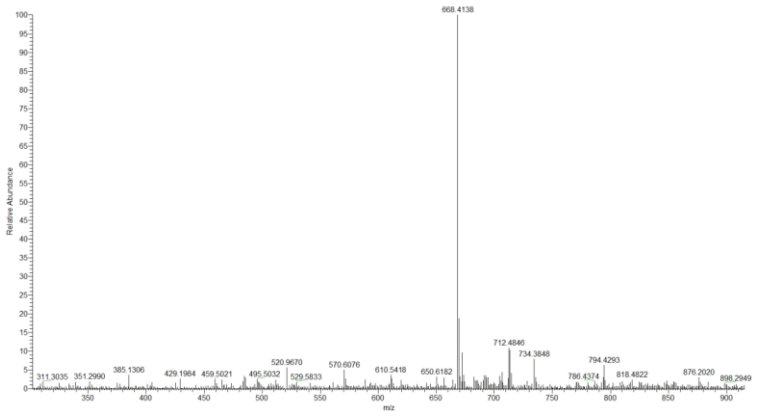

^{1}H NMR of compound **45** in CD_3OD

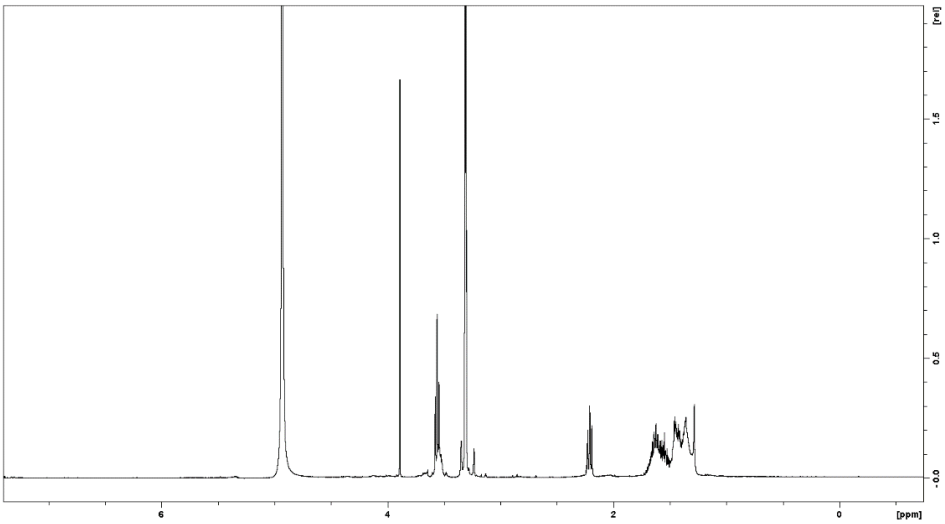

HR-ESIMS spectrum of compound **45**

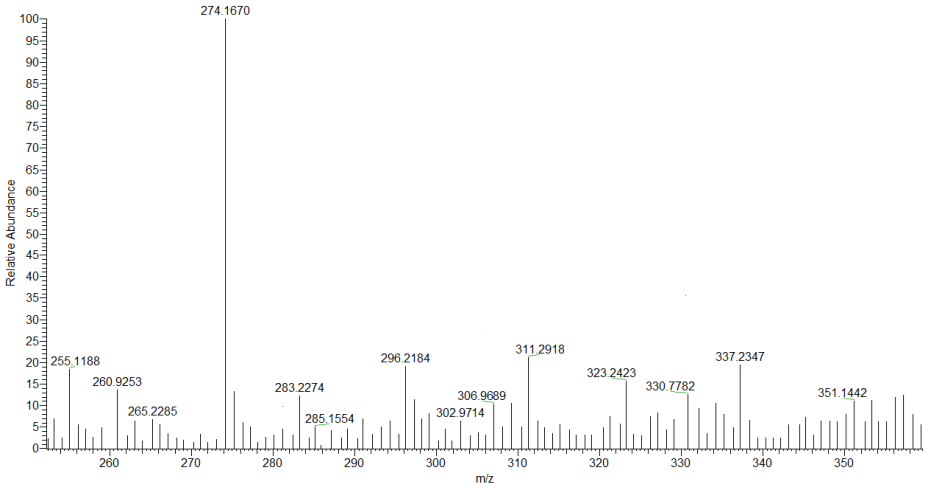

^{1}H NMR of compound **46** in CD_3OD

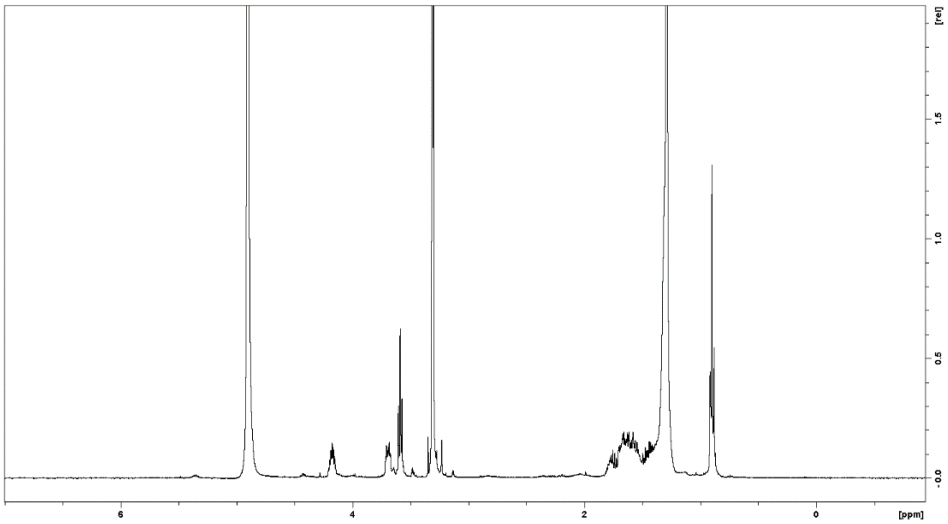

HR-ESIMS spectrum of compound **46**

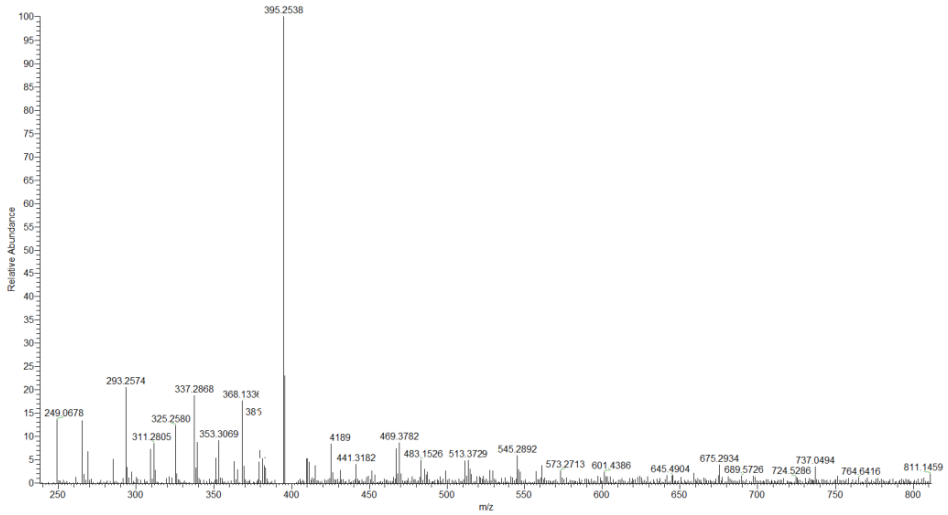

^{1}H NMR of compound **47a** in CD_3OD

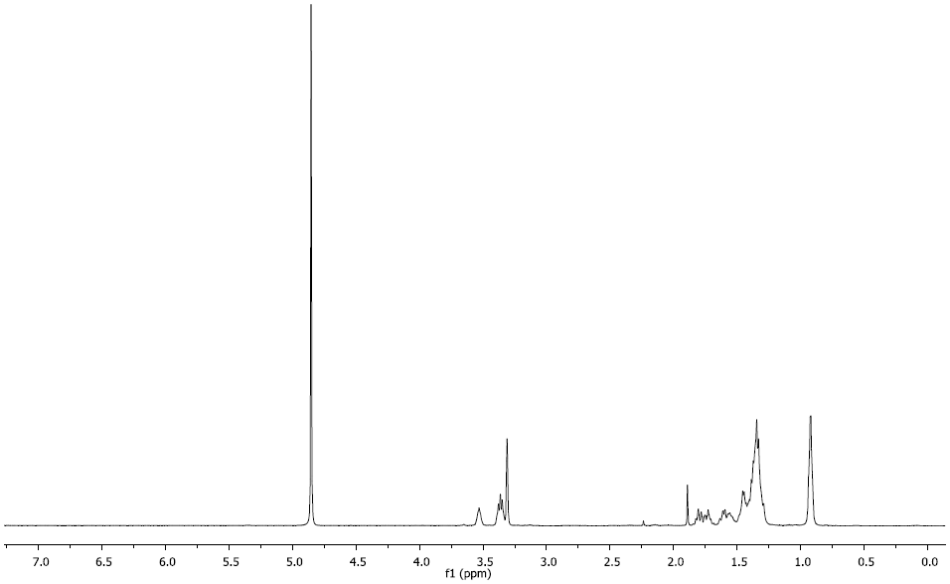

HR-ESIMS spectrum of compound **47a**

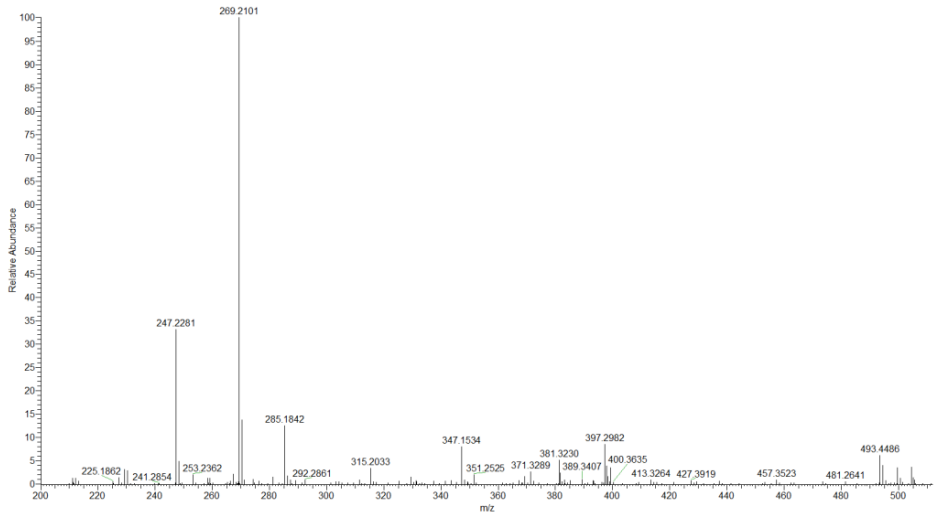

^{1}H NMR of compound **47b** in CD_3OD

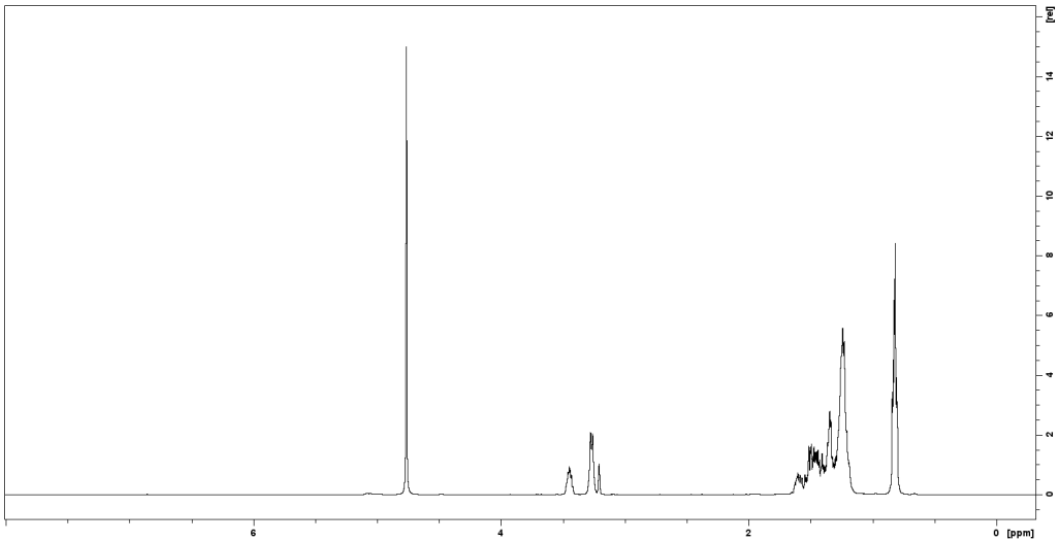

HR-ESIMS spectrum of compound **47b**

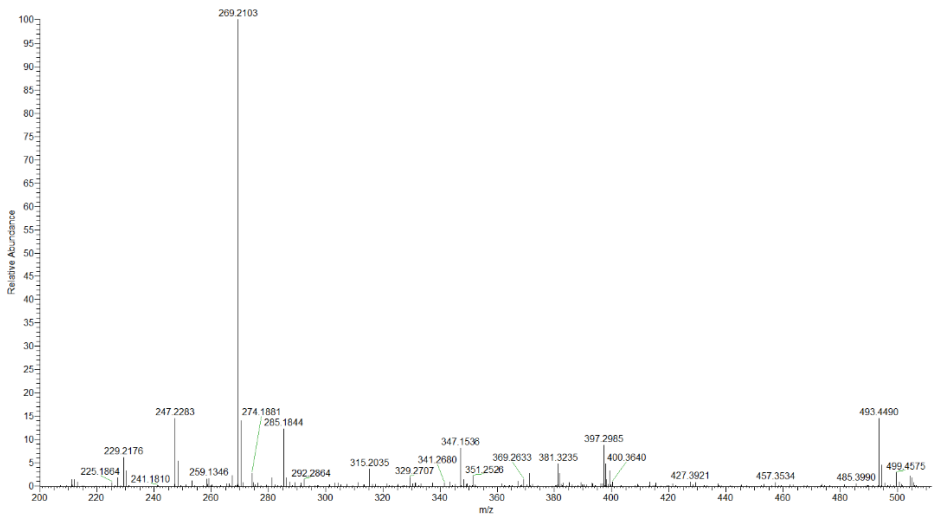

^{1}H NMR of compound **51a** in CD_3OD

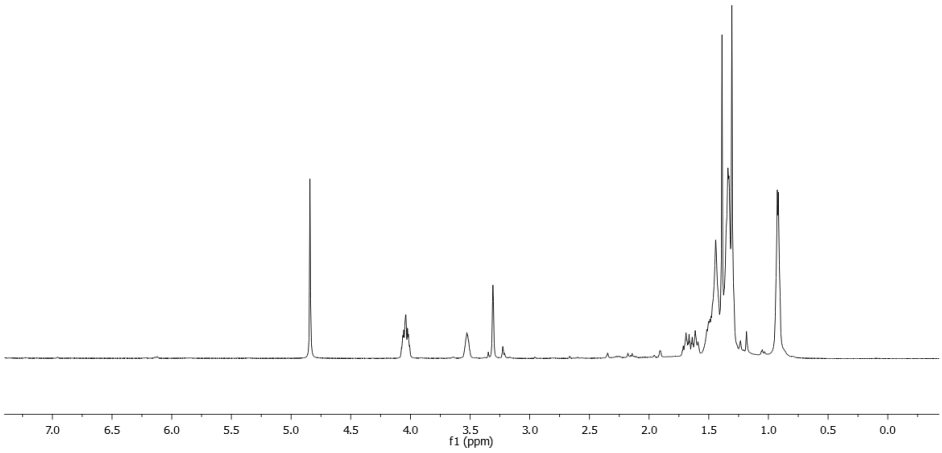

HR-ESIMS spectrum of compound **51a**

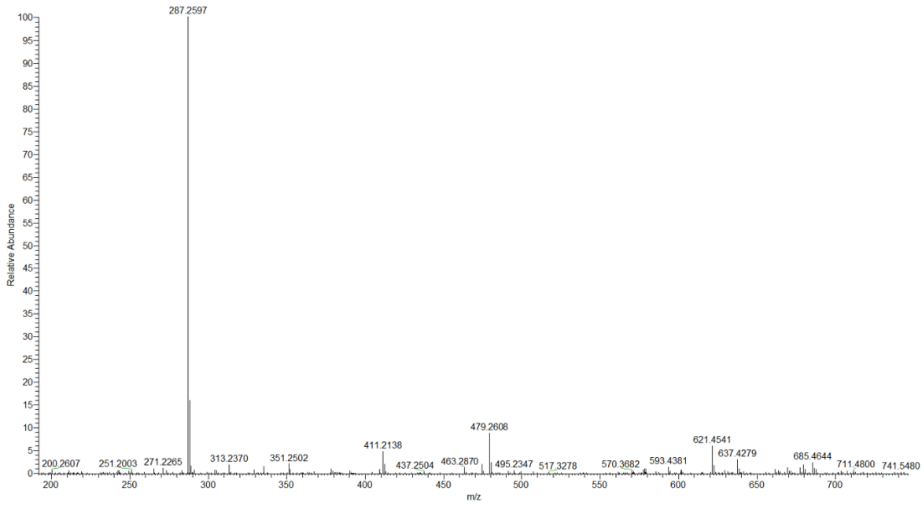

^{1}H NMR of compound **51b** in CD_3OD

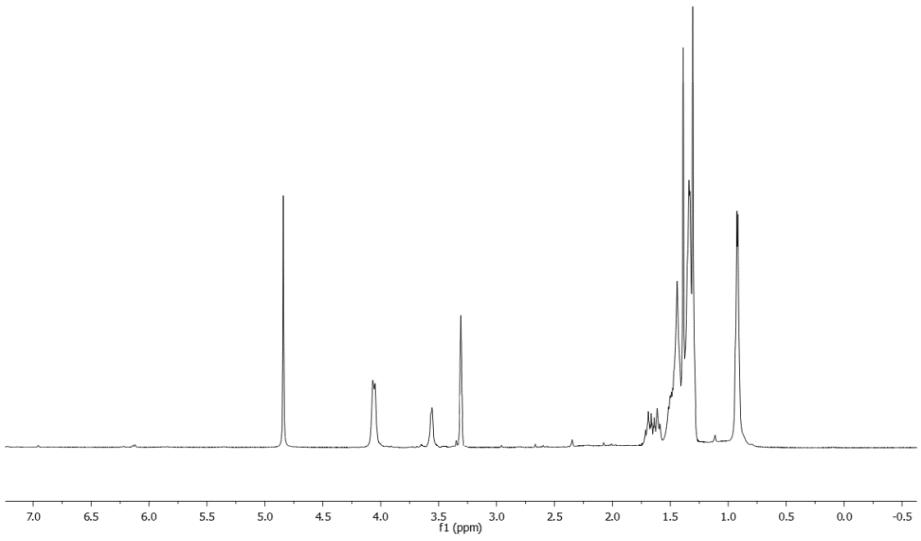

HR-ESIMS spectrum of compound **51b**

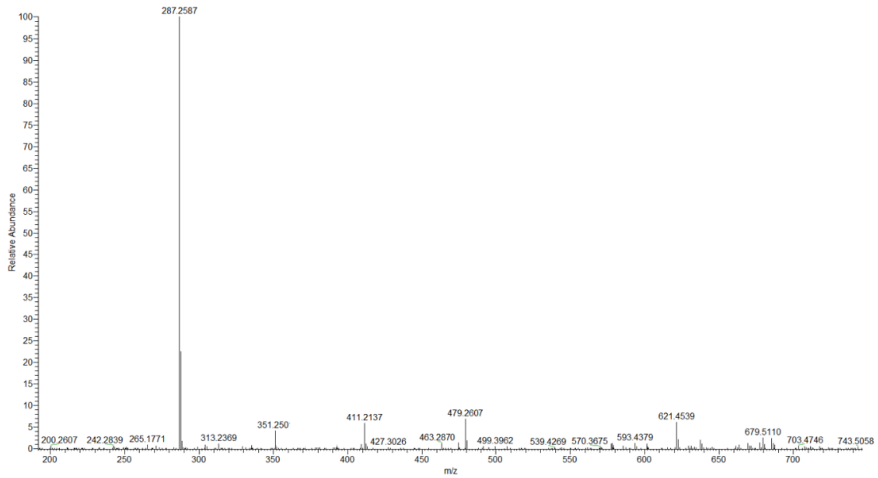

HR-ESIMS spectrum of compound **52b**

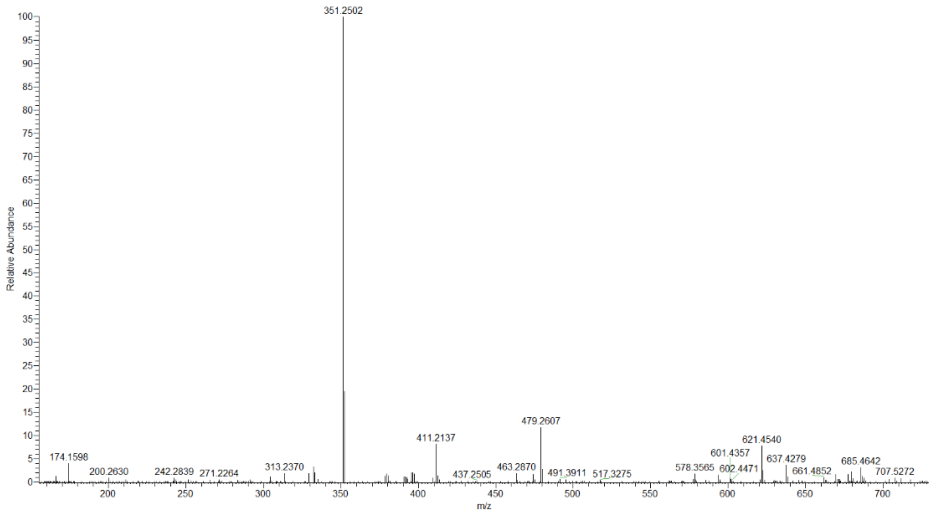

HR-ESIMS spectrum of compound **52b**

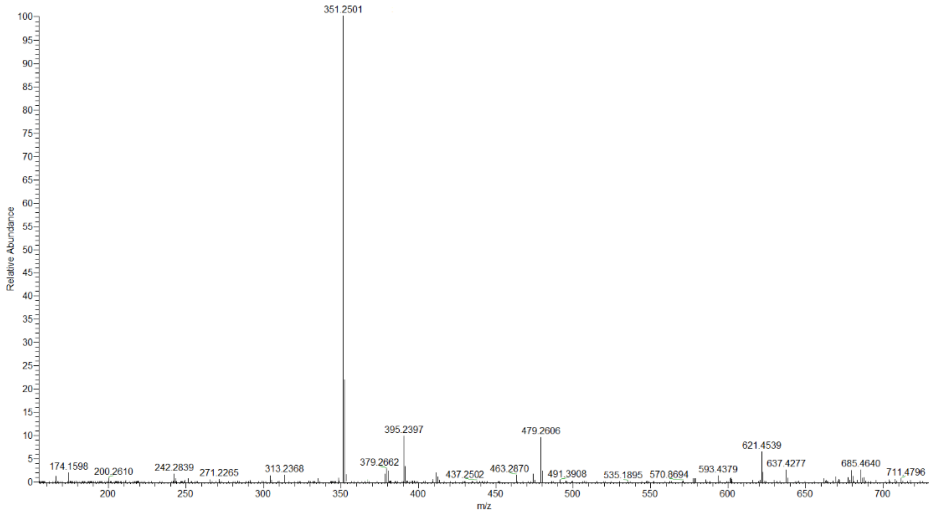

^{1}H NMR of compound **48a** in CD_3OD

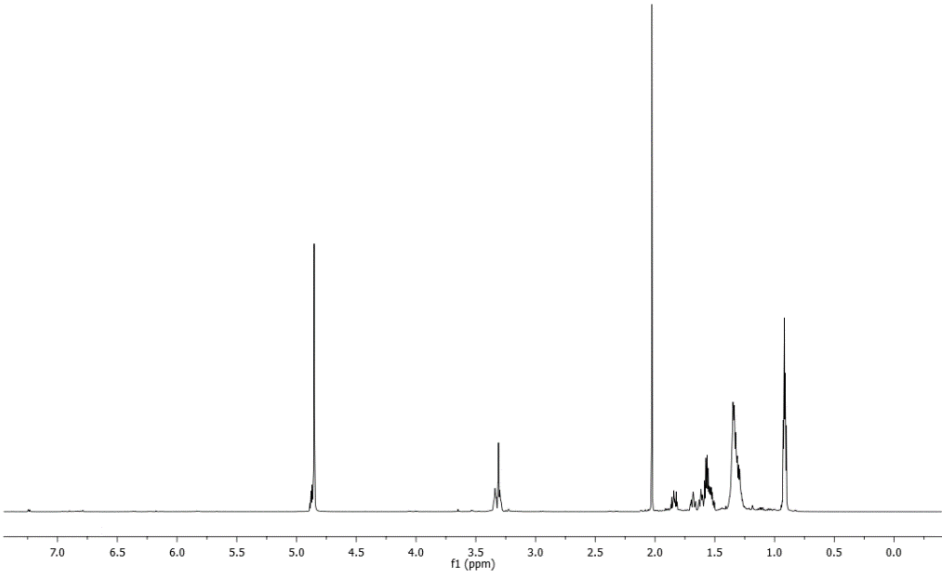

^{13}C NMR of compound **48a** in CD_3OD

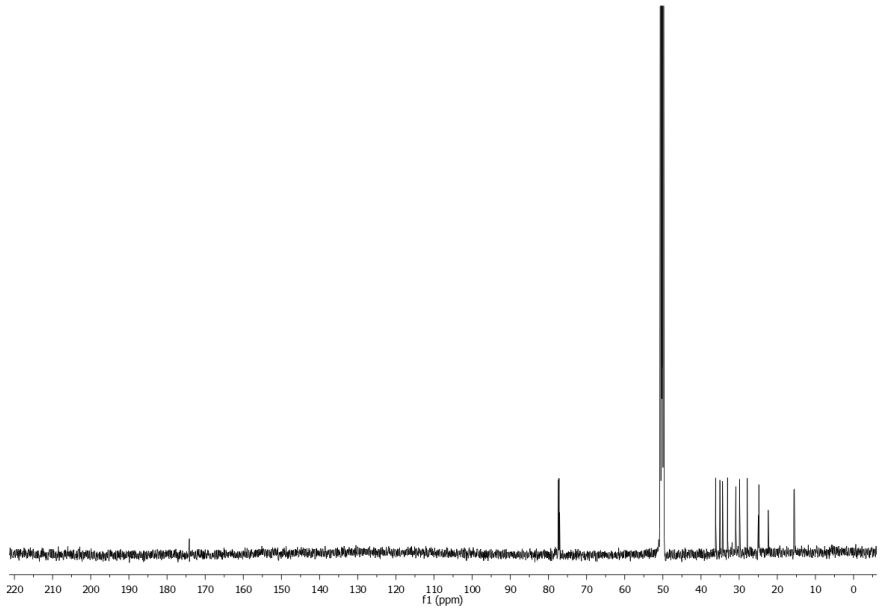

HR-ESIMS spectrum of compound **48a**

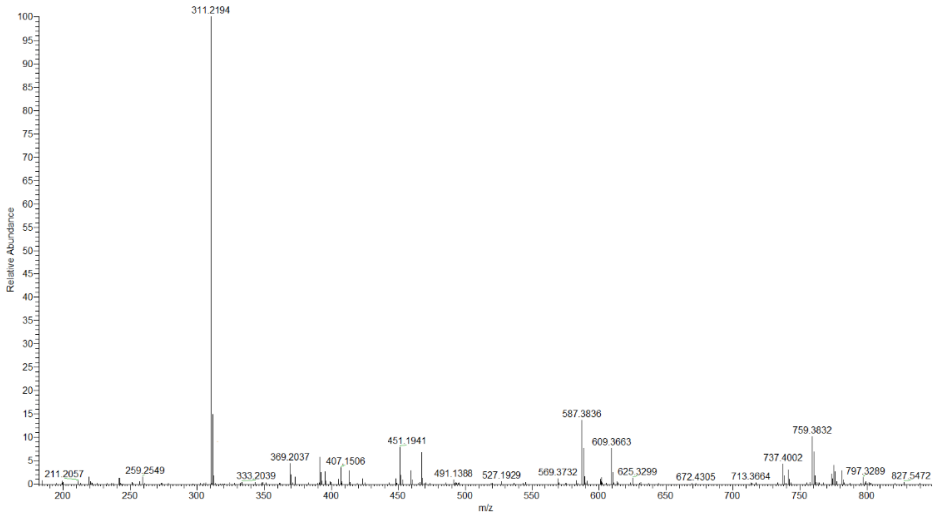

^{1}H NMR of compound **48b** in CD_3OD

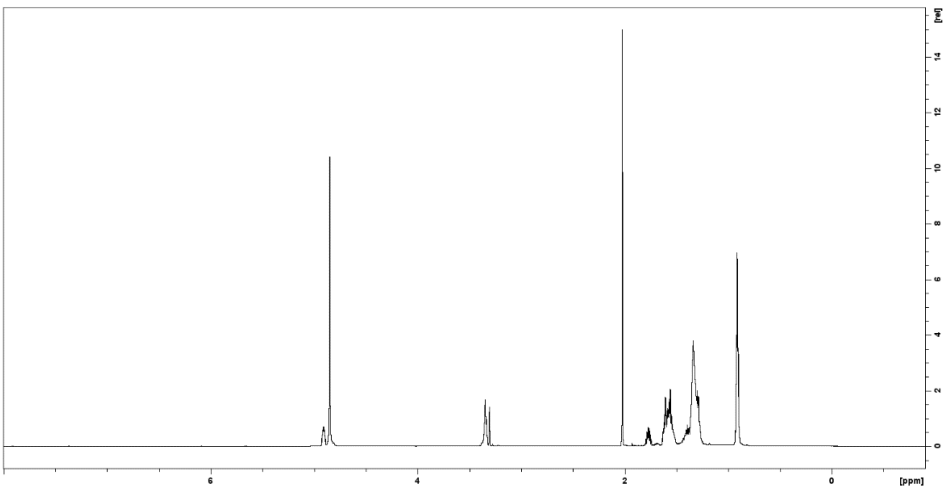

^{13}C NMR of compound **48b** in CD_3OD

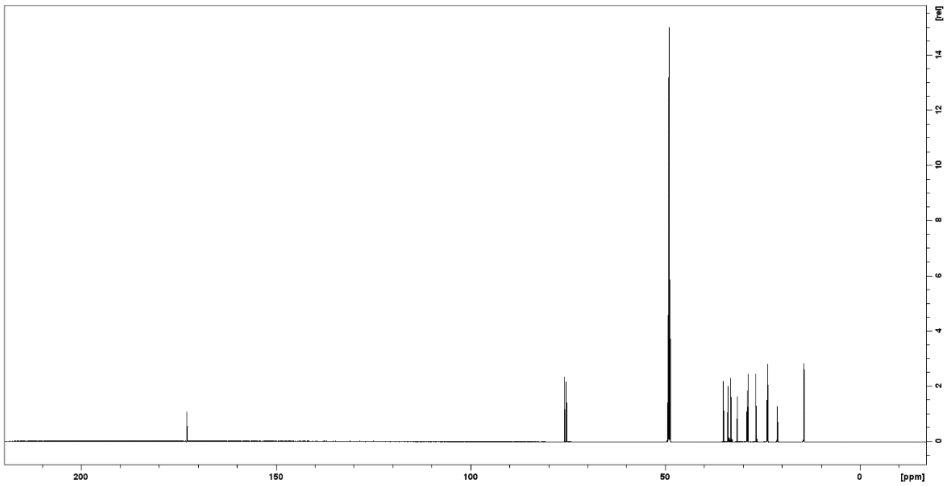

HR-ESIMS spectrum of compound **48b**

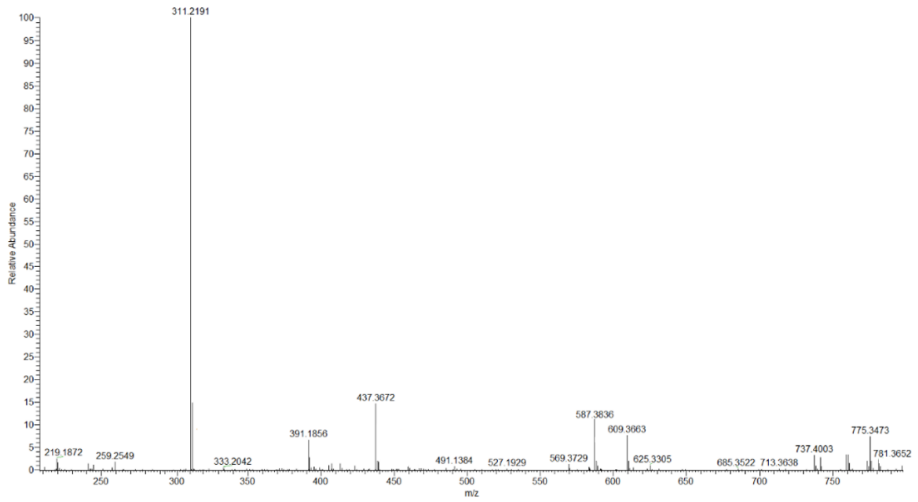

^{1}H NMR of compound **49a** in CD_3OD

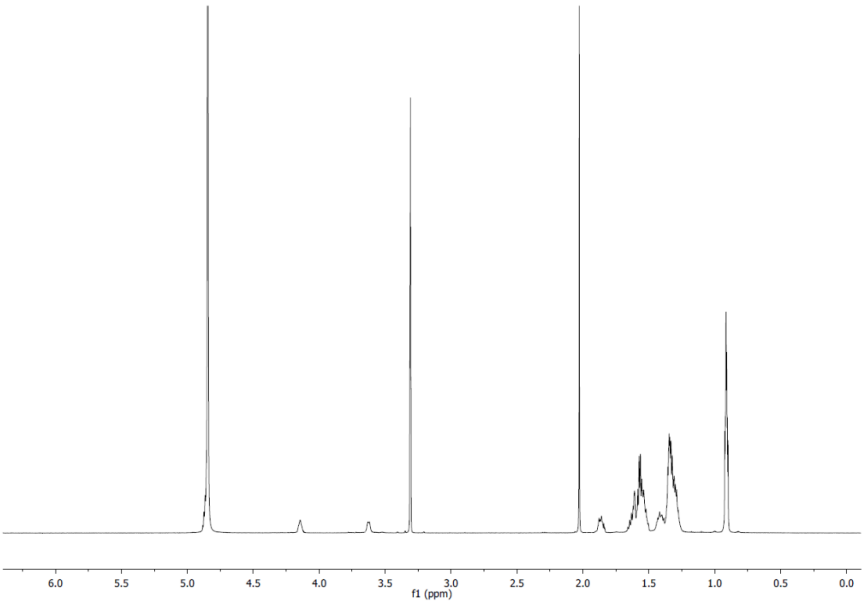

^{1}H-^{1}H COSY spectrum in CD_3OD of compound **49a**

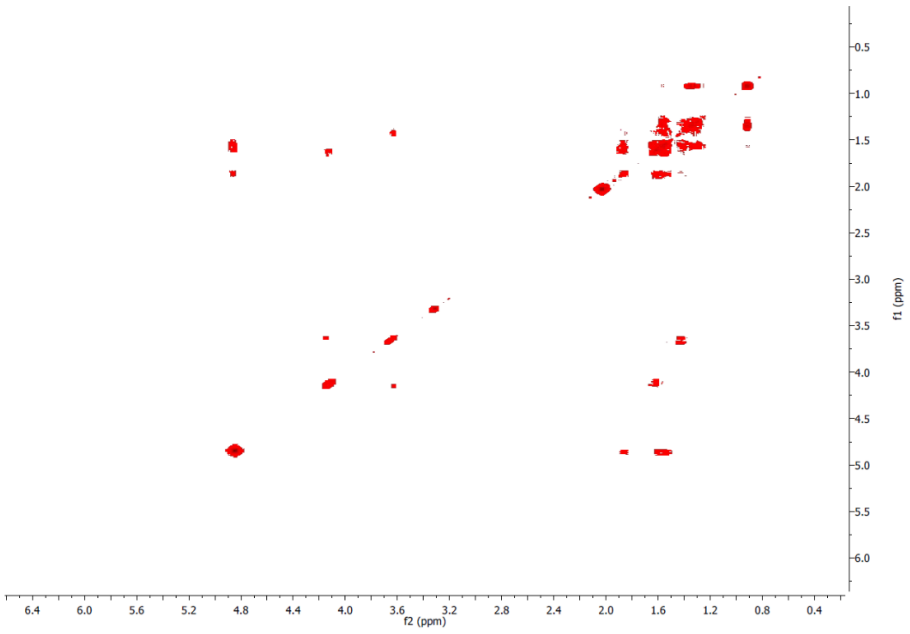

HR-ESIMS spectrum of compound **49a**

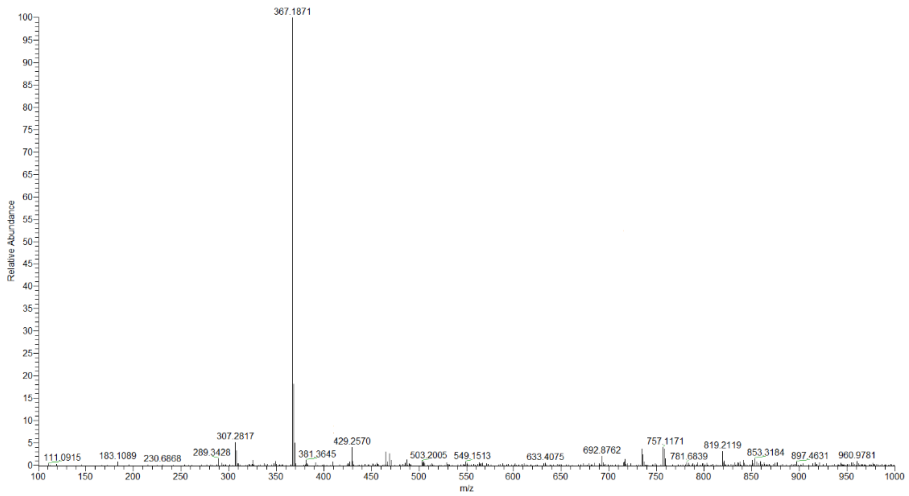

^{1}H NMR of compound **50a** in CD_3OD

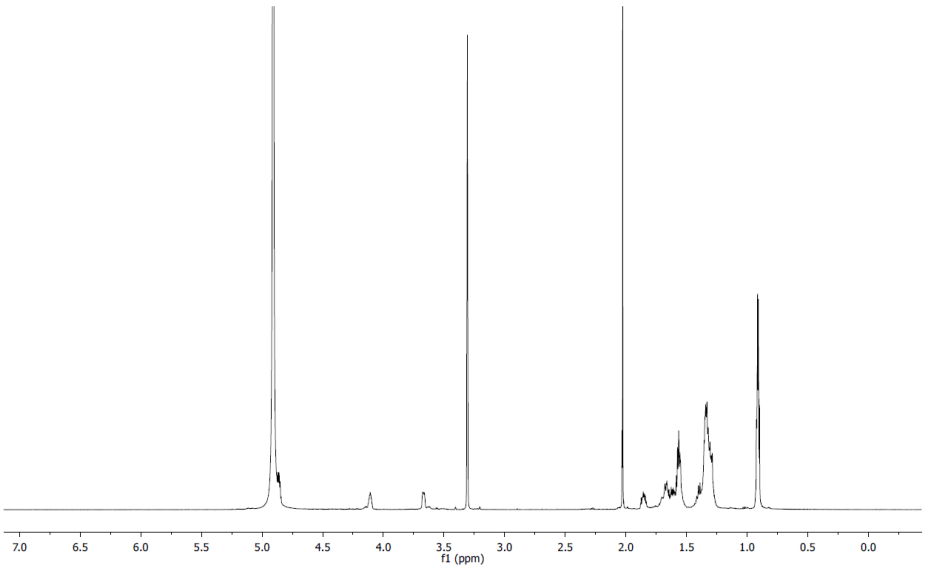

^{1}H-^{1}H COSY spectrum in CD_3OD of compound **50a**

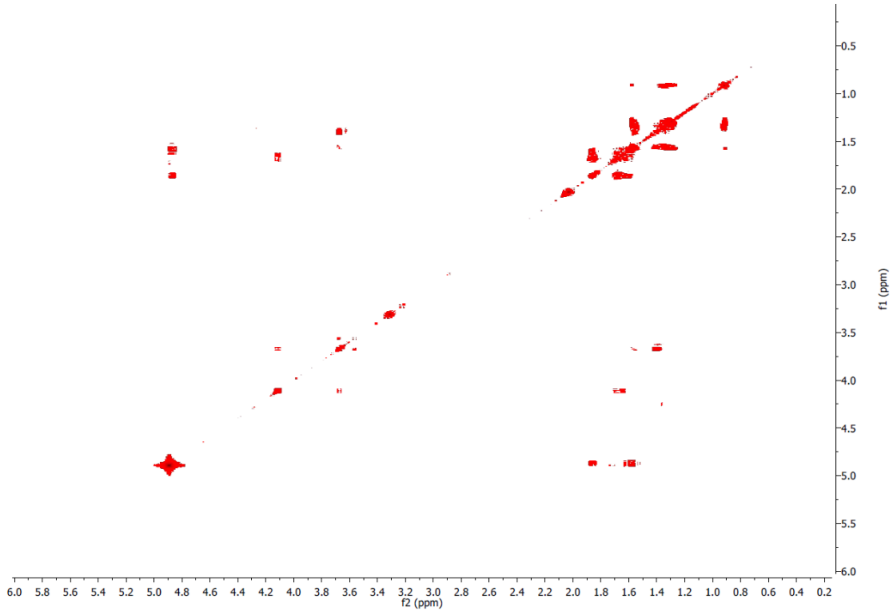

^{1}H-^{13}C HSQC spectrum in CD_3OD of compound **50a**

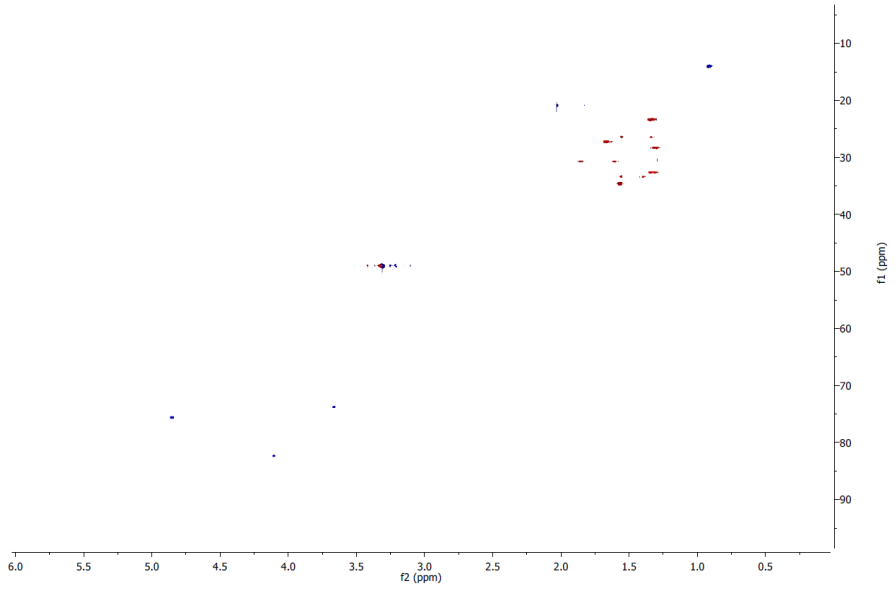

HR-ESIMS spectrum of compound **50b**

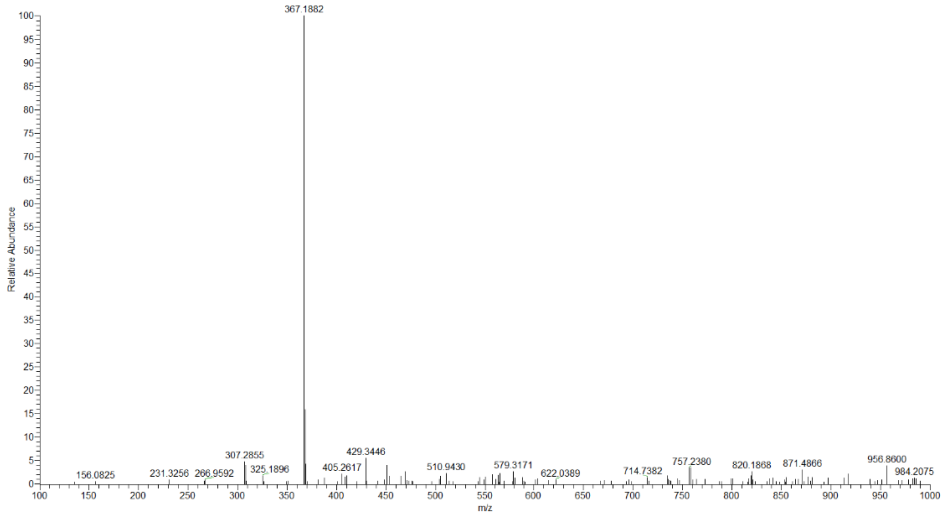

^{1}H NMR of compound **49b** in CD_3OD

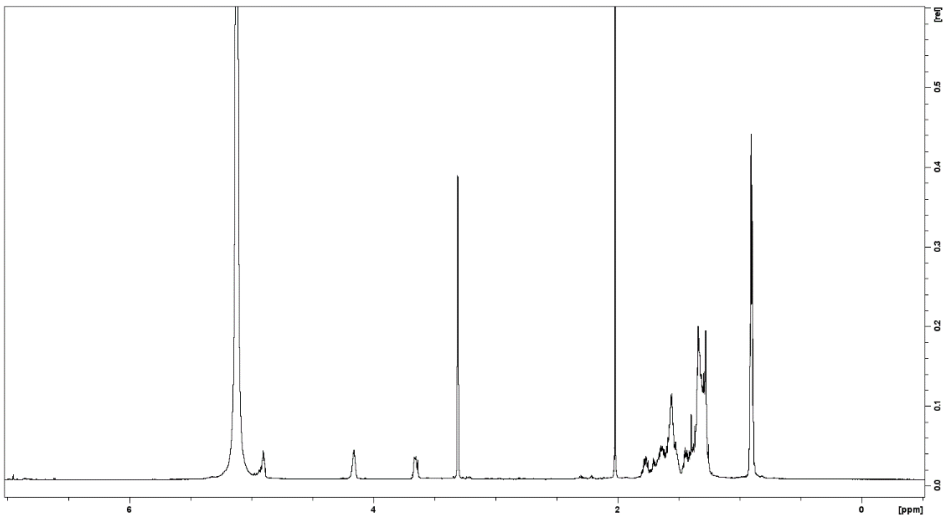

^{1}H-^{1}H COSY spectrum in CD_3OD of compound **49b**

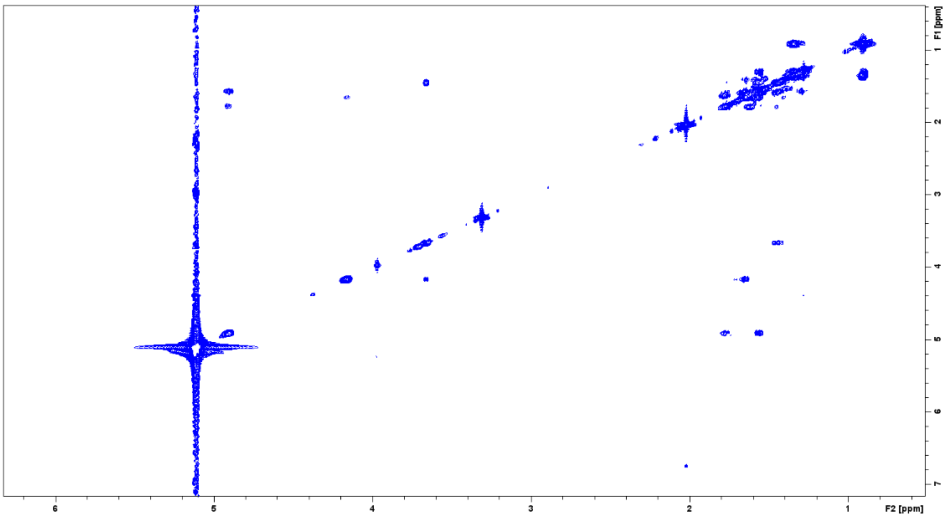

^{1}H-^{13}C HSQC spectrum in CD_3OD of compound **49b**

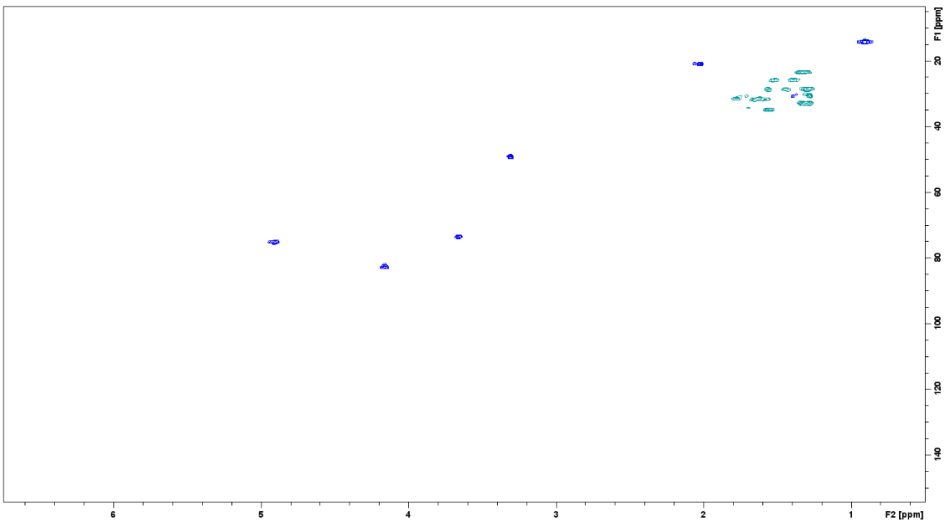

HR-ESIMS spectrum of compound **49b**

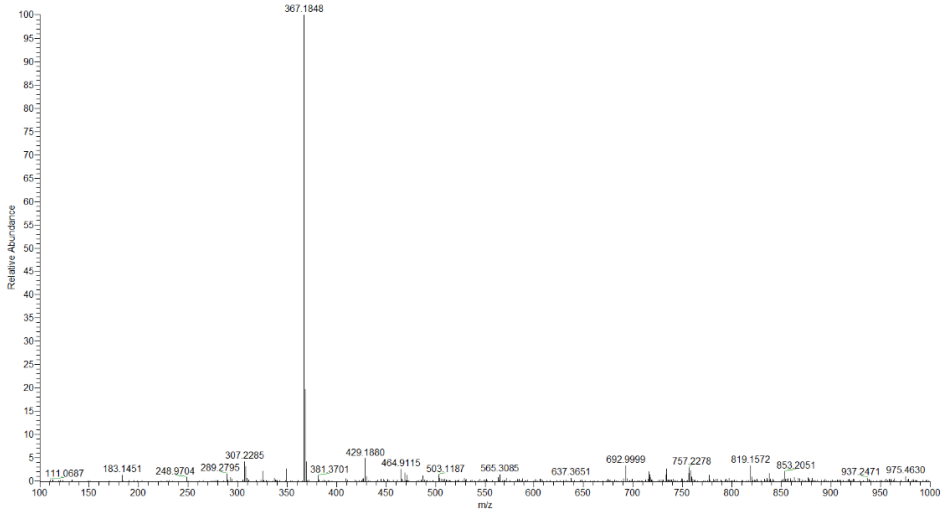

^{1}H NMR of compound **50b** in CD_3OD

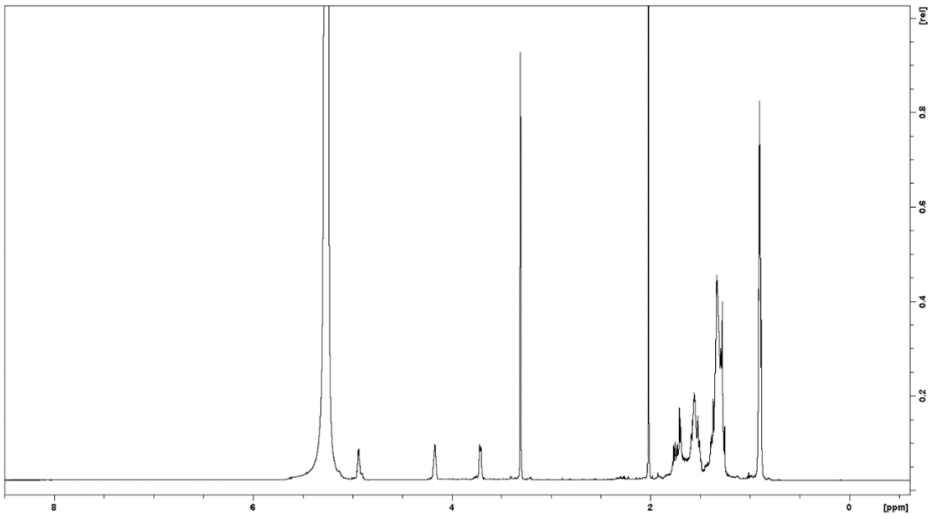

^{1}H-^{1}H COSY spectrum in CD_3OD of compound **49b**

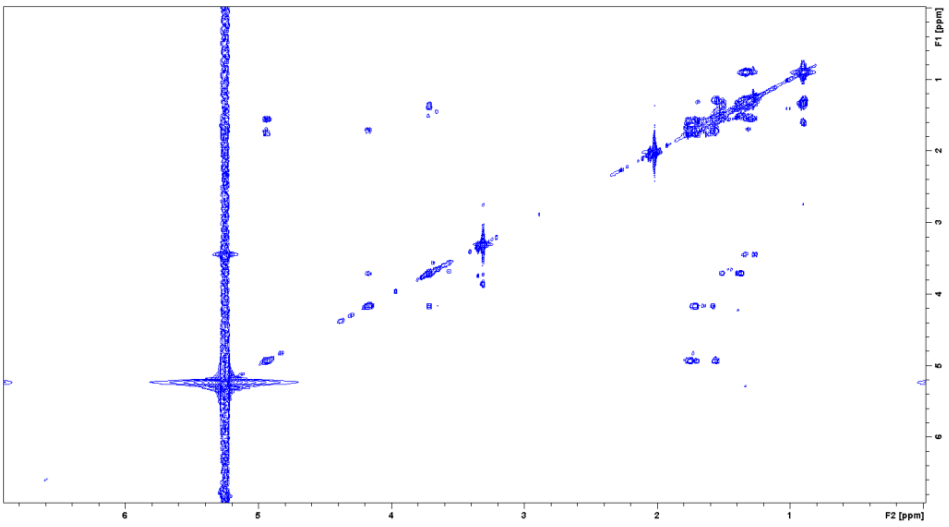

^{1}H-^{13}C HSQC spectrum in CD_3OD of compound **50b**

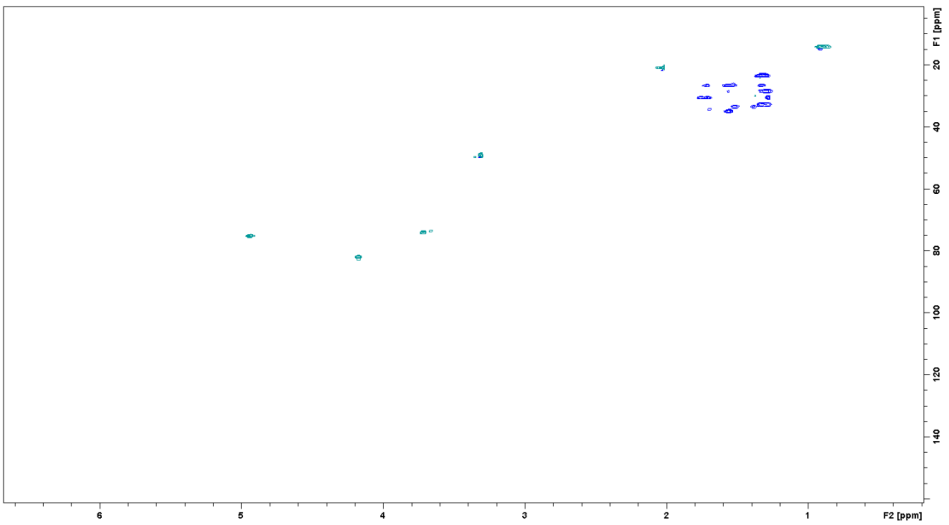

HR-ESIMS spectrum of compound **50b**

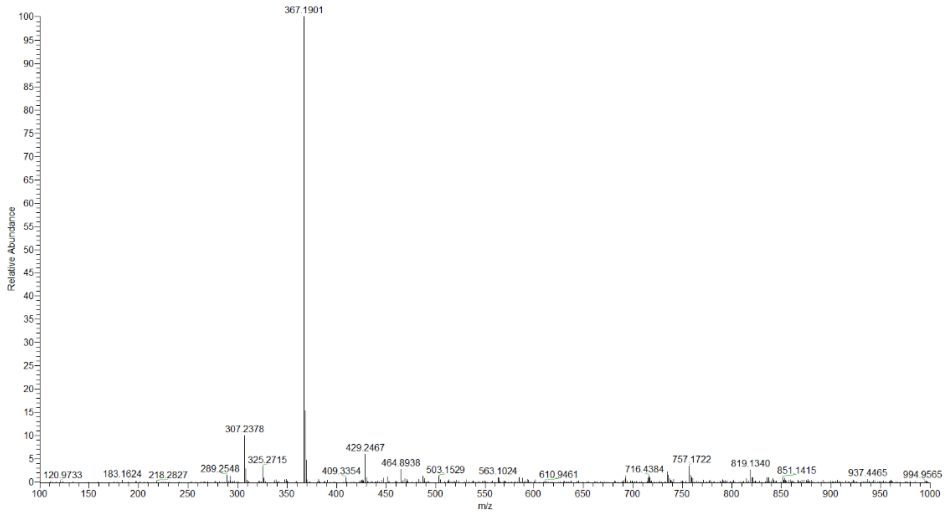

^{1}H NMR of compound **71** in CD_3OD

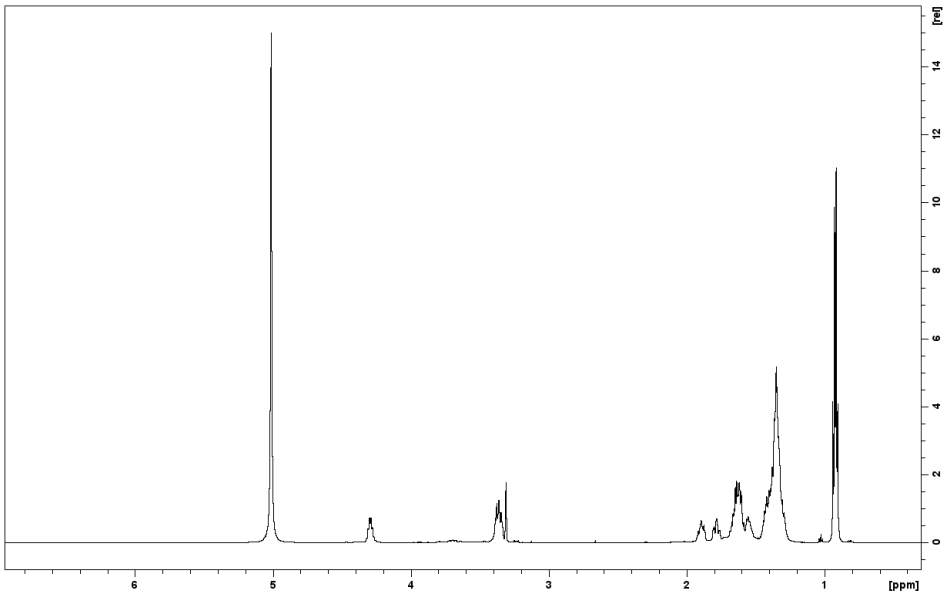

^{1}H-^{13}C HSQC spectrum of compound **71** in CD_3OD

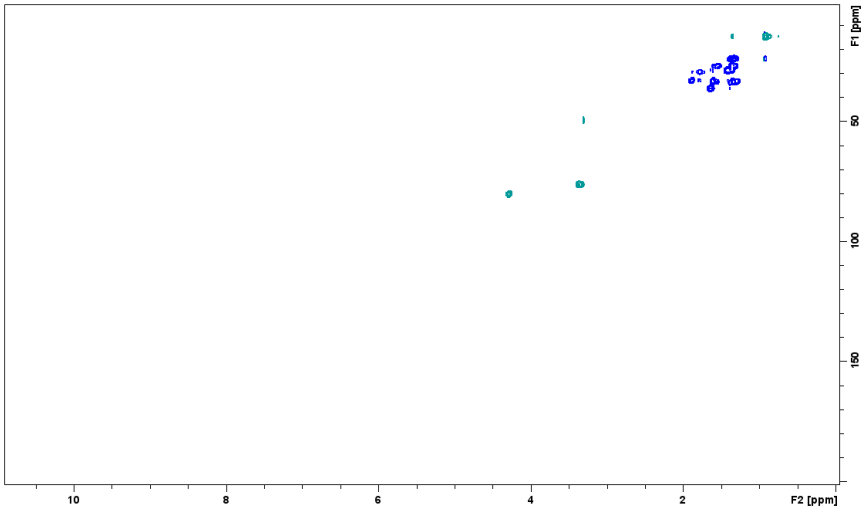

^{1}H NMR of compound **72** in CD_3OD

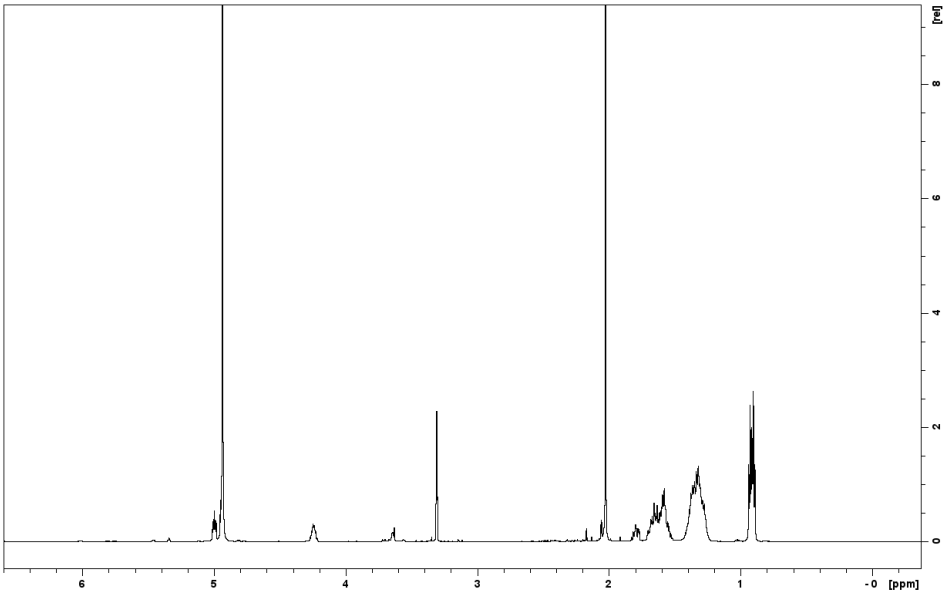

^{1}H-^{13}C HSQC spectrum of compound **72** in CD_3OD

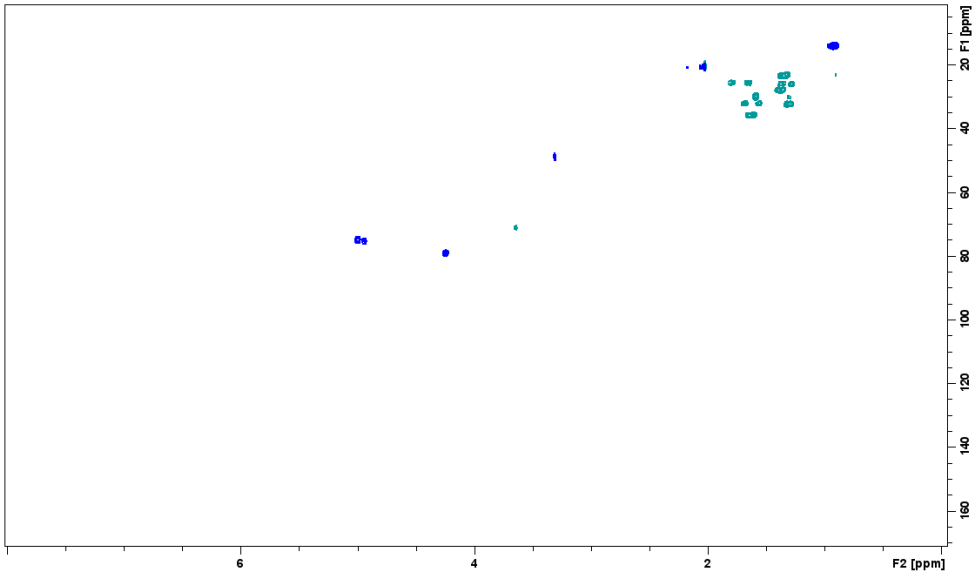

^{1}H NMR of compound **76** in CD_3OD

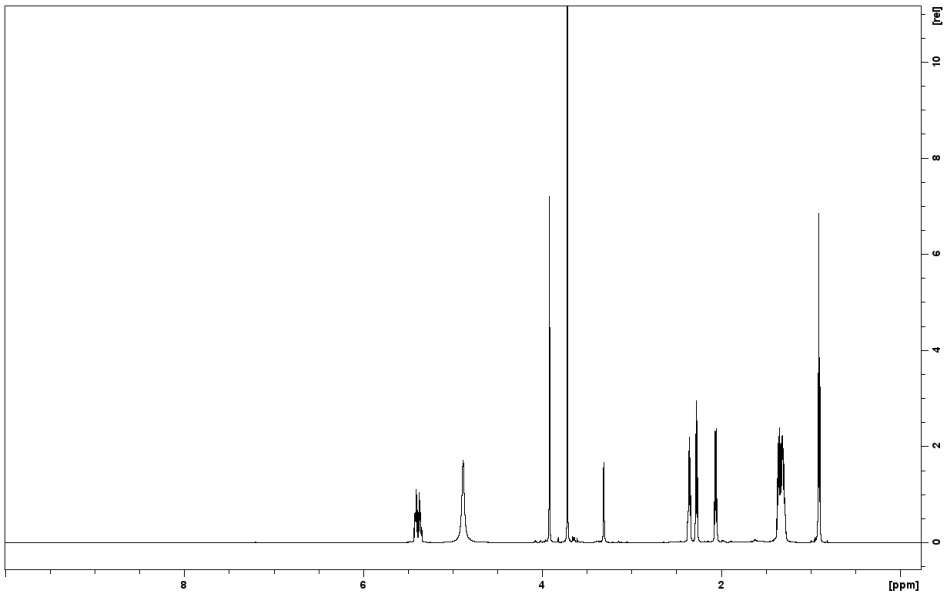

HR-ESIMS spectrum of compound **76**

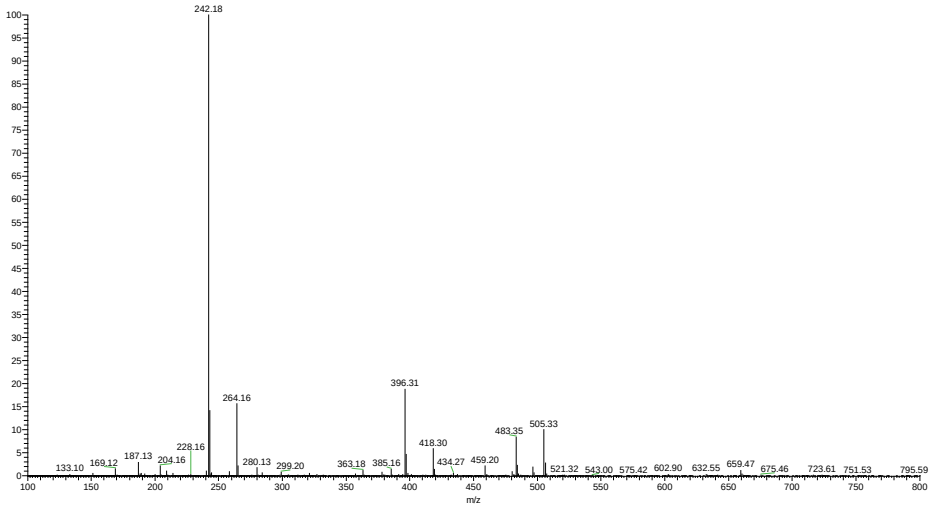

^{1}H NMR of compound **73a** in CD_3OD

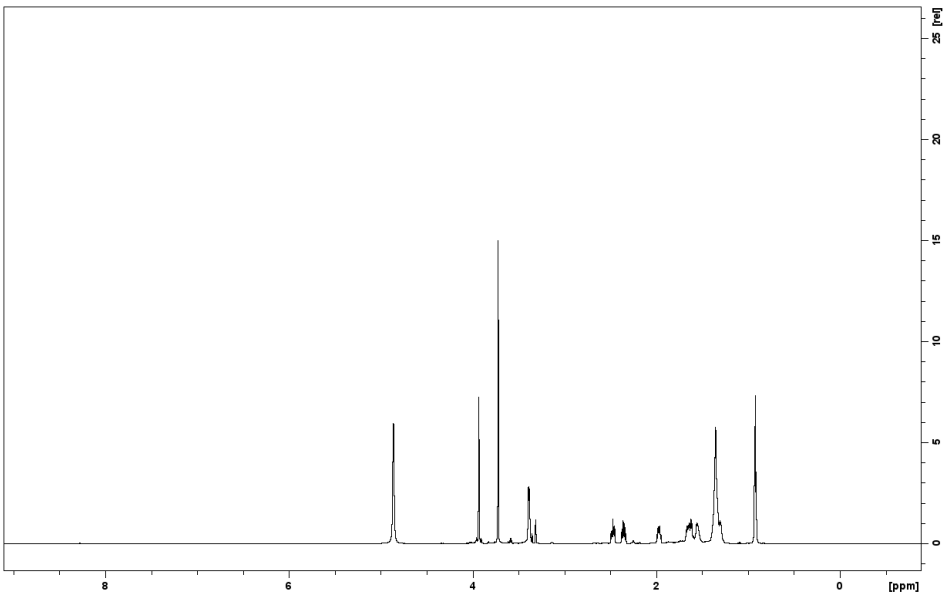

^{13}C NMR of compound **73a** in CD_3OD

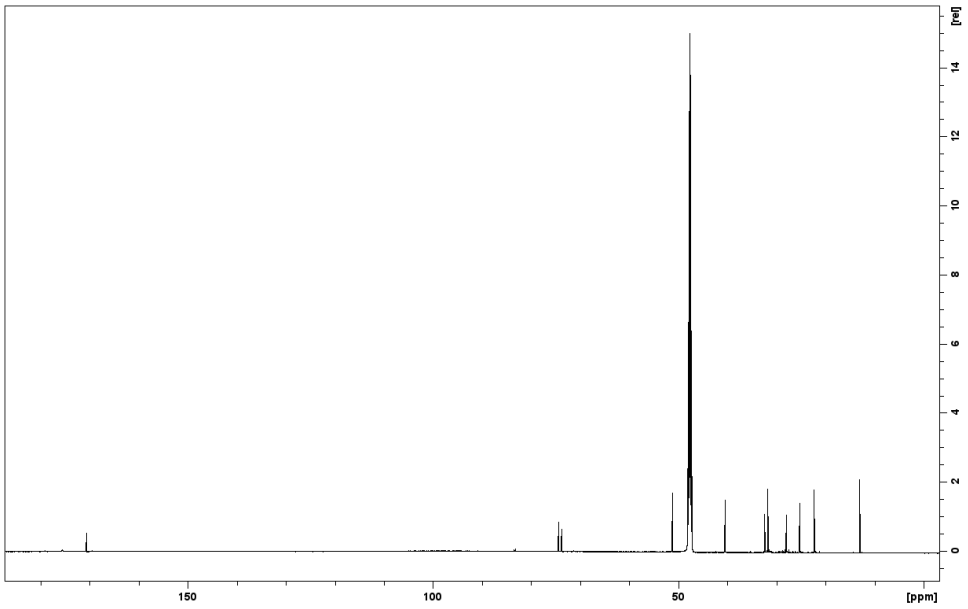

^{1}H NMR of compound **73b** in CD_3OD

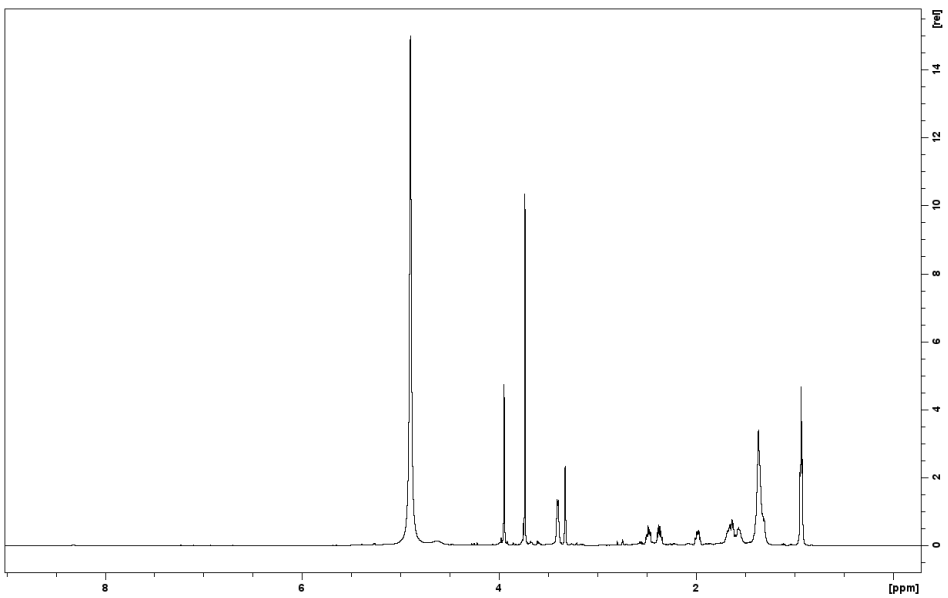

^{13}C NMR of compound **73b** in CD_3OD

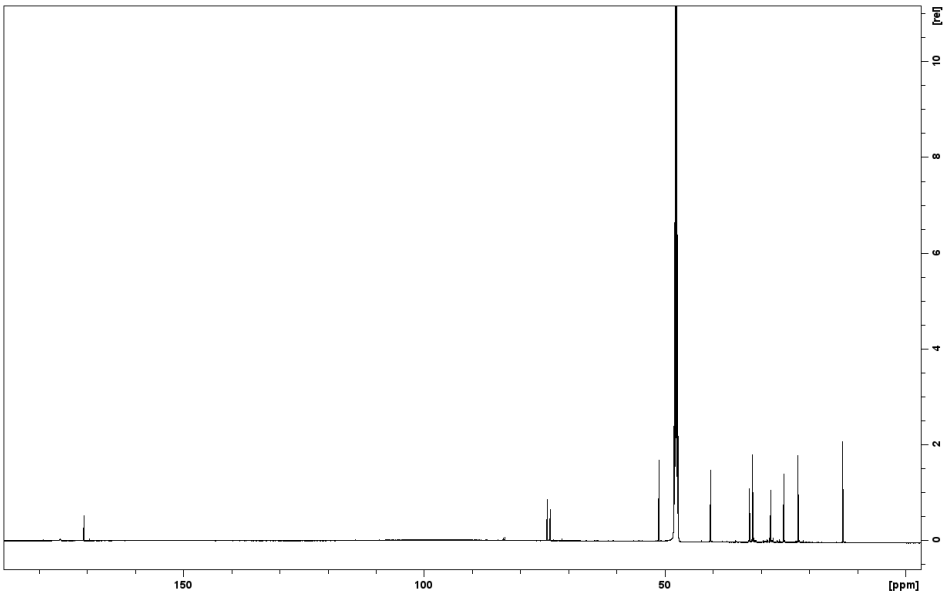

HR-ESIMS spectrum of compound **73b**

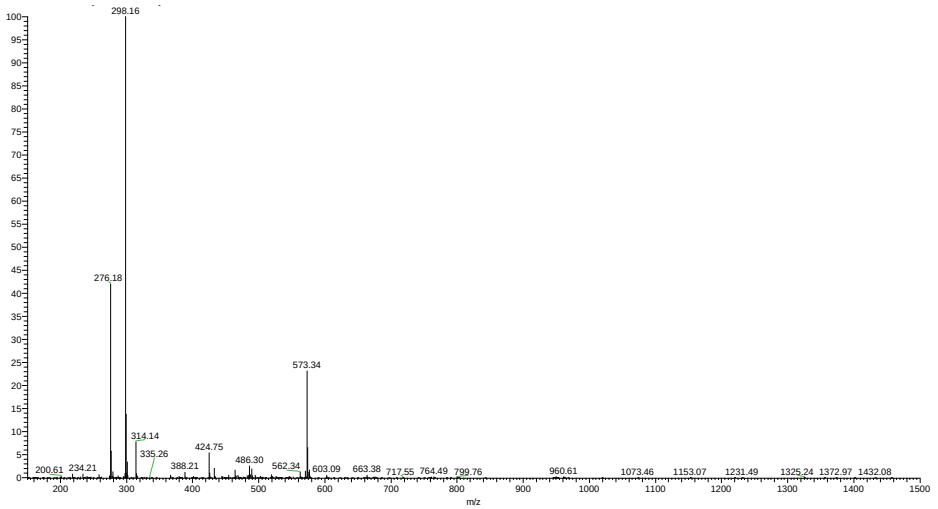

^{1}H NMR of compound **77** in $CDCl_3$

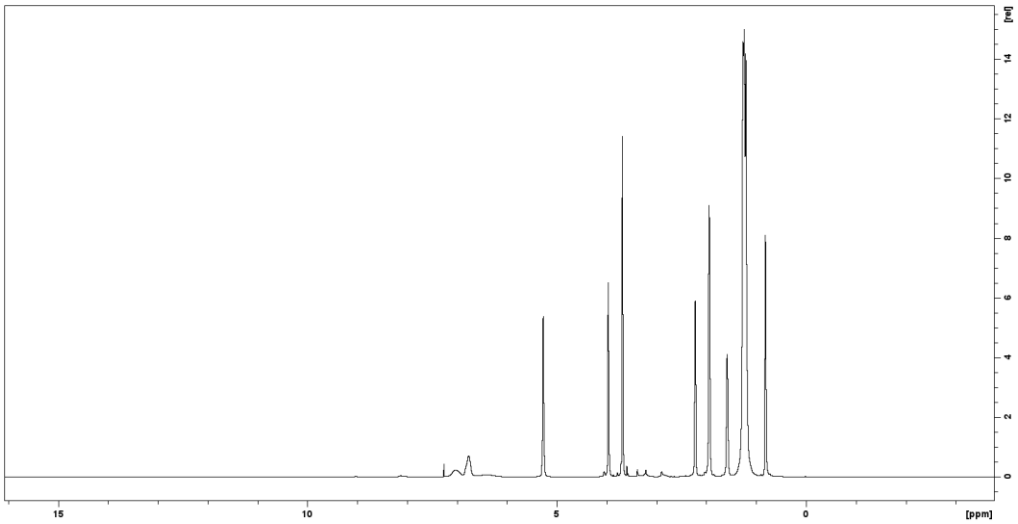

HR-ESIMS spectrum of compound **77**

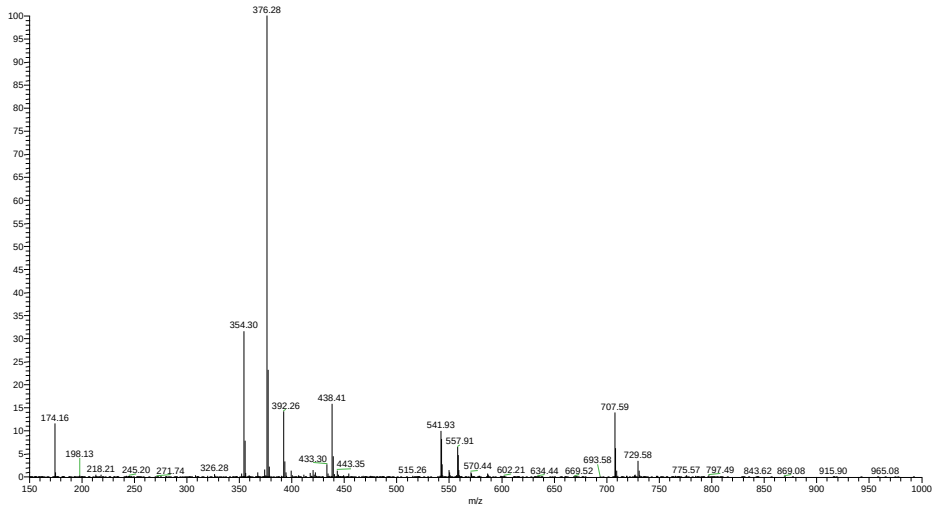

^{1}H NMR of compound **78a** in $CDCl_3$

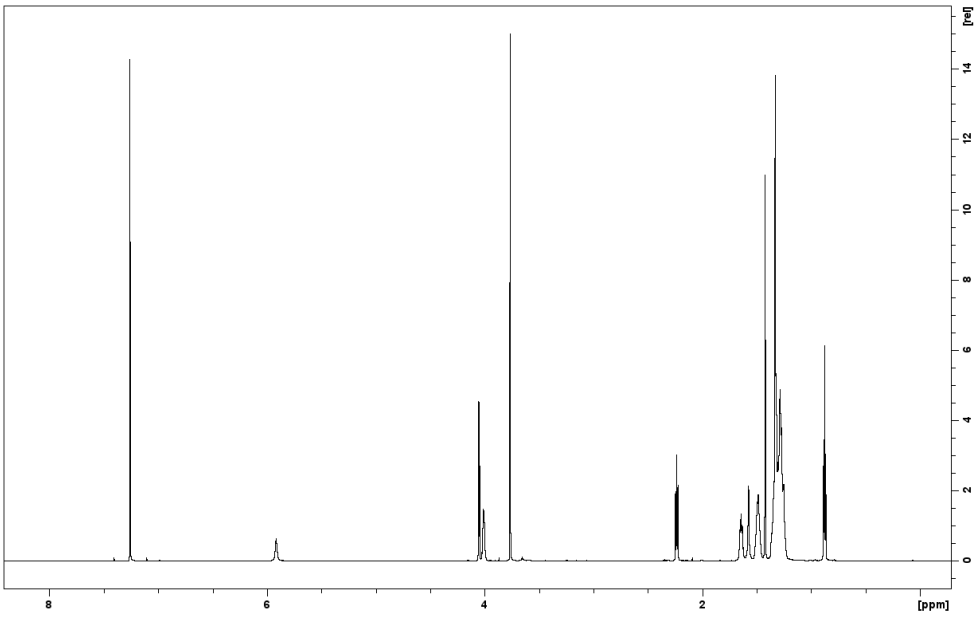

^{13}C NMR of compound **78a** in $CDCl_3$

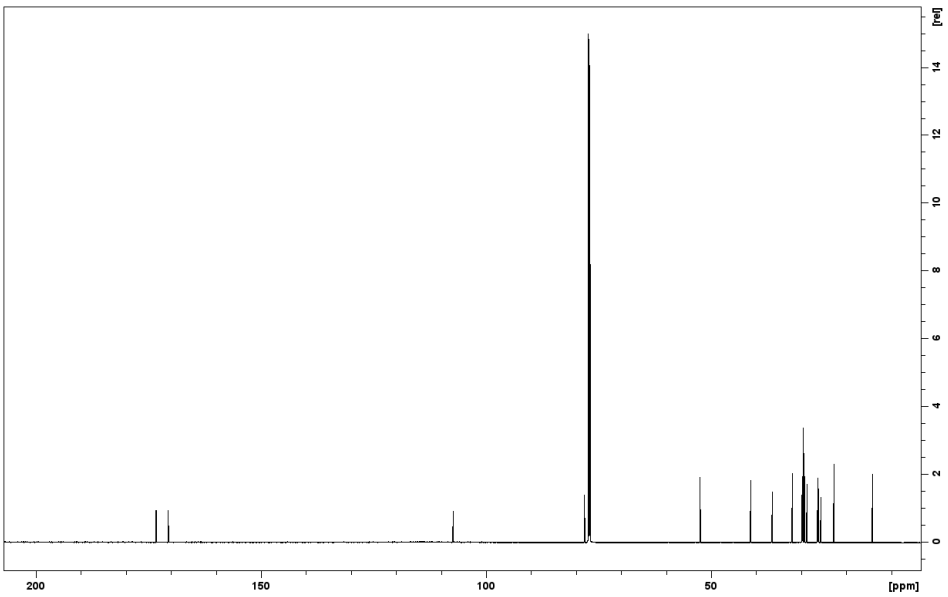

^{1}H NMR of compound **78b** in $CDCl_3$

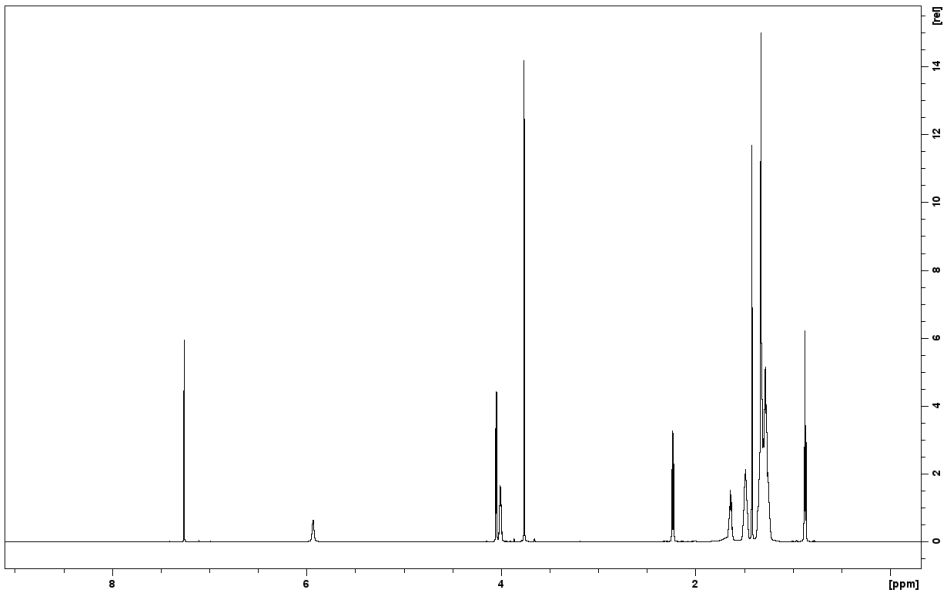

^{13}C NMR of compound **78b** in $CDCl_3$

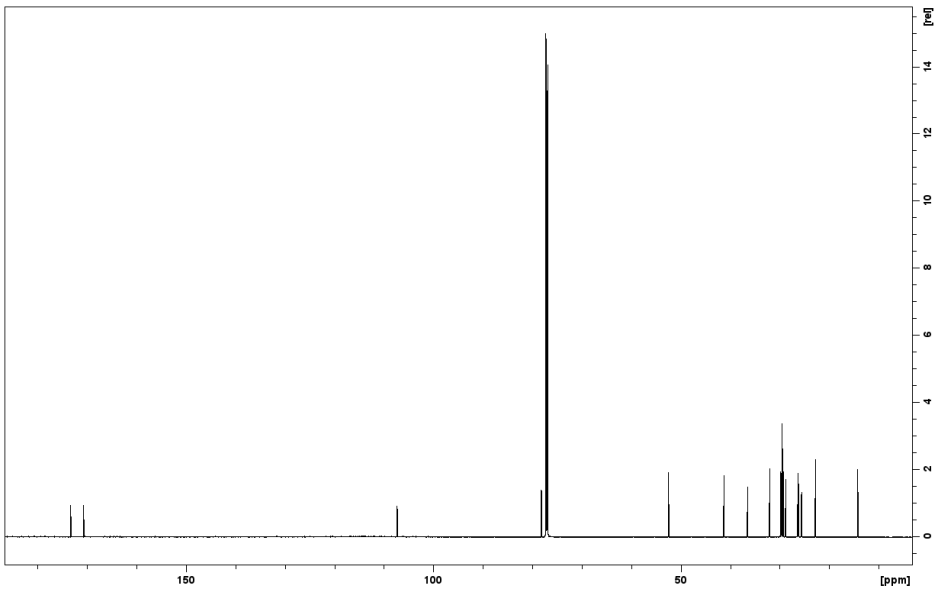

HR-ESIMS spectrum of compound **78b**

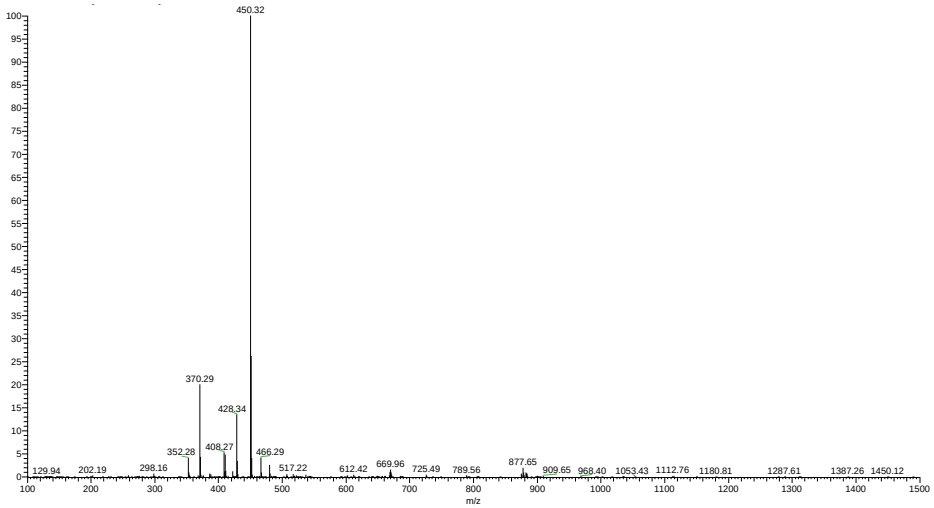

^{1}H NMR (700 MHz) of compound **74a** in $CDCl_3$

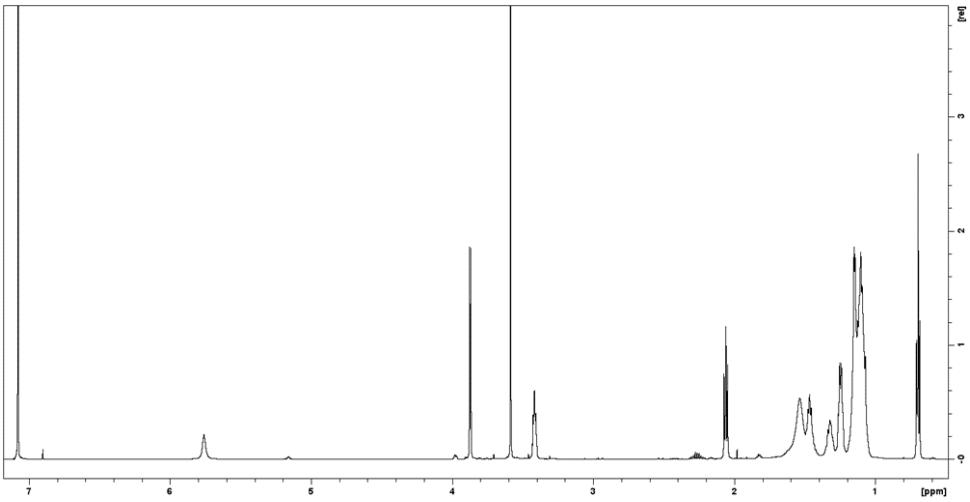

^{1}H NMR (700 MHz) of compound **74b** in $CDCl_3$

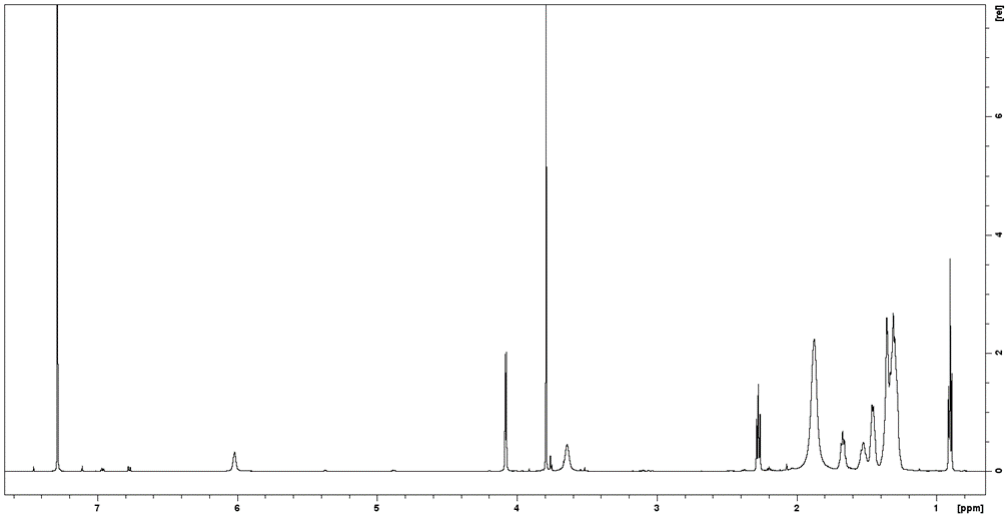

^{1}H NMR of compound **79** in $CDCl_3$

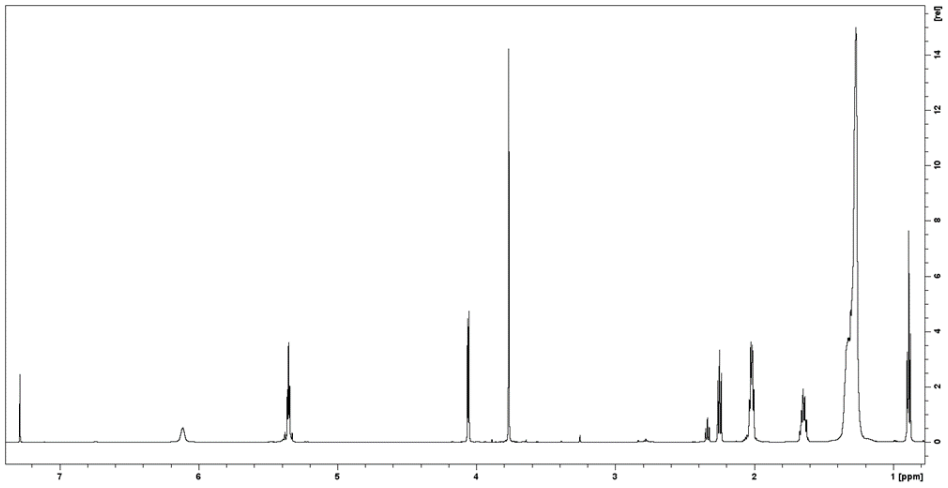

^{1}H NMR of compound **80a** in $CDCl_3$

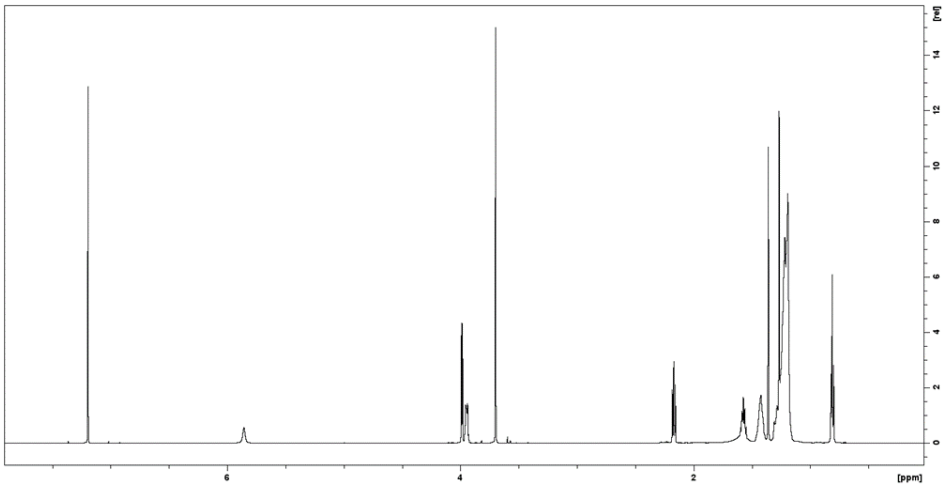

^{13}C NMR of compound **80a** in $CDCl_3$

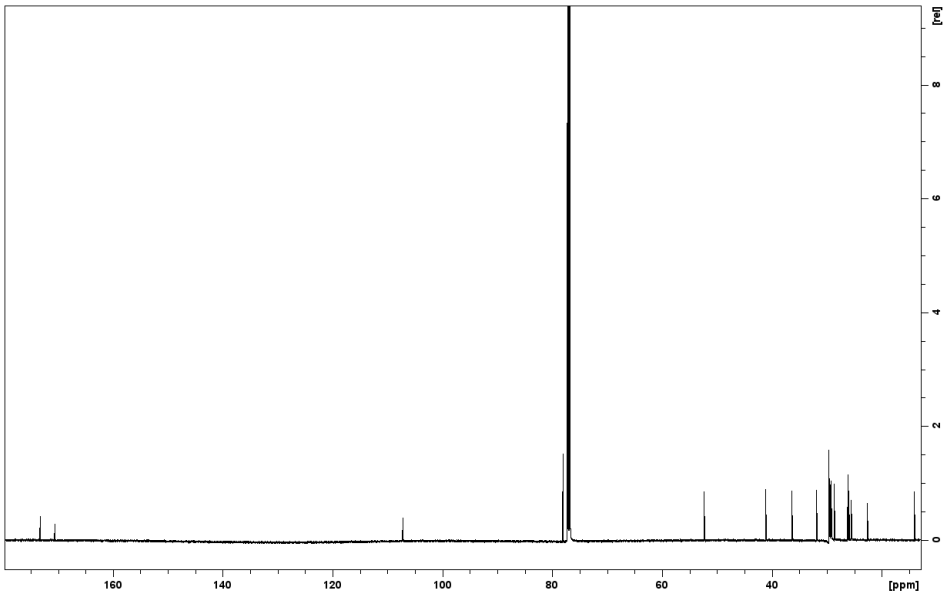

^{1}H NMR of compound **80b** in $CDCl_3$

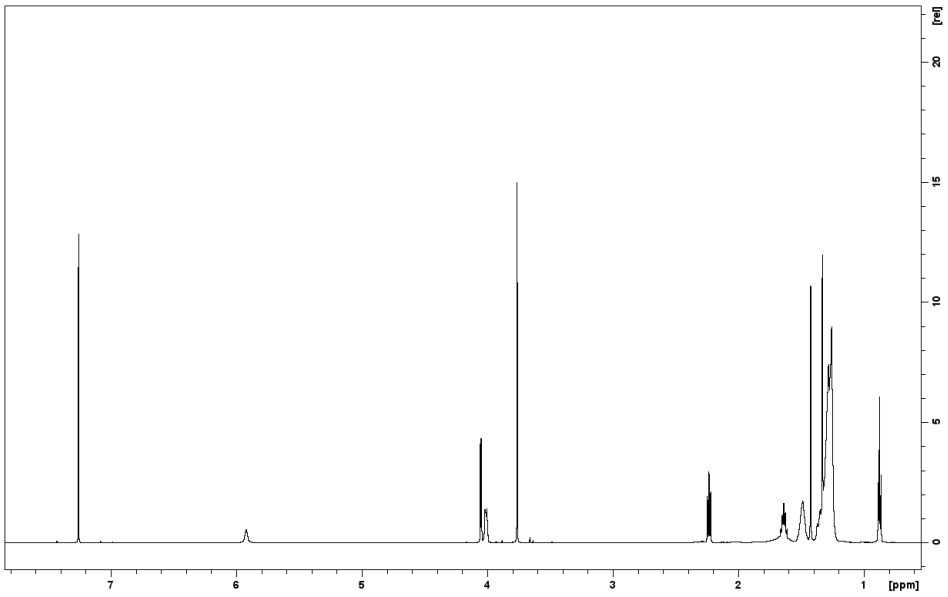

^{13}C NMR of compound **80b** in $CDCl_3$

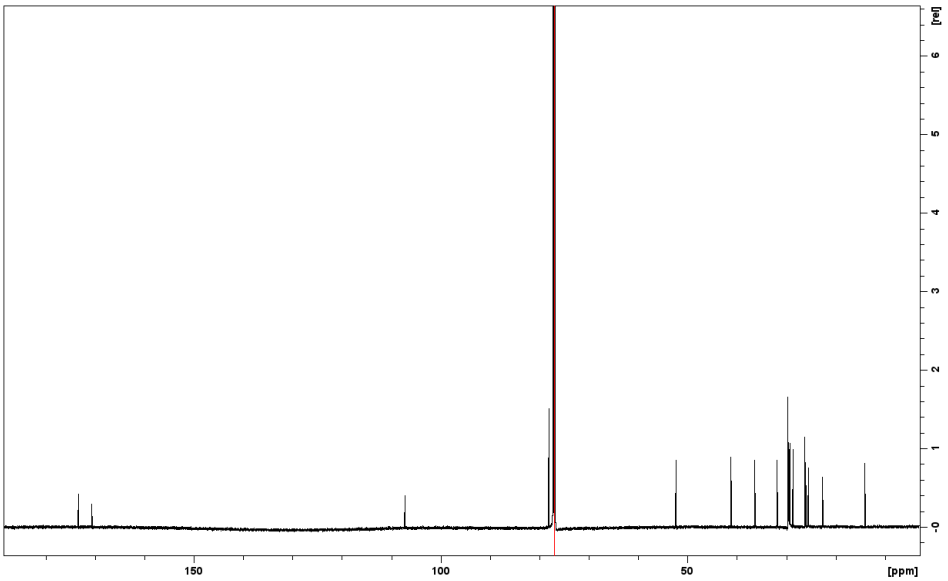

^{1}H NMR of compound **81a** in $CDCl_3$

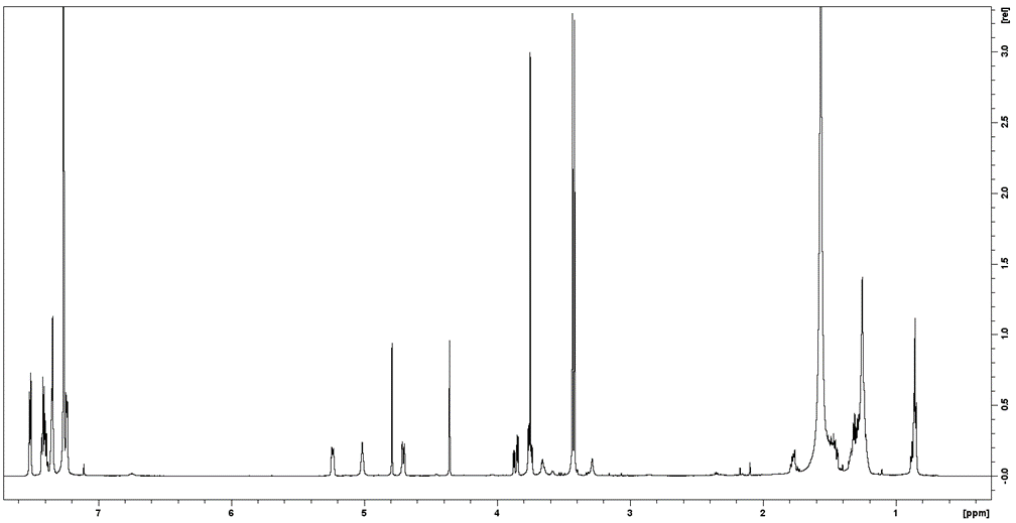

^{1}H-^{13}C HSQC spectrum in $CDCl_3$ of compound **81a**

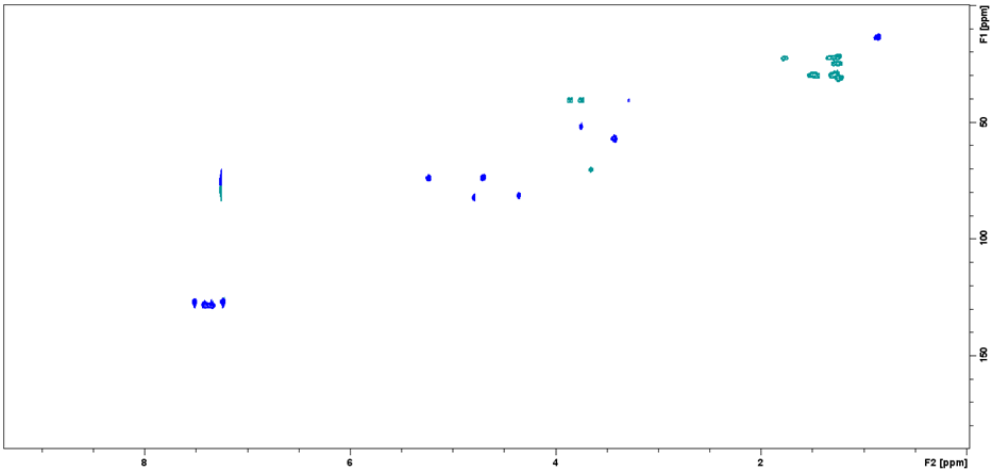

^{1}H-^{13}C HMBC spectrum in $CDCl_3$ of compound **81a**

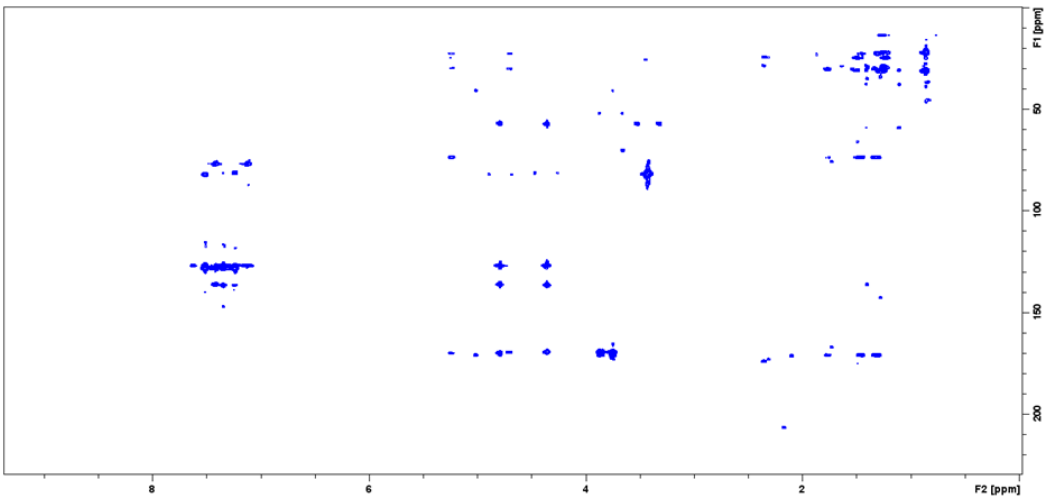

^{1}H-^{1}H COSY spectrum in $CDCl_3$ of compound **81a**

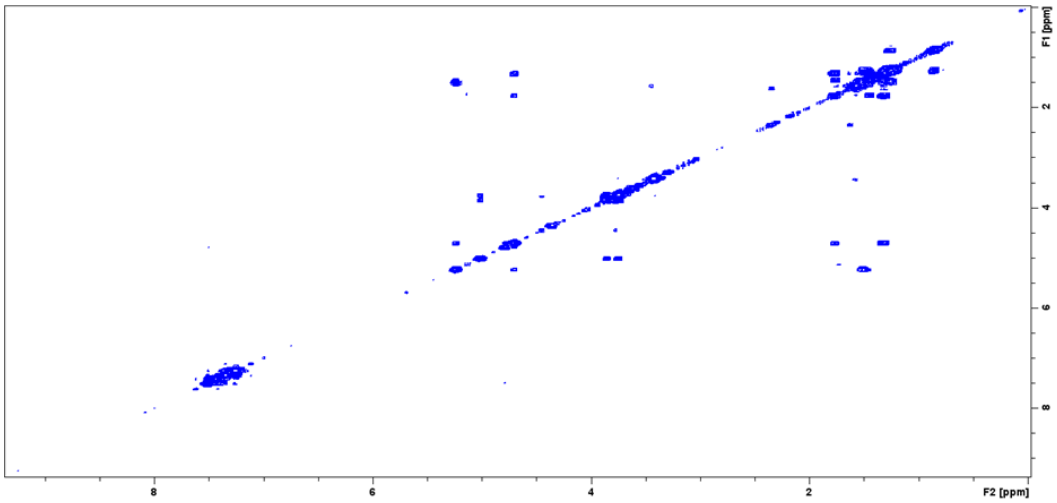

^{1}H NMR spectrum of compound **81b** in $CDCl_3$

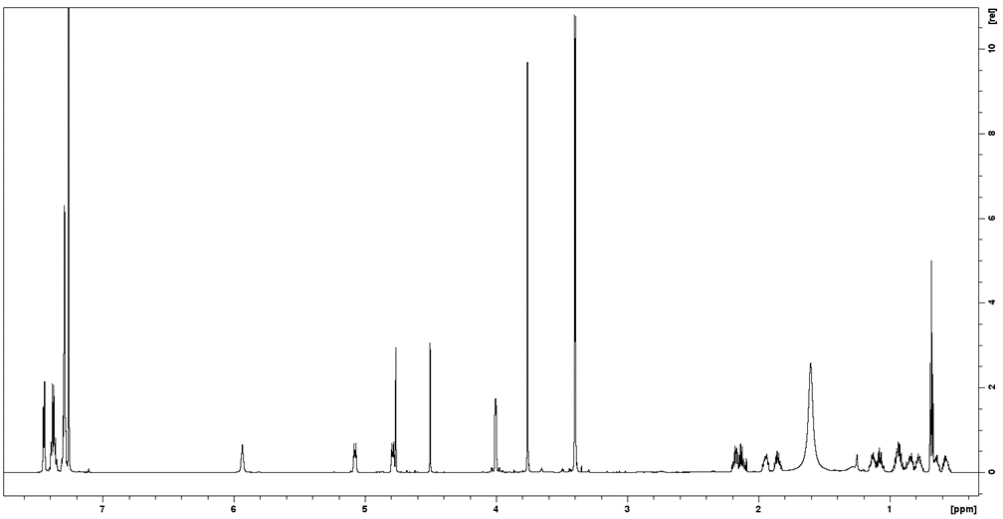

^{1}H-^{13}C HSQC spectrum in $CDCl_3$ of compound **81b**

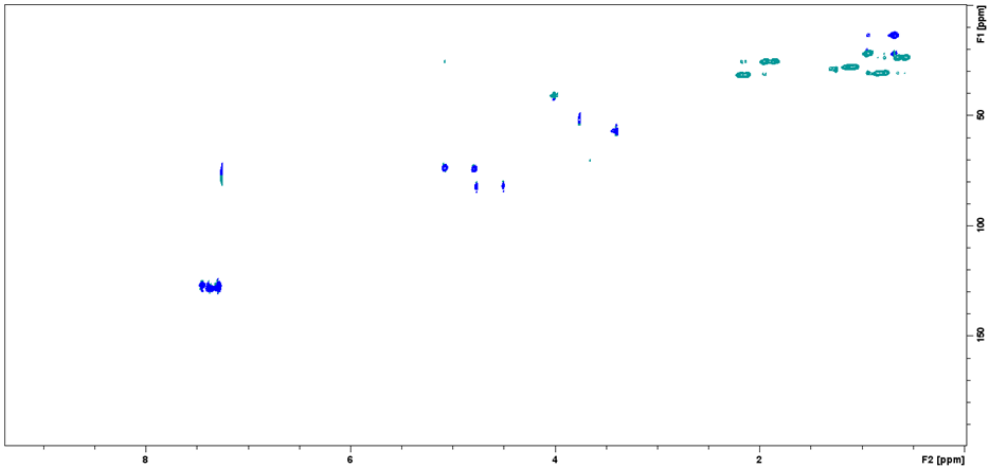

^{1}H-^{13}C HMBC spectrum in $CDCl_3$ of compound **81b**

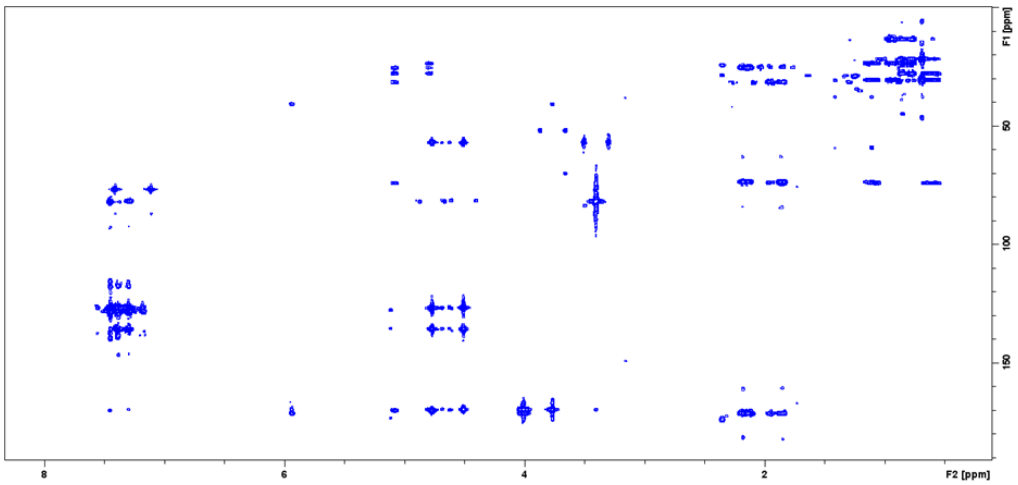

^{1}H-^{1}H COSY spectrum of compound **81b** in $CDCl_3$

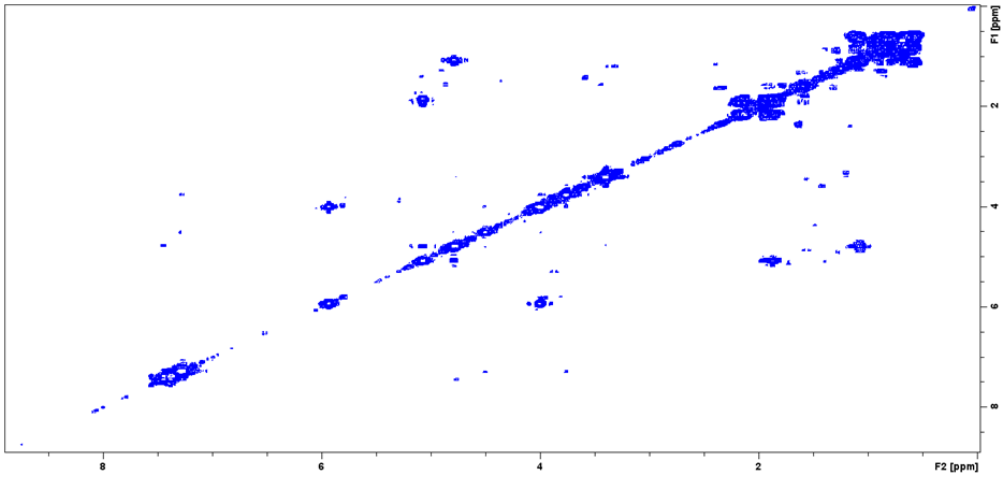

^{1}H NMR spectrum of compound **82a** in $CDCl_3$

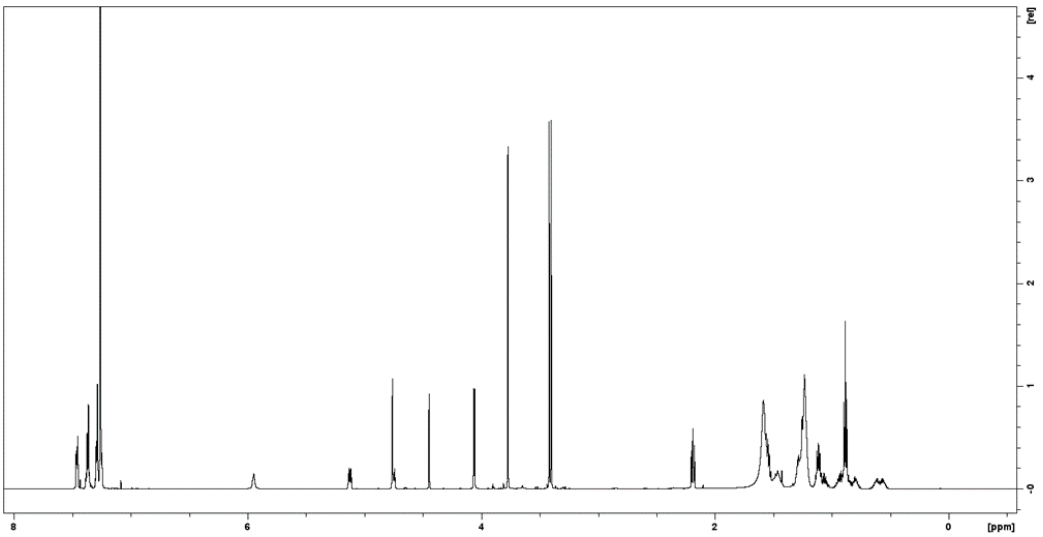

^{1}H-^{13}C HSQC spectrum in $CDCl_3$ of compound **82a**

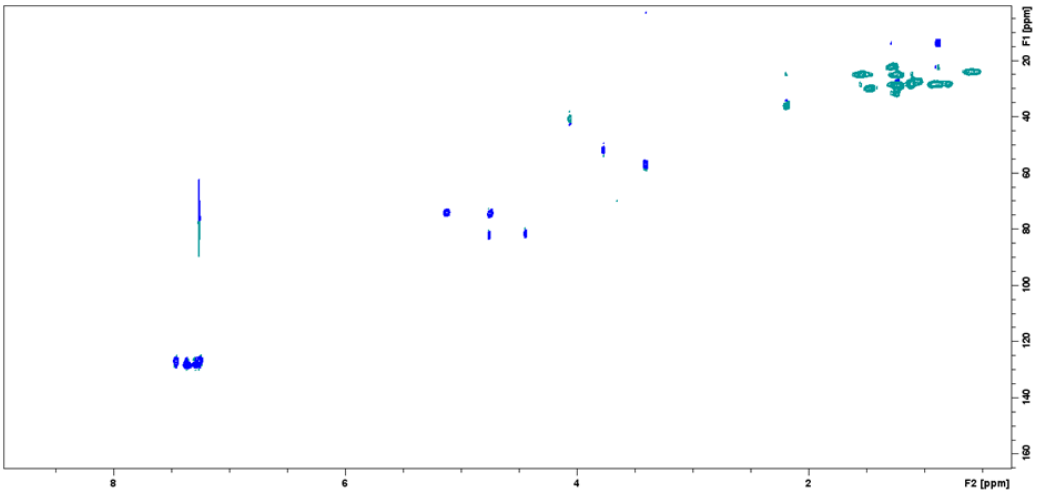

^{1}H-^{13}C HMBC spectrum in $CDCl_3$ of compound **82a**

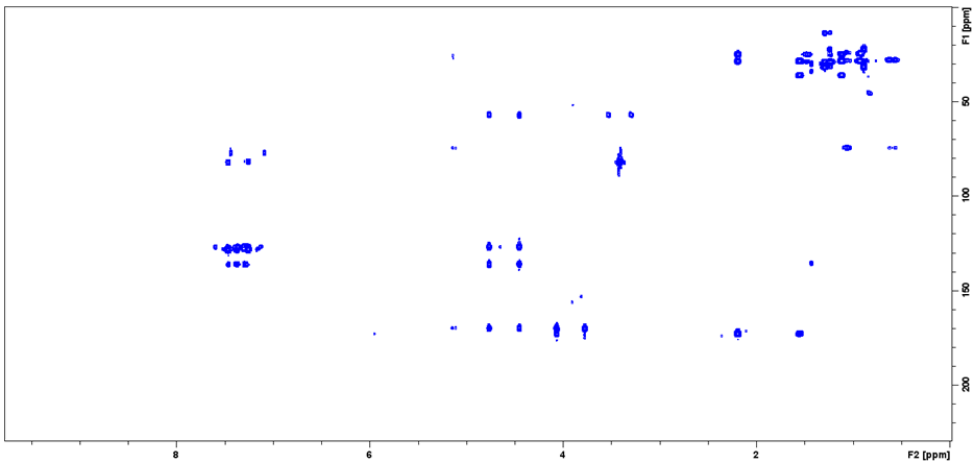

^{1}H-^{1}H COSY spectrum of compound **82a** in $CDCl_3$

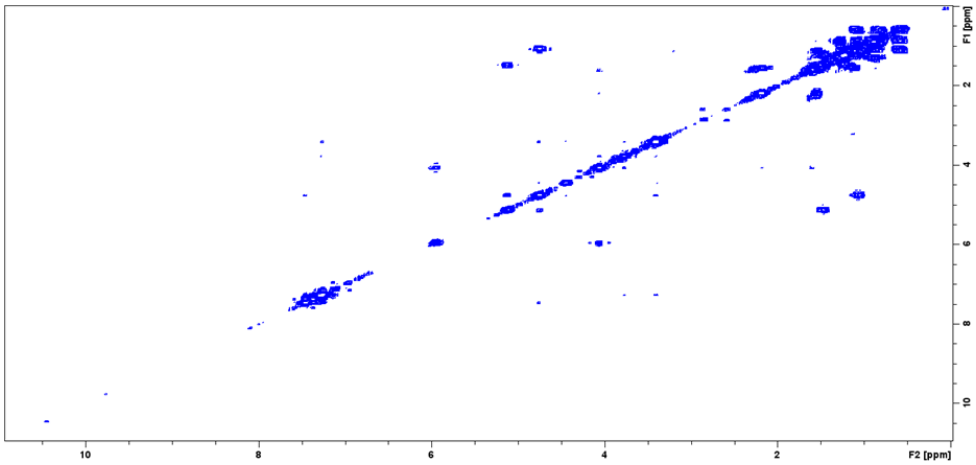

^{1}H NMR spectrum of compound **82b** in $CDCl_3$

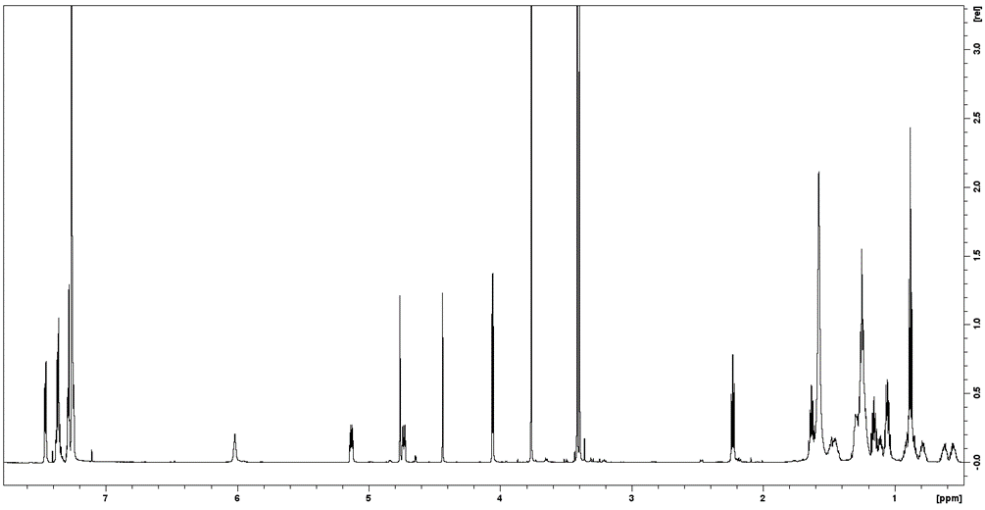

^{1}H-^{13}C HSQC spectrum in $CDCl_3$ of compound **82b**

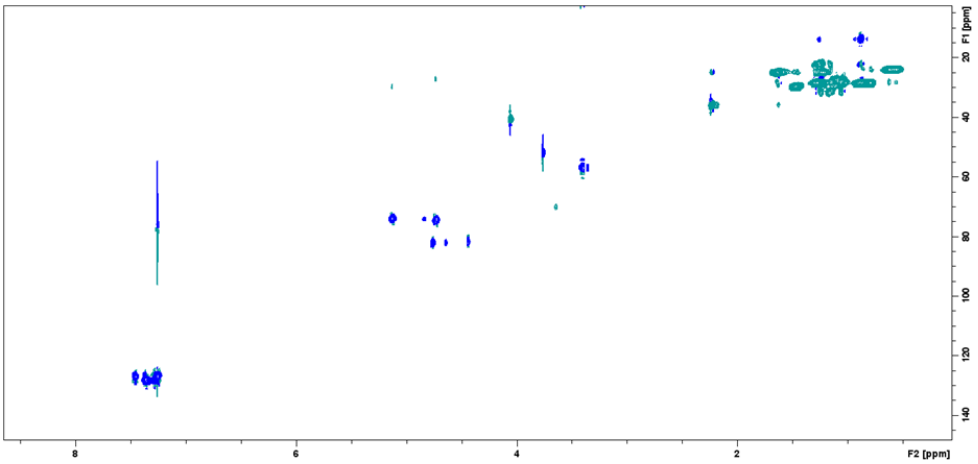

^{1}H-^{13}C HMBC spectrum in $CDCl_3$ of compound **82b**

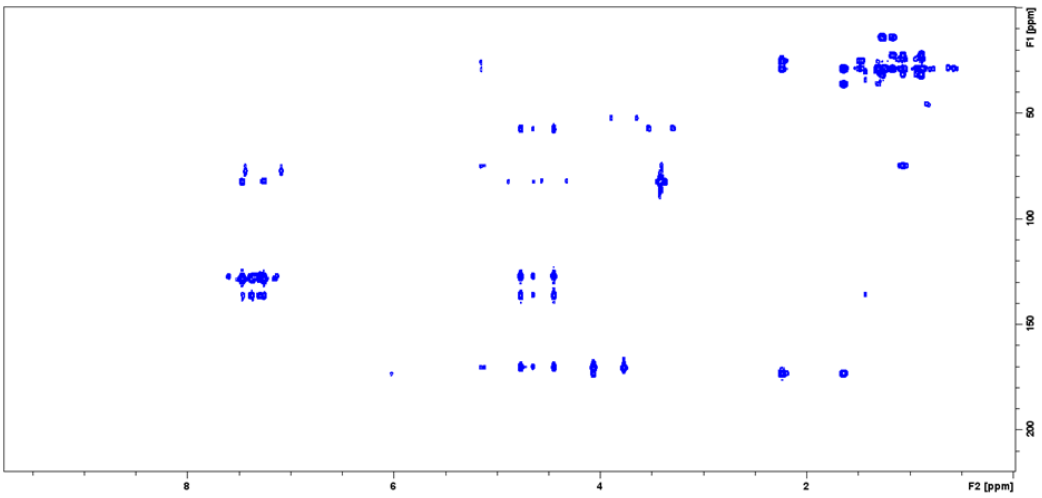

1H-1H COSY spectrum in $CDCl_3$ of compound **82b**

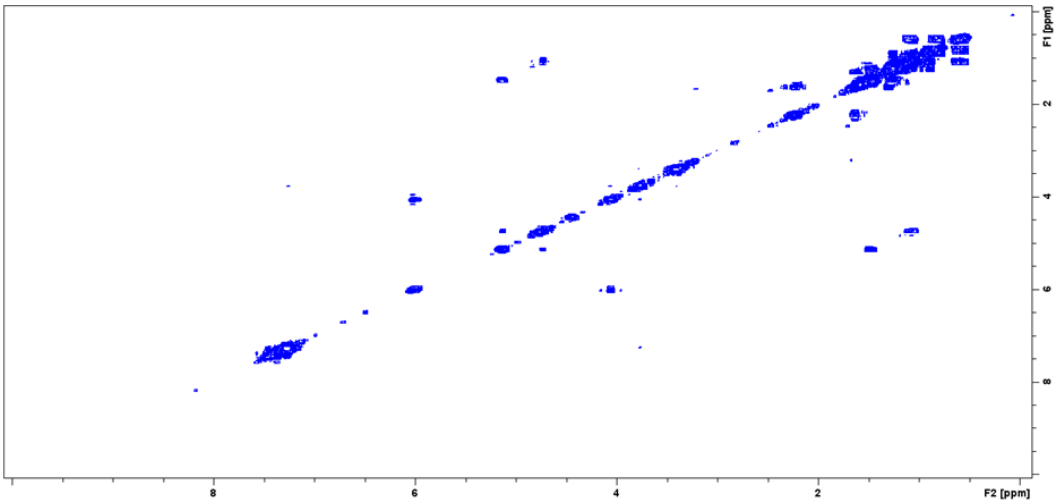

REFERENCES

1. Hughes, J.; Rees, S.; Kalindjian, S.; Philpott, K. Principles of Early Drug Discovery. *Br J Pharmacol* **2011**, *162*, 1239–1249, doi:10.1111/j.1476-5381.2010.01127.x.
2. Nicolaou, K.C. Advancing the Drug Discovery and Development Process. *Angewandte Chemie* **2014**, *126*, 9280–9292, doi:10.1002/ange.201404761.
3. Deore, A.B.; Dhumane, J.R.; Wagh, R.; Sonawane, R. The Stages of Drug Discovery and Development Process. *Asian Journal of Pharmaceutical Research and Development* **2019**, *7*, 62–67, doi:10.22270/ajprd.v7i6.616.

4. Owens, J. Determining Druggability. *Nat Rev Drug Discov* **2007**, *6*, 187–187, doi:10.1038/nrd2275.
5. Kopec, K.K.; Bozyczko-Coyne, D.; Williams, M. Target Identification and Validation in Drug Discovery: The Role of Proteomics. *Biochem Pharmacol* **2005**, *69*, 1133–1139, doi:10.1016/j.bcp.2005.01.004.
6. Doyle, S.K.; Pop, M.S.; Evans, H.L.; Koehler, A.N. Advances in Discovering Small Molecules to Probe Protein Function in a Systems Context. *Curr Opin Chem Biol* **2016**, *30*, 28–36, doi:10.1016/j.cbpa.2015.10.032.
7. Fox, S.; Farr-Jones, S.; Sopchak, L.; Boggs, A.; Nicely, H.W.; Khoury, R.; Biros, M. High-Throughput Screening: Update on Practices and Success. *SLAS Discovery* **2006**, *11*, 864–869, doi:10.1177/1087057106292473.
8. Liu, R.; Li, X.; Lam, K.S. Combinatorial Chemistry in Drug Discovery. *Curr Opin Chem Biol* **2017**, *38*, 117–126, doi:10.1016/j.cbpa.2017.03.017.
9. Dias, D.A.; Urban, S.; Roessner, U. A Historical Overview of Natural Products in Drug Discovery. *Metabolites* **2012**, *2*, 303–336, doi:10.3390/metabo2020303.
10. Fabricant, D.S.; Farnsworth, N.R. The Value of Plants Used in Traditional Medicine for Drug Discovery. *Environ Health Perspect* **2001**, *109*, 69–75, doi:10.1289/ehp.01109s169.
11. Verpoorte, R. Exploration of Nature's Chemodiversity: The Role of Secondary Metabolites as Leads in Drug Development. *Drug Discov Today* **1998**, *3*, 232–238, doi:10.1016/S1359-6446(97)01167-7.

12. Maplestone, R.A.; Stone, M.J.; Williams, D.H. The Evolutionary Role of Secondary Metabolites — a Review. *Gene* **1992**, *115*, 151–157, doi:10.1016/0378-1119(92)90553-2.
13. Newman, D.J.; Cragg, G.M. Natural Products as Sources of New Drugs over the Last 25 Years. *J Nat Prod* **2007**, *70*, 461–477, doi:10.1021/np068054v.
14. Newman, D.J.; Cragg, G.M. Natural Products as Sources of New Drugs over the Nearly Four Decades from 01/1981 to 09/2019. *J Nat Prod* **2020**, *83*, 770–803, doi:10.1021/acs.jnatprod.9b01285.
15. Atanasov, A.G.; Zotchev, S.B.; Dirsch, V.M.; Supuran, C.T. Natural Products in Drug Discovery: Advances and Opportunities. *Nat Rev Drug Discov* **2021**, *20*, 200–216, doi:10.1038/s41573-020-00114-z.
16. HARVEY, A. Natural Products in Drug Discovery. *Drug Discov Today* **2008**, *13*, 894–901, doi:10.1016/j.drudis.2008.07.004.
17. Koehn, F.E.; Carter, G.T. The Evolving Role of Natural Products in Drug Discovery. *Nat Rev Drug Discov* **2005**, *4*, 206–220, doi:10.1038/nrd1657.
18. Chen, Y.; Garcia de Lomana, M.; Friedrich, N.-O.; Kirchmair, J. Characterization of the Chemical Space of Known and Readily Obtainable Natural Products. *J Chem Inf Model* **2018**, *58*, 1518–1532, doi:10.1021/acs.jcim.8b00302.
19. Lovering, F.; Bikker, J.; Humblet, C. Escape from Flatland: Increasing Saturation as an Approach to Improving Clinical Success. *J Med Chem* **2009**, *52*, 6752–6756, doi:10.1021/jm901241e.
20. Chen, Y.; Garcia de Lomana, M.; Friedrich, N.-O.; Kirchmair, J. Characterization of the Chemical Space of Known and Readily

Obtainable Natural Products. *J Chem Inf Model* **2018**, *58*, 1518–1532, doi:10.1021/acs.jcim.8b00302.

21. Crawford, J.M.; Tang, G.-L.; Herzon, S.B. Natural Products: An Era of Discovery in Organic Chemistry. *J Org Chem* **2021**, *86*, 10943–10945, doi:10.1021/acs.joc.1c01753.
22. Baran, P.S. Natural Product Total Synthesis: As Exciting as Ever and Here To Stay. *J Am Chem Soc* **2018**, *140*, 4751–4755, doi:10.1021/jacs.8b02266.
23. Truax, N.J.; Romo, D. Bridging the Gap between Natural Product Synthesis and Drug Discovery. *Nat Prod Rep* **2020**, *37*, 1436–1453, doi:10.1039/D0NP00048E.
24. Vollmann, D.J.; Winand, L.; Nett, M. Emerging Concepts in the Semisynthetic and Mutasynthetic Production of Natural Products. *Curr Opin Biotechnol* **2022**, *77*, 102761, doi:10.1016/j.copbio.2022.102761.
25. Majhi, S.; Das, D. Chemical Derivatization of Natural Products: Semisynthesis and Pharmacological Aspects- A Decade Update. *Tetrahedron* **2021**, *78*, 131801, doi:10.1016/j.tet.2020.131801.
26. Scott, D.E.; Coyne, A.G.; Hudson, S.A.; Abell, C. Fragment-Based Approaches in Drug Discovery and Chemical Biology. *Biochemistry* **2012**, *51*, 4990–5003, doi:10.1021/bi3005126.
27. Murray, C.W.; Rees, D.C. The Rise of Fragment-Based Drug Discovery. *Nat Chem* **2009**, *1*, 187–192, doi:10.1038/nchem.217.
28. Dandapani, S.; Marcaurelle, L.A. Current Strategies for Diversity-Oriented Synthesis. *Curr Opin Chem Biol* **2010**, *14*, 362–370, doi:10.1016/j.cbpa.2010.03.018.

29. Spandl, R.J.; Díaz-Gavilán, M.; O'Connell, K.M.G.; Thomas, G.L.; Spring, D.R. Diversity-oriented Synthesis. *The Chemical Record* **2008**, *8*, 129–142, doi:10.1002/tcr.20144.
30. Cordier, C.; Morton, D.; Murrison, S.; Nelson, A.; O'Leary-Steele, C. Natural Products as an Inspiration in the Diversity-Oriented Synthesis of Bioactive Compound Libraries. *Nat Prod Rep* **2008**, *25*, 719, doi:10.1039/b706296f.
31. Over, B.; Wetzel, S.; Grütter, C.; Nakai, Y.; Renner, S.; Rauh, D.; Waldmann, H. Natural-Product-Derived Fragments for Fragment-Based Ligand Discovery. *Nat Chem* **2013**, *5*, 21–28, doi:10.1038/nchem.1506.
32. Newman, D.J.; Cragg, G.M. Marine Natural Products and Related Compounds in Clinical and Advanced Preclinical Trials. *J Nat Prod* **2004**, *67*, 1216–1238, doi:10.1021/np040031y.
33. Blunt, J.W.; Copp, B.R.; Munro, M.H.G.; Northcote, P.T.; Prinsep, M.R. Marine Natural Products. *Nat. Prod. Rep.* **2011**, *28*, 196–268, doi:10.1039/C005001F.
34. Li, K.; Chung-Davidson, Y.-W.; Bussy, U.; Li, W. Recent Advances and Applications of Experimental Technologies in Marine Natural Product Research. *Mar Drugs* **2015**, *13*, 2694–2713, doi:10.3390/md13052694.
35. Wang, S.; Dong, G.; Sheng, C. Structural Simplification of Natural Products. *Chem Rev* **2019**, *119*, 4180–4220, doi:10.1021/acs.chemrev.8b00504.
36. Chávez-Hernández, A.L.; Sánchez-Cruz, N.; Medina-Franco, J.L. A Fragment Library of Natural Products and Its Comparative Chemoinformatic Characterization. *Mol Inform* **2020**, *39*, doi:10.1002/minf.202000050.

37. Molinski, T.F.; Dalisay, D.S.; Lievens, S.L.; Saludes, J.P. Drug Development from Marine Natural Products. *Nat Rev Drug Discov* **2009**, *8*, 69–85, doi:10.1038/nrd2487.
38. Montaser, R.; Luesch, H. Marine Natural Products: A New Wave of Drugs? *Future Med Chem* **2011**, *3*, 1475–1489, doi:10.4155/fmc.11.118.
39. Schwartsmann, G.; da Rocha, A.B.; Berlinck, R.G.; Jimeno, J. Marine Organisms as a Source of New Anticancer Agents. *Lancet Oncol* **2001**, *2*, 221–225, doi:10.1016/S1470-2045(00)00292-8.
40. Dyshlovoy, S.A.; Honecker, F. Marine Compounds and Cancer: Updates 2020. *Mar Drugs* **2020**, *18*, 643, doi:10.3390/md18120643.
41. Sagar, S.; Kaur, M.; Minneman, K.P. Antiviral Lead Compounds from Marine Sponges. *Mar Drugs* **2010**, *8*, 2619–2638, doi:10.3390/md8102619.
42. Cuevas, C.; Francesch, A. Development of Yondelis® (Trabectedin, ET-743). A Semisynthetic Process Solves the Supply Problem. *Nat Prod Rep* **2009**, *26*, 322, doi:10.1039/b808331m.
43. Cappello, E.; Nieri, P. From Life in the Sea to the Clinic: The Marine Drugs Approved and under Clinical Trial. *Life* **2021**, *11*, 1390, doi:10.3390/life11121390.
44. Innes, J.K.; Calder, P.C. Marine Omega-3 (N-3) Fatty Acids for Cardiovascular Health: An Update for 2020. *Int J Mol Sci* **2020**, *21*, 1362, doi:10.3390/ijms21041362.
45. Safavi-Hemami, H.; Brogan, S.E.; Olivera, B.M. Pain Therapeutics from Cone Snail Venoms: From Ziconotide to Novel Non-Opioid Pathways. *J Proteomics* **2019**, *190*, 12–20, doi:10.1016/j.jprot.2018.05.009.

46. Pereira, F. Have Marine Natural Product Drug Discovery Efforts Been Productive and How Can We Improve Their Efficiency? *Expert Opin Drug Discov* **2019**, *14*, 717–722, doi:10.1080/17460441.2019.1604675.
47. Liu, L.; Zheng, Y.-Y.; Shao, C.-L.; Wang, C.-Y. Metabolites from Marine Invertebrates and Their Symbiotic Microorganisms: Molecular Diversity Discovery, Mining, and Application. *Mar Life Sci Technol* **2019**, *1*, 60–94, doi:10.1007/s42995-019-00021-2.
48. Shaw, J.E.; Sicree, R.A.; Zimmet, P.Z. Global Estimates of the Prevalence of Diabetes for 2010 and 2030. *Diabetes Res Clin Pract* **2010**, *87*, 4–14, doi:10.1016/j.diabres.2009.10.007.
49. Zghebi, S.S.; Steinke, D.T.; Carr, M.J.; Rutter, M.K.; Emsley, R.A.; Ashcroft, D.M. Examining Trends in Type 2 Diabetes Incidence, Prevalence and Mortality in the <scp>UK</Scp> between 2004 and 2014. *Diabetes Obes Metab* **2017**, *19*, 1537–1545, doi:10.1111/dom.12964.
50. Mosenzon, O.; Del Prato, S.; Schechter, M.; Leiter, L.A.; Ceriello, A.; DeFronzo, R.A.; Raz, I. From Glucose Lowering Agents to Disease/Diabetes Modifying Drugs: A “SIMPLE” Approach for the Treatment of Type 2 Diabetes. *Cardiovasc Diabetol* **2021**, *20*, 92, doi:10.1186/s12933-021-01281-y.
51. Nolan, C.J.; Damm, P.; Prentki, M. Type 2 Diabetes across Generations: From Pathophysiology to Prevention and Management. *The Lancet* **2011**, *378*, 169–181, doi:10.1016/S0140-6736(11)60614-4.
52. Wondmkun, Y.T. <p>Obesity, Insulin Resistance, and Type 2 Diabetes: Associations and Therapeutic Implications</P>. *Diabetes*

Metab Syndr Obes **2020**, *Volume 13*, 3611–3616, doi:10.2147/DMSO.S275898.

53. Dandona, P.; Aljada, A.; Chaudhuri, A.; Mohanty, P.; Garg, R. Metabolic Syndrome. *Circulation* **2005**, *111*, 1448–1454, doi:10.1161/01.CIR.0000158483.13093.9D.
54. Mosenzon, O.; Del Prato, S.; Schechter, M.; Leiter, L.A.; Ceriello, A.; DeFronzo, R.A.; Raz, I. From Glucose Lowering Agents to Disease/Diabetes Modifying Drugs: A "SIMPLE" Approach for the Treatment of Type 2 Diabetes. *Cardiovasc Diabetol* **2021**, *20*, 92, doi:10.1186/s12933-021-01281-y.
55. Hamdy, O.; Goodyear, L.J.; Horton, E.S. DIET AND EXERCISE IN TYPE 2 DIABETES MELLITUS. *Endocrinol Metab Clin North Am* **2001**, *30*, 883–907, doi:10.1016/S0889-8529(05)70220-6.
56. Seino, S.; Sugawara, K.; Yokoi, N.; Takahashi, H. B-Cell Signalling and Insulin Secretagogues: A Path for Improved Diabetes Therapy. *Diabetes Obes Metab* **2017**, *19*, 22–29, doi:10.1111/dom.12995.
57. Quillen, D.M.; Samraj, G.; Kuritzky, L. Improving Management of Type 2 Diabetes Mellitus: 2. Biguanides. *Hosp Pract* **1999**, *34*, 41–44, doi:10.1080/21548331.1999.11443925.
58. Thangavel, N.; Al Bratty, M.; Akhtar Javed, S.; Ahsan, W.; Alhazmi, H.A. Targeting Peroxisome Proliferator-Activated Receptors Using Thiazolidinediones: Strategy for Design of Novel Antidiabetic Drugs. *Int J Med Chem* **2017**, *2017*, 1–20, doi:10.1155/2017/1069718.
59. Padhi, S.; Nayak, A.K.; Behera, A. Type II Diabetes Mellitus: A Review on Recent Drug Based Therapeutics. *Biomedicine &*

Pharmacotherapy **2020**, *131*, 110708, doi:10.1016/j.biopha.2020.110708.

60. Sharma, P.; Singh, S.; Thakur, V.; Sharma, N.; Grewal, A.S. Novel and Emerging Therapeutic Drug Targets for Management of Type 2 Diabetes Mellitus. *Obes Med* **2021**, *23*, 100329, doi:10.1016/j.obmed.2021.100329.
61. Gong, L.; Feng, D.; Wang, T.; Ren, Y.; Liu, Y.; Wang, J. Inhibitors of A-amylase and A-glucosidase: Potential Linkage for Whole Cereal Foods on Prevention of Hyperglycemia. *Food Sci Nutr* **2020**, *8*, 6320–6337, doi:10.1002/fsn3.1987.
62. Ferrannini, E.; Solini, A. SGLT2 Inhibition in Diabetes Mellitus: Rationale and Clinical Prospects. *Nat Rev Endocrinol* **2012**, *8*, 495–502, doi:10.1038/nrendo.2011.243.
63. Kaur, R.; Dahiya, L.; Kumar, M. Fructose-1,6-Bisphosphatase Inhibitors: A New Valid Approach for Management of Type 2 Diabetes Mellitus. *Eur J Med Chem* **2017**, *141*, 473–505, doi:10.1016/j.ejmech.2017.09.029.
64. Henriksen, E.; Dokken, B. Role of Glycogen Synthase Kinase-3 in Insulin Resistance and Type 2 Diabetes. *Curr Drug Targets* **2006**, *7*, 1435–1441, doi:10.2174/1389450110607011435.
65. ZHANG, S.; ZHANG, Z. PTP1B as a Drug Target: Recent Developments in PTP1B Inhibitor Discovery. *Drug Discov Today* **2007**, *12*, 373–381, doi:10.1016/j.drudis.2007.03.011.
66. Oyama, T.; Miyasita, Y.; Watanabe, H.; Shirai, K. The Role of Polyol Pathway in High Glucose-Induced Endothelial Cell Damages. *Diabetes Res Clin Pract* **2006**, *73*, 227–234, doi:10.1016/j.diabres.2006.02.010.

67. Casertano, M.; Vito, A.; Aiello, A.; Imperatore, C.; Menna, M. Natural Bioactive Compounds from Marine Invertebrates That Modulate Key Targets Implicated in the Onset of Type 2 Diabetes Mellitus (T2DM) and Its Complications. *Pharmaceutics* **2023**, *15*, 2321, doi:10.3390/pharmaceutics15092321.
68. Zhang, Y.; Li, Y.; Guo, Y.; Jiang, H.; Shen, X. A Sesquiterpene Quinone, Dysidine, from the Sponge Dysidea Villosa, Activates the Insulin Pathway through Inhibition of PTPases. *Acta Pharmacol Sin* **2009**, *30*, 333–345, doi:10.1038/aps.2009.5.
69. Abdjul, D.B.; Yamazaki, H.; Takahashi, O.; Kirikoshi, R.; Ukai, K.; Namikoshi, M. Sesquiterpene Hydroquinones with Protein Tyrosine Phosphatase 1B Inhibitory Activities from a *Dysidea* Sp. Marine Sponge Collected in Okinawa. *J Nat Prod* **2016**, *79*, 1842–1847, doi:10.1021/acs.jnatprod.6b00367.
70. Jiao, W.-H.; Li, J.; Zhang, M.-M.; Cui, J.; Gui, Y.-H.; Zhang, Y.; Li, J.-Y.; Liu, K.-C.; Lin, H.-W. Frondoplysins A and B, Unprecedented Terpene-Alkaloid Bioconjugates from *Dysidea Frondosa*. *Org Lett* **2019**, *21*, 6190–6193, doi:10.1021/acs.orglett.9b01754.
71. He, W.-F.; Xue, D.-Q.; Yao, L.-G.; Li, J.; Liu, H.-L.; Guo, Y.-W. A New Bioactive Steroidal Ketone from the South China Sea Sponge *Xestospongia Testudinaria*. *J Asian Nat Prod Res* **2016**, *18*, 195–199, doi:10.1080/10286020.2015.1056521.
72. Yamazaki, H.; Sumilat, D.A.; Kanno, S.; Ukai, K.; Rotinsulu, H.; Wewengkang, D.S.; Ishikawa, M.; Mangindaan, R.E.P.; Namikoshi, M. A Polybromodiphenyl Ether from an Indonesian Marine Sponge Lamellodysidea Herbacea and Its Chemical Derivatives Inhibit Protein Tyrosine Phosphatase 1B, an Important

Target for Diabetes Treatment. *J Nat Med* **2013**, *67*, 730–735, doi:10.1007/s11418-012-0735-y.

73. Takada, K.; Uehara, T.; Nakao, Y.; Matsunaga, S.; van Soest, R.W.M.; Fusetani, N. Schulzeines A−C, New α-Glucosidase Inhibitors from the Marine Sponge *Penares Schulzei* [1]. *J Am Chem Soc* **2004**, *126*, 187–193, doi:10.1021/ja037368r.
74. Costantino, L.; Rastelli, G.; Cignarella, G.; Vianello, P.; Barlocco, D. New Aldose Reductase Inhibitors as Potential Agents for the Prevention of Long-Term Diabetic Complications. *Expert Opin Ther Pat* **1997**, *7*, 843–858, doi:10.1517/13543776.7.8.843.
75. Manzanaro, S.; Salvá, J.; de la Fuente, J.Á. Phenolic Marine Natural Products as Aldose Reductase Inhibitors. *J Nat Prod* **2006**, *69*, 1485–1487, doi:10.1021/np0503698.
76. Hamann, M.; Alonso, D.; Martín-Aparicio, E.; Fuertes, A.; Pérez-Puerto, M.J.; Castro, A.; Morales, S.; Navarro, M.L.; del Monte-Millán, M.; Medina, M.; et al. Glycogen Synthase Kinase-3 (GSK-3) Inhibitory Activity and Structure–Activity Relationship (SAR) Studies of the Manzamine Alkaloids. Potential for Alzheimer's Disease. *J Nat Prod* **2007**, *70*, 1397–1405, doi:10.1021/np060092r.
77. Chianese, G.; Yu, H.-B.; Yang, F.; Sirignano, C.; Luciano, P.; Han, B.-N.; Khan, S.; Lin, H.-W.; Taglialatela-Scafati, O. PPAR Modulating Polyketides from a Chinese *Plakortis Simplex* and Clues on the Origin of Their Chemodiversity. *J Org Chem* **2016**, *81*, 5135–5143, doi:10.1021/acs.joc.6b00695.
78. Festa, C.; D'Amore, C.; Renga, B.; Lauro, G.; Marino, S.; D'Auria, M.; Bifulco, G.; Zampella, A.; Fiorucci, S. Oxygenated Polyketides from Plakinastrella Mamillaris as a New Chemotype of PXR

Agonists. *Mar Drugs* **2013**, *11*, 2314–2327, doi:10.3390/md11072314.

79. Anighoro, A.; Bajorath, J.; Rastelli, G. Polypharmacology: Challenges and Opportunities in Drug Discovery. *J Med Chem* **2014**, *57*, 7874–7887, doi:10.1021/jm5006463.
80. Wermuth, C.G. Multitargeted Drugs: The End of the 'One-Target-One-Disease' Philosophy? *Drug Discov Today* **2004**, *9*, 826–827, doi:10.1016/S1359-6446(04)03213-1.
81. Ramsay, R.R.; Popovic-Nikolic, M.R.; Nikolic, K.; Uliassi, E.; Bolognesi, M.L. A Perspective on Multi-target Drug Discovery and Design for Complex Diseases. *Clin Transl Med* **2018**, *7*, doi:10.1186/s40169-017-0181-2.
82. Casertano, M.; Genovese, M.; Santi, A.; Pranzini, E.; Balestri, F.; Piazza, L.; Del Corso, A.; Avunduk, S.; Imperatore, C.; Menna, M.; et al. Evidence of Insulin-Sensitizing and Mimetic Activity of the Sesquiterpene Quinone Avarone, a Protein Tyrosine Phosphatase 1B and Aldose Reductase Dual Targeting Agent from the Marine Sponge Dysidea Avara. *Pharmaceutics* **2023**, *15*, 528, doi:10.3390/pharmaceutics15020528.
83. DELIORMAN ORHAN, D. PHENOLIC CONTENT, ANTIOXIDANT AND IN VITRO ANTIDIABETIC EFFECTS OF THIRTEEN MARINE ORGANISMS FROM MEDITERRANEAN SEA. *Farmacia* **2021**, *69*, 68–74, doi:10.31925/farmacia.2021.1.9.
84. Francis, P.; Chakraborty, K. Clathriketal, a New Tricyclic Spiroketal Compound from Marine Sponge *Clathria Prolifera* Attenuates Serine Exopeptidase Dipeptidyl Peptidase-IV. *Nat Prod Res* **2022**, *36*, 3069–3077, doi:10.1080/14786419.2021.1956491.

85. D'Aniello, E.; Iannotti, F.; Falkenberg, L.; Martella, A.; Gentile, A.; De Maio, F.; Ciavatta, M.; Gavagnin, M.; Waxman, J.; Di Marzo, V.; et al. In Silico Identification and Experimental Validation of (−)-Muqubilin A, a Marine Norterpene Peroxide, as PPARα/γ-RXRα Agonist and RARα Positive Allosteric Modulator. *Mar Drugs* **2019**, *17*, 110, doi:10.3390/md17020110.
86. Liang, X.; Luo, D.; Luesch, H. Advances in Exploring the Therapeutic Potential of Marine Natural Products. *Pharmacol Res* **2019**, *147*, 104373, doi:10.1016/j.phrs.2019.104373.
87. Blunt, J.W.; Copp, B.R.; Hu, W.-P.; Munro, M.H.G.; Northcote, P.T.; Prinsep, M.R. Marine Natural Products. *Nat Prod Rep* **2009**, *26*, 170, doi:10.1039/b805113p.
88. Liu, X.-Y.; Qin, Y. Industrial Total Synthesis of Natural Medicines. *Nat Prod Rep* **2023**, *40*, 1694–1700, doi:10.1039/D3NP00020F.
89. Ganesan, A. The Impact of Natural Products upon Modern Drug Discovery. *Curr Opin Chem Biol* **2008**, *12*, 306–317, doi:10.1016/j.cbpa.2008.03.016.
90. Gordaliza, M. Natural Products as Leads to Anticancer Drugs. *Clinical and Translational Oncology* **2007**, *9*, 767–776, doi:10.1007/s12094-007-0138-9.
91. Barnes, E.C.; Kumar, R.; Davis, R.A. The Use of Isolated Natural Products as Scaffolds for the Generation of Chemically Diverse Screening Libraries for Drug Discovery. *Nat Prod Rep* **2016**, *33*, 372–381, doi:10.1039/C5NP00121H.
92. Galloway, W.R.J.D.; Isidro-Llobet, A.; Spring, D.R. Diversity-Oriented Synthesis as a Tool for the Discovery of Novel Biologically Active Small Molecules. *Nat Commun* **2010**, *1*, 80, doi:10.1038/ncomms1081.

93. Burke, M.D.; Schreiber, S.L. A Planning Strategy for Diversity-Oriented Synthesis. *Angewandte Chemie International Edition* **2004**, *43*, 46–58, doi:10.1002/anie.200300626.

94. Kim, J.; Kim, H.; Park, S.B. Privileged Structures: Efficient Chemical "Navigators" toward Unexplored Biologically Relevant Chemical Spaces. *J Am Chem Soc* **2014**, *136*, 14629–14638, doi:10.1021/ja508343a.

95. Marcaurelle, L.A.; Johannes, C.W. Application of Natural Product-Inspired Diversity-Oriented Synthesis to Drug Discovery. In *Natural Compounds as Drugs*; Birkhäuser Basel: Basel; pp. 187–216.

96. Morley, A.D.; Pugliese, A.; Birchall, K.; Bower, J.; Brennan, P.; Brown, N.; Chapman, T.; Drysdale, M.; Gilbert, I.H.; Hoelder, S.; et al. Fragment-Based Hit Identification: Thinking in 3D. *Drug Discov Today* **2013**, *18*, 1221–1227, doi:10.1016/j.drudis.2013.07.011.

97. Liu, M.; Quinn, R.J. Fragment-Based Screening with Natural Products for Novel Anti-Parasitic Disease Drug Discovery. *Expert Opin Drug Discov* **2019**, *14*, 1283–1295, doi:10.1080/17460441.2019.1653849.

98. McConathy, J.; Owens, M.J. Stereochemistry in Drug Action. *Prim Care Companion CNS Disord* **2003**, *5*, doi:10.4088/PCC.v05n0202.

99. Flack, H.D.; Bernardinelli, G. The Use of X-ray Crystallography to Determine Absolute Configuration. *Chirality* **2008**, *20*, 681–690, doi:10.1002/chir.20473.

100. Wenzel, T.J. Strategies for Using NMR Spectroscopy to Determine Absolute Configuration. *Tetrahedron Asymmetry* **2017**, *28*, 1212–1219, doi:10.1016/j.tetasy.2017.09.009.
101. Seco, J.M.; Quiñoá, E.; Riguera, R. The Assignment of Absolute Configuration by NMR. *Chem Rev* **2004**, *104*, 17–118, doi:10.1021/cr000665j.
102. Mishra, S.K.; Suryaprakash, N. Some New Protocols for the Assignment of Absolute Configuration by NMR Spectroscopy Using Chiral Solvating Agents and CDAs. *Tetrahedron Asymmetry* **2017**, *28*, 1220–1232, doi:10.1016/j.tetasy.2017.09.017.
103. Wenzel, T.J.; Chisholm, C.D. Assignment of Absolute Configuration Using Chiral Reagents and NMR Spectroscopy. *Chirality* **2011**, *23*, 190–214, doi:10.1002/chir.20889.
104. Seco, J.M.; Riguera, R. NMR Methods for the Assignment of Absolute Stereochemistry of Bioactive Compounds. In *eMagRes*; John Wiley & Sons, Ltd: Chichester, UK, 2015; pp. 1–30.
105. Lallana, E.; Freire, F.; Seco, J.M.; Quiñoá, E.; Riguera, R. The ^{1}H NMR Method for the Determination of the Absolute Configuration of 1,2,3- *p Rim* , *s Ec* , *s Ec*- Triols. *Org Lett* **2006**, *8*, 4449–4452, doi:10.1021/ol0616135.
106. Hoye, T.R.; Jeffrey, C.S.; Shao, F. Mosher Ester Analysis for the Determination of Absolute Configuration of Stereogenic (Chiral) Carbinol Carbons. *Nat Protoc* **2007**, *2*, 2451–2458, doi:10.1038/nprot.2007.354.
107. Imperatore, C.; Luciano, P.; Aiello, A.; Vitalone, R.; Irace, C.; Santamaria, R.; Li, J.; Guo, Y.-W.; Menna, M. Structure and Configuration of Phosphoeleganin, a Protein Tyrosine Phosphatase

1B Inhibitor from the Mediterranean Ascidian *Sidnyum Elegans*. *J Nat Prod* **2016**, *79*, 1144–1148, doi:10.1021/acs.jnatprod.6b00063.

108. Luciano, P.; Imperatore, C.; Senese, M.; Aiello, A.; Casertano, M.; Guo, Y.-W.; Menna, M. Assignment of the Absolute Configuration of Phosphoeleganin via Synthesis of Model Compounds. *J Nat Prod* **2017**, *80*, 2118–2123, doi:10.1021/acs.jnatprod.7b00397.
109. Genovese, M.; Imperatore, C.; Casertano, M.; Aiello, A.; Balestri, F.; Piazza, L.; Menna, M.; Del Corso, A.; Paoli, P. Dual Targeting of PTP1B and Aldose Reductase with Marine Drug Phosphoeleganin: A Promising Strategy for Treatment of Type 2 Diabetes. *Mar Drugs* **2021**, *19*, 535, doi:10.3390/md19100535.
110. Casertano, M.; Genovese, M.; Piazza, L.; Balestri, F.; Del Corso, A.; Vito, A.; Paoli, P.; Santi, A.; Imperatore, C.; Menna, M. Identifying Human PTP1B Enzyme Inhibitors from Marine Natural Products: Perspectives for Developing of Novel Insulin-Mimetic Drugs. *Pharmaceuticals* **2022**, *15*, 325, doi:10.3390/ph15030325.
111. Burt, A.; Lackner, C.; Tiniakos, D. Diagnosis and Assessment of NAFLD: Definitions and Histopathological Classification. *Semin Liver Dis* **2015**, *35*, 207–220, doi:10.1055/s-0035-1562942.
112. Papatheodoridi, M.; Cholongitas, E. Diagnosis of Non-Alcoholic Fatty Liver Disease (NAFLD): Current Concepts. *Curr Pharm Des* **2019**, *24*, 4574–4586, doi:10.2174/1381612825666190117102111.
113. Younossi, Z.M.; Golabi, P.; Paik, J.M.; Henry, A.; Van Dongen, C.; Henry, L. The Global Epidemiology of Nonalcoholic Fatty Liver Disease (NAFLD) and Nonalcoholic Steatohepatitis (NASH): A Systematic Review. *Hepatology* **2023**, *77*, 1335–1347, doi:10.1097/HEP.0000000000000004.

114. Boccatonda, A.; Andreetto, L.; D'Ardes, D.; Cocco, G.; Rossi, I.; Vicari, S.; Schiavone, C.; Cipollone, F.; Guagnano, M.T. From NAFLD to MAFLD: Definition, Pathophysiological Basis and Cardiovascular Implications. *Biomedicines* **2023**, *11*, 883, doi:10.3390/biomedicines11030883.
115. Eslam, M.; Newsome, P.N.; Sarin, S.K.; Anstee, Q.M.; Targher, G.; Romero-Gomez, M.; Zelber-Sagi, S.; Wai-Sun Wong, V.; Dufour, J.-F.; Schattenberg, J.M.; et al. A New Definition for Metabolic Dysfunction-Associated Fatty Liver Disease: An International Expert Consensus Statement. *J Hepatol* **2020**, *73*, 202–209, doi:10.1016/j.jhep.2020.03.039.
116. Lin, S.; Huang, J.; Wang, M.; Kumar, R.; Liu, Y.; Liu, S.; Wu, Y.; Wang, X.; Zhu, Y. Comparison of MAFLD and NAFLD Diagnostic Criteria in Real World. *Liver International* **2020**, *40*, 2082–2089, doi:10.1111/liv.14548.
117. Kaya, E.; Yilmaz, Y. Metabolic-Associated Fatty Liver Disease (MAFLD): A Multi-Systemic Disease Beyond the Liver. *J Clin Transl Hepatol* **2022**, *10*, 329–338, doi:10.14218/JCTH.2021.00178.
118. Younossi, Z.M.; Koenig, A.B.; Abdelatif, D.; Fazel, Y.; Henry, L.; Wymer, M. Global Epidemiology of Nonalcoholic Fatty Liver Disease—Meta-analytic Assessment of Prevalence, Incidence, and Outcomes. *Hepatology* **2016**, *64*, 73–84, doi:10.1002/hep.28431.
119. Xia, M.-F.; Bian, H.; Gao, X. NAFLD and Diabetes: Two Sides of the Same Coin? Rationale for Gene-Based Personalized NAFLD Treatment. *Front Pharmacol* **2019**, *10*, doi:10.3389/fphar.2019.00877.

120. Sakurai, Y.; Kubota, N.; Yamauchi, T.; Kadowaki, T. Role of Insulin Resistance in MAFLD. *Int J Mol Sci* **2021**, *22*, 4156, doi:10.3390/ijms22084156.
121. Alam, S.; Mustafa, G.; Alam, M.; Ahmad, N. Insulin Resistance in Development and Progression of Nonalcoholic Fatty Liver Disease. *World J Gastrointest Pathophysiol* **2016**, *7*, 211, doi:10.4291/wjgp.v7.i2.211.
122. Chen, Y.; Liu, T.; Teia, F.K.F.; Xie, M. Exploring the Underlying Mechanisms of Obesity and Diabetes and the Potential of Traditional Chinese Medicine: An Overview of the Literature. *Front Endocrinol (Lausanne)* **2023**, *14*, doi:10.3389/fendo.2023.1218880.
123. Gallagher, E.J.; LeRoith, D.; Karnieli, E. The Metabolic Syndrome—from Insulin Resistance to Obesity and Diabetes. *Endocrinol Metab Clin North Am* **2008**, *37*, 559–579, doi:10.1016/j.ecl.2008.05.002.
124. Souza, M.R. de A.; Diniz, M. de F.F. de M.; Medeiros-Filho, J.E.M. de; Araújo, M.S.T. de Metabolic Syndrome and Risk Factors for Non-Alcoholic Fatty Liver Disease. *Arq Gastroenterol* **2012**, *49*, 89–96, doi:10.1590/S0004-28032012000100015.
125. Katsiki, N.; Perez-Martinez, P.; Anagnostis, P.; Mikhailidis, D.P.; Karagiannis, A. Is Nonalcoholic Fatty Liver Disease Indeed the Hepatic Manifestation of Metabolic Syndrome? *Curr Vasc Pharmacol* **2018**, *16*, 219–227, doi:10.2174/1570161115666170621075619.
126. Cole, B.K.; Feaver, R.E.; Wamhoff, B.R.; Dash, A. Non-Alcoholic Fatty Liver Disease (NAFLD) Models in Drug Discovery. *Expert*

Opin Drug Discov **2018**, *13*, 193–205, doi:10.1080/17460441.2018.1410135.

127. Jeeyavudeen, M.S.; Khan, S.K.; Fouda, S.; Pappachan, J.M. Management of Metabolic-Associated Fatty Liver Disease: The Diabetology Perspective. *World J Gastroenterol* **2023**, *29*, 126–143, doi:10.3748/wjg.v29.i1.126.
128. Titchenell, P.M.; Lazar, M.A.; Birnbaum, M.J. Unraveling the Regulation of Hepatic Metabolism by Insulin. *Trends in Endocrinology & Metabolism* **2017**, *28*, 497–505, doi:10.1016/j.tem.2017.03.003.
129. Li, M.; Chi, X.; Wang, Y.; Setrerrahmane, S.; Xie, W.; Xu, H. Trends in Insulin Resistance: Insights into Mechanisms and Therapeutic Strategy. *Signal Transduct Target Ther* **2022**, *7*, 216, doi:10.1038/s41392-022-01073-0.
130. Spooner, M.H.; Jump, D.B. Omega-3 Fatty Acids and Nonalcoholic Fatty Liver Disease in Adults and Children. *Curr Opin Clin Nutr Metab Care* **2019**, *22*, 103–110, doi:10.1097/MCO.0000000000000539.
131. Goldstein, B.J. Protein-Tyrosine Phosphatase 1B (PTP1B): A Novel Therapeutic Target for Type 2 Diabetes Mellitus, Obesity and Related States of Insulin Resistance. *Curr Drug Targets Immune Endocr Metabol Disord* **2001**, *1*, 265–275, doi:10.2174/1568008013341163.
132. Ramana, K. V.; Srivastava, S.K. Aldose Reductase: A Novel Therapeutic Target for Inflammatory Pathologies. *Int J Biochem Cell Biol* **2010**, *42*, 17–20, doi:10.1016/j.biocel.2009.09.009.
133. Livak, K.J.; Schmittgen, T.D. Analysis of Relative Gene Expression Data Using Real-Time Quantitative PCR and the

2−ΔΔCT Method. *Methods* **2001**, *25*, 402–408, doi:10.1006/meth.2001.1262.

134. Cimmino, I.; Lorenzo, V.; Fiory, F.; Doti, N.; Ricci, S.; Cabaro, S.; Liotti, A.; Vitagliano, L.; Longo, M.; Miele, C.; et al. A Peptide Antagonist of Prep1-P160 Interaction Improves Ceramide-Induced Insulin Resistance in Skeletal Muscle Cells. *Oncotarget* **2017**, *8*, 71845–71858, doi:10.18632/oncotarget.18286.
135. Chauhan, J.; Luthra, T.; Gundla, R.; Ferraro, A.; Holzgrabe, U.; Sen, S. A Diversity Oriented Synthesis of Natural Product Inspired Molecular Libraries. *Org Biomol Chem* **2017**, *15*, 9108–9120, doi:10.1039/C7OB02230A.
136. Hoffer, L.; Voitovich, Y. V.; Raux, B.; Carrasco, K.; Muller, C.; Fedorov, A.Y.; Derviaux, C.; Amouric, A.; Betzi, S.; Horvath, D.; et al. Integrated Strategy for Lead Optimization Based on Fragment Growing: The Diversity-Oriented-Target-Focused-Synthesis Approach. *J Med Chem* **2018**, *61*, 5719–5732, doi:10.1021/acs.jmedchem.8b00653.
137. Prescher, H.; Koch, G.; Schuhmann, T.; Ertl, P.; Bussenault, A.; Glick, M.; Dix, I.; Petersen, F.; Lizos, D.E. Construction of a 3D-Shaped, Natural Product like Fragment Library by Fragmentation and Diversification of Natural Products. *Bioorg Med Chem* **2017**, *25*, 921–925, doi:10.1016/j.bmc.2016.12.005.
138. Hung, A.W.; Ramek, A.; Wang, Y.; Kaya, T.; Wilson, J.A.; Clemons, P.A.; Young, D.W. Route to Three-Dimensional Fragments Using Diversity-Oriented Synthesis. *Proceedings of the National Academy of Sciences* **2011**, *108*, 6799–6804, doi:10.1073/pnas.1015271108.

139. Kidd, S.L.; Osberger, T.J.; Mateu, N.; Sore, H.F.; Spring, D.R. Recent Applications of Diversity-Oriented Synthesis Toward Novel, 3-Dimensional Fragment Collections. *Front Chem* **2018**, *6*, doi:10.3389/fchem.2018.00460.

140. Lira, L.M.; Vasilev, D.; Pilli, R.A.; Wessjohann, L.A. One-Pot Synthesis of Organophosphate Monoesters from Alcohols. *Tetrahedron Lett* **2013**, *54*, 1690–1692, doi:10.1016/j.tetlet.2013.01.059.

141. Ottanà, R.; Paoli, P.; Lori, G.; Adornato, I.; Previti, S.; Naß, A.; Wolber, G.; Maccari, R. Design and Evaluation of Non-Carboxylate 5-Arylidene-2-Thioxo-4-Imidazolidinones as Novel Non-Competitive Inhibitors of Protein Tyrosine Phosphatase 1B. *Bioorg Chem* **2019**, *92*, 103211, doi:10.1016/j.bioorg.2019.103211.

142. Balestri, F.; Cappiello, M.; Moschini, R.; Rotondo, R.; Buggiani, I.; Pelosi, P.; Mura, U.; Del-Corso, A. L-Idose: An Attractive Substrate Alternative to d-Glucose for Measuring Aldose Reductase Activity. *Biochem Biophys Res Commun* **2015**, *456*, 891–895, doi:10.1016/j.bbrc.2014.12.054.

143. Liavonchanka, A.; Feussner, I. Lipoxygenases: Occurrence, Functions and Catalysis. *J Plant Physiol* **2006**, *163*, 348–357, doi:10.1016/j.jplph.2005.11.006.

144. Mashima, R.; Okuyama, T. The Role of Lipoxygenases in Pathophysiology; New Insights and Future Perspectives. *Redox Biol* **2015**, *6*, 297–310, doi:10.1016/j.redox.2015.08.006.

145. Ivanov, I.; Heydeck, D.; Hofheinz, K.; Roffeis, J.; O'Donnell, V.B.; Kuhn, H.; Walther, M. Molecular Enzymology of Lipoxygenases. *Arch Biochem Biophys* **2010**, *503*, 161–174, doi:10.1016/j.abb.2010.08.016.

146. Yamamoto, S. Mammalian Lipoxygenases: Molecular Structures and Functions. *Biochimica et Biophysica Acta (BBA) - Lipids and Lipid Metabolism* **1992**, *1128*, 117–131, doi:10.1016/0005-2760(92)90297-9.

147. Ivanov, I.; Kuhn, H.; Heydeck, D. Structural and Functional Biology of Arachidonic Acid 15-Lipoxygenase-1 (ALOX15). *Gene* **2015**, *573*, 1–32, doi:10.1016/j.gene.2015.07.073.

148. Kuhn, H.; Walther, M.; Kuban, R.J. Mammalian Arachidonate 15-Lipoxygenases. *Prostaglandins Other Lipid Mediat* **2002**, *68–69*, 263–290, doi:10.1016/S0090-6980(02)00035-7.

149. Singh, N.K.; Rao, G.N. Emerging Role of 12/15-Lipoxygenase (ALOX15) in Human Pathologies. *Prog Lipid Res* **2019**, *73*, 28–45, doi:10.1016/j.plipres.2018.11.001.

150. Snodgrass, R.G.; Brüne, B. Regulation and Functions of 15-Lipoxygenases in Human Macrophages. *Front Pharmacol* **2019**, *10*, doi:10.3389/fphar.2019.00719.

151. Xu, X.; Li, J.; Zhang, Y.; Zhang, L. Arachidonic Acid 15-Lipoxygenase: Effects of Its Expression, Metabolites, and Genetic and Epigenetic Variations on Airway Inflammation. *Allergy Asthma Immunol Res* **2021**, *13*, 684, doi:10.4168/aair.2021.13.5.684.

152. Joshi, Y.B.; Giannopoulos, P.F.; Praticò, D. The 12/15-Lipoxygenase as an Emerging Therapeutic Target for Alzheimer's Disease. *Trends Pharmacol Sci* **2015**, *36*, 181–186, doi:10.1016/j.tips.2015.01.005.

153. Tobaben, S.; Grohm, J.; Seiler, A.; Conrad, M.; Plesnila, N.; Culmsee, C. Bid-Mediated Mitochondrial Damage Is a Key Mechanism in Glutamate-Induced Oxidative Stress and AIF-

Dependent Cell Death in Immortalized HT-22 Hippocampal Neurons. *Cell Death Differ* **2011**, *18*, 282–292, doi:10.1038/cdd.2010.92.

154. Meng, H.; McClendon, C.L.; Dai, Z.; Li, K.; Zhang, X.; He, S.; Shang, E.; Liu, Y.; Lai, L. Discovery of Novel 15-Lipoxygenase Activators To Shift the Human Arachidonic Acid Metabolic Network toward Inflammation Resolution. *J Med Chem* **2016**, *59*, 4202–4209, doi:10.1021/acs.jmedchem.5b01011.
155. Sadeghian, H.; Jabbari, A. 15-Lipoxygenase Inhibitors: A Patent Review. *Expert Opin Ther Pat* **2016**, *26*, 65–88, doi:10.1517/13543776.2016.1113259.
156. Fu, X.; Schmitz, F.J.; Govindan, M.; Abbas, S.A.; Hanson, K.M.; Horton, P.A.; Crews, P.; Laney, M.; Schatzman, R.C. Enzyme Inhibitors: New and Known Polybrominated Phenols and Diphenyl Ethers from Four Indo-Pacific Dysidea Sponges. *J Nat Prod* **1995**, *58*, 1384–1391, doi:10.1021/np50123a008.
157. Cichewicz, R.H.; Kenyon, V.A.; Whitman, S.; Morales, N.M.; Arguello, J.F.; Holman, T.R.; Crews, P. Redox Inactivation of Human 15-Lipoxygenase by Marine-Derived Meroditerpenes and Synthetic Chromanes: Archetypes for a Unique Class of Selective and Recyclable Inhibitors. *J Am Chem Soc* **2004**, *126*, 14910–14920, doi:10.1021/ja046082z.
158. Alzarea, S.I.; Elmaidomy, A.H.; Saber, H.; Musa, A.; Al-Sanea, M.M.; Mostafa, E.M.; Hendawy, O.M.; Youssif, K.A.; Alanazi, A.S.; Alharbi, M.; et al. Potential Anticancer Lipoxygenase Inhibitors from the Red Sea-Derived Brown Algae Sargassum Cinereum: An In-Silico-Supported In-Vitro Study. *Antibiotics* **2021**, *10*, 416, doi:10.3390/antibiotics10040416.

159. Sadeghian, H.; Jabbari, A. 15-Lipoxygenase Inhibitors: A Patent Review. *Expert Opin Ther Pat* **2016**, *26*, 65–88, doi:10.1517/13543776.2016.1113259.

160. Eleftheriadis, N.; Thee, S.; te Biesebeek, J.; van der Wouden, P.; Baas, B.-J.; Dekker, F.J. Identification of 6-Benzyloxysalicylates as a Novel Class of Inhibitors of 15-Lipoxygenase-1. *Eur J Med Chem* **2015**, *94*, 265–275, doi:10.1016/j.ejmech.2015.03.007.